



A University of Sussex PhD thesis

Available online via Sussex Research Online:

<http://sro.sussex.ac.uk/>

This thesis is protected by copyright which belongs to the author.

This thesis cannot be reproduced or quoted extensively from without first obtaining permission in writing from the Author

The content must not be changed in any way or sold commercially in any format or medium without the formal permission of the Author

When referring to this work, full bibliographic details including the author, title, awarding institution and date of the thesis must be given

Please visit Sussex Research Online for more information and further details

**Modulation of feeding and its role in appetitive
memory consolidation in *Lymnaea stagnalis***

Daniel Price

Submitted for the degree of Doctor of Philosophy

University of Sussex

September 2018

Declaration

The work in this thesis is entirely my own, except where references to the work of others are acknowledged. This thesis has not been and will not be submitted in whole or in part to this or any other university as part of a degree.

Signature:

Daniel Price

Acknowledgements

I would like to thank my supervisors Ildiko Kemenes and Thomas Nowotny for the many hours of supervision, guidance and encouragement they have given me. I'd also like to thank George Kemenes and Paul Benjamin who have frequently provided me with helpful advice and comments. Thank you to Felix Kern for helping me to learn the dynamic clamp technique and how to write basic scripts. Thanks to Michael Crossley for providing an expert understanding of the feeding system and working alongside me to collect the semi-intact recordings of the PIB and the CGC. I'd also like to thank Terri Roberts for helping me with modifications to my rig. Thank you to Hazel Smulders and her team for always doing a fantastic job looking after the snails. Thank you to Souvik, Lenzie, Sian and Simon for your help at various points of my PhD. Lastly, I'd like to thank my family for always supporting me during my studies.

Abstract

Feeding in the pond snail (*Lymnaea stagnalis*) is heavily regulated by modulatory neurons throughout the brain. Following appetitive conditioning many of these identified neurons show changes in electrophysiological properties that contribute to the conditioned feeding response. The aim of this thesis was to further characterise modulatory feeding neurons and the neural plasticity that occurs within them during appetitive memory consolidation.

Previous research had shown that the cerebral giant cell (CGC) is persistently depolarised 16-24 hours following appetitive conditioning and onwards. A Hodgkin-Huxley model of the CGC predicted this nonsynaptic plasticity to occur via an increase in the maximum conductance of the persistent sodium current (I_{NaP}), delayed rectifier current (I_K) and high voltage activated calcium current (I_{HVA}). To test this hypothesis these three modelled conductances were introduced into the membrane of the CGC of untrained snails, using dynamic clamp. Little effect on electrophysiological properties was initially seen due to an unexpectedly large cell surface area. To correct for this underestimation the response of the membrane to sine wave current injection was used to calculate the total cell surface area prior to dynamic clamp. When correctly scaled conductances were applied to the cell, there was still no significant change in the resting membrane potential (RMP). This suggests that the changes in ionic conductances causing CGC nonsynaptic plasticity during long term memory are more complex than previously realised and may involve other membrane conductances. A simpler attempt to depolarise the CGC with pattern clamp was able to cause significant RMP depolarisation, but also led to ectopic spike initiation in the proximal axon.

Sub-optimal classical conditioning of *Lymnaea* with dilute sucrose (US) results in memory expression which is temporarily undetectable both at 30 minutes and 2 hours after training. The neural mechanisms involved during these memory lapses are unknown. Therefore, two key modulatory neurons, the CGC and the pleural buccal interneuron (PIB) were recorded during lapse and non-lapse time points after sub-optimal conditioning. These neurons were targeted as they can upregulate and downregulate the entire feeding system, and modulatory cells have previously been

shown to play a role in memory consolidation. When conditioned preparations were compared to unconditioned preparations there was no significant difference in spontaneous firing frequency or CS-induced firing frequency in the CGC or PIB. This suggests that neither of these identified modulatory neurons play a role at 1 hr (non-lapse), 2 hr (lapse), and 3 hr (non-lapse) following sub-optimal appetitive conditioning.

To better understand the neural mechanisms of appetitive memory storage it is also important to characterise the feeding network. Particularly little is known about the control of the modulatory feeding neurons which project to the buccal ganglia, where the feeding CPG and motoneurons are located. Therefore, a search was made for a neuron presynaptic to modulatory projection cells. Such a cell was identified in the parietal ganglion and was termed parietal dorsal 4 (PD4). Intracellular dye filling revealed an expansive morphology with a large axon projecting through the pleural ganglion, cerebral ganglion, and lastly the buccal ganglion. The axon was also seen to branch extensively and cross both the cerebral and buccal commissure. Furthermore, a peripheral projection was observed from a nerve of the visceral ganglion. This extensive morphology makes this neuron an ideal candidate to regulate control of the feeding system as a whole. When artificially activated by depolarisation PD4 caused monosynaptic excitation of both the ipsilateral and contralateral CGC. Delayed excitation was also observed on the ipsilateral CV1a and inhibition on the ipsilateral PIB. However, no direct connection was found between PD4 and identified dorsal buccal feeding neurons. Depolarisation of PD4 could occasionally cause feeding cycles to occur but could also inhibit spontaneous fictive feeding. This differential effect is likely due to polysynaptic depolarisation of the inhibitory CPG neuron N3t, which becomes dominant when there are high frequency action potentials in the CGC. In a semi-intact preparation PD4 did not respond to sucrose applied to the lips, demonstrating it is not involved in the unconditioned feeding response. PD4 was depolarised to threshold by extracellular stimulation of multiple nerves including the lip, tentacle, anal/intestinal and parietal nerves. Activation of PD4 also caused inhibition of the caudodorsal cells (CDCs) and excitation of the ring neuron (RN), suggesting that the neuron may be involved in controlling modulation of the feeding network during egg laying behaviour.

In summary, this thesis examines important conceptual gaps in the understanding of appetitive memory consolidation in *Lymnaea*. It also provides the characterisation of an entirely new cell with widespread influence over the feeding system.

Table of contents

ABBREVIATIONS	VI
CHAPTER 1: GENERAL INTRODUCTION	1
1.1. OUTLINE	1
1.2. THE NEURAL BASIS OF BEHAVIOUR	1
1.3 CLASSIFICATION OF LEARNING AND MEMORY	2
1.4. ASSOCIATIVE LEARNING AND MEMORY	3
1.4.1. <i>Operant conditioning</i>	3
1.4.2. <i>Classical conditioning</i>	3
1.5. THE NEUROPHYSIOLOGICAL BASIS OF MEMORY	4
1.5.1. <i>The engram concept</i>	4
1.5.2. <i>Early evidence of the engram</i>	4
1.5.3. <i>The engram is often highly distributed</i>	4
1.6. FEATURES OF ASSOCIATIVE CONDITIONING	5
1.6.1. <i>Coincidence detection</i>	5
1.6.2. <i>Consolidation and reconsolidation</i>	5
1.6.3. <i>Synaptic plasticity</i>	6
1.6.4. <i>Nonsynaptic plasticity</i>	6
1.7. <i>LYMNAEA</i> AS A MODEL FOR ASSOCIATIVE LEARNING	7
1.7.1. <i>Operant conditioning of respiration</i>	7
1.7.1.1 Behaviour	7
1.7.1.2. Network.....	7
1.7.1.3. Plasticity	8
1.7.2. <i>Classical conditioning of feeding</i>	8
1.7.2.1 Behaviour	8
1.7.2.2 Network.....	9
CPG and motoneurons	9
Modulatory neurons	11
1.7.2.3 Plasticity	16
Tactile appetitive conditioning	16
Chemical appetitive conditioning.....	18
1.8. CONCEPTUAL GAPS IN THE CURRENT UNDERSTANDING OF CHEMICAL APPETITIVE CONDITIONING IN <i>LYMNAEA</i>	20
1.8.1. <i>The ionic conductances responsible for nonsynaptic plasticity in CGC during LTM are theorised but not fully tested</i>	20

1.8.2. <i>The monosynaptic connections of the lip and tentacle chemosensory neurons are uncharacterised</i>	21
1.8.3. <i>The neural basis for memory lapses in Lymnaea is unknown</i>	22
1.8.4. <i>Presynaptic control of modulatory projection neurons is largely unexplored</i>	23
1.9. THESIS OUTLINE	24
CHAPTER 2: GENERAL METHODS	26
2.1. ANIMAL MAINTENANCE	26
2.2. ELECTROPHYSIOLOGICAL PREPARATIONS.....	26
2.3. INTRACELLULAR RECORDING	28
2.4. RECORDING AND DATA PROCESSING SOFTWARE	29
2.5. STATISTICAL ANALYSIS OF DATA	29
CHAPTER 3: ELECTROPHYSIOLOGICAL BASIS FOR NONSYNAPTIC PLASTICITY IN A KEY MODULATORY NEURON OF THE FEEDING SYSTEM	31
3.1. INTRODUCTION.....	31
3.2. METHODS	33
3.2.1. <i>Preparation</i>	33
3.2.2. <i>Cell surface estimation</i>	33
3.2.3. <i>Insertion of artificial conductances using dynamic clamp</i>	34
3.2.4. <i>Collection and analysis of dynamic clamp data</i>	36
3.2.5. <i>Pattern Clamp</i>	37
3.3. RESULTS.....	38
3.3.1. <i>Addition of model conductances has little effect when CGC is assumed to be a sphere</i>	38
3.3.2. <i>The surface area of CGC is much larger than a sphere</i>	42
3.3.3. <i>Addition of modelled conductances still does not depolarise CGC, when based on measured cell surface area</i>	43
3.3.4. <i>Pattern clamp can depolarise the CGC soma, but induces irrepressible action potentials elsewhere in the cell</i>	47
3.4. DISCUSSION	51
3.4.1. <i>Neuronal surface area</i>	51
3.4.2. <i>The ionic basis of nonsynaptic plasticity</i>	52
3.4.3. <i>Spike initiation outside the soma</i>	53
CHAPTER 4: THE ROLE OF MODULATORY NEURONS IN MEMORY LAPSES	55

4.1. INTRODUCTION.....	55
4.2. METHODS	57
4.2.1. <i>Sub-optimal behavioural conditioning</i>	57
4.2.2. <i>Semi-intact preparations</i>	59
4.2.3. <i>Time course of the electrophysiology experiments</i>	59
4.2.4. <i>Analysis of electrophysiological recordings</i>	60
4.3. RESULTS.....	61
4.3.1. <i>Sub-optimal conditioning using GNL as the CS shows memory lapses</i>	61
4.3.2. <i>Sub-optimal conditioning did not reveal significant change in spontaneous or CS-evoked PIB firing rates</i>	62
4.3.3. <i>No significant changes were found in PIB spike characteristics following sub-optimal conditioning</i>	65
4.3.4. <i>No change in PIB firing rate was found by application of the US before or after sub-optimal conditioning</i>	66
4.3.5. <i>GNL causes a direct depolarisation of CGC without the lips</i>	69
4.3.6. <i>Sub-optimal conditioning using AA as the CS shows memory lapses</i>	71
4.3.7. <i>Sub-optimal conditioning did not reveal significant change in spontaneous or CS-evoked CGC firing rates</i>	72
4.3.8. <i>No significant changes were found in CGC spike characteristics following sub-optimal conditioning</i>	75
4.3.9. <i>Sucrose caused significant increases in CGC firing frequency both in conditioned and unconditioned preparations</i>	76
4.4. DISCUSSION	79
4.4.1. <i>Nonsynaptic plasticity in the CGS and PIB neurons was not detected within either the lapse or non-lapse periods during memory consolidation</i>	79
4.4.2. <i>No response to the CS was detected in either the CGC or the PIB neurons after conditioning</i>	80
4.4.3. <i>Low statistical power makes interpretation of the electrophysiological results of this chapter inconclusive</i>	80
4.4.4. <i>Other possible loci underlying memory lapses</i>	81
CV1a	81
N1M	81
4.4.5. <i>Alternative experimental approaches</i>	81
Nerve stimulation.....	81
<i>In vitro</i> conditioning	82

CHAPTER 5: A NOVEL PARIETAL NEURON THAT CONTROLS FEEDING MODULATION	83
5.1. INTRODUCTION.....	83
5.2. METHODS	85
5.2.1. Preparations.....	85
5.2.2. Cell identification	85
5.2.3. Intracellular dye filling	87
5.2.4. Modified saline.....	87
5.2.5. Nerve stimulation.....	88
5.3. RESULTS.....	88
5.3.1. PD4 has a widespread morphology	88
5.3.2. Each PD4 directly excites both the ipsilateral and contralateral CGC.....	92
5.3.3. PD4 also synapses with other modulatory projection neurons of the feeding system	94
5.3.4. PD4 does not synapse with identified dorsal buccal feeding neurons	96
5.3.5. PD4 influences feeding but is not a command neuron	98
5.3.6. PD4 responds to touch but not sucrose to the lips.....	100
5.3.7. PD4 inhibits the egg laying neurons.....	101
5.3.8. PD4 does not synapse with key cells of the cardiorespiratory and withdrawal networks.....	102
5.3.9. PD4 can be activated by nerve stimulation.....	103
5.4. DISCUSSION	106
5.4.1. PD4 influences feeding through modulatory projection neurons	106
5.4.2. PD4 may play a role in the later stages of egg laying.....	107
5.4.3. PD4 was not found to have connections with the withdrawal or cardiorespiratory networks.....	109
5.4.4. Similar higher order neurons exist in other molluscs	109
CHAPTER 6: GENERAL DISCUSSION.....	111
6.1. USING DYNAMIC CLAMP TO SIMULATE NONSYNAPTIC PLASTICITY IN A MODULATORY NEURON	112
6.1.1. Testing learning-induced changes predicted by a mathematical model revealed that further physiological parameters need to be taken in to consideration.....	112
6.1.2. Ectopic spikes prevent artificial CGC depolarisation	113
6.2. SEARCHING FOR THE NEURAL BASIS OF THE KAMIN EFFECT	114
6.2.1. Training with different conditioning stimuli results in identical temporal occurrence of the Kamin effect.....	114

6.2.2. A functional role for two key modulatory feeding neurons, CGC and PIB, in the Kamin effect, could not be found	115
6.3. A NEWLY IDENTIFIED NEURON, PD4, HAS A STRONG INFLUENCE OVER THE FEEDING AND EGG LAYING NETWORKS	116
6.3.1. PD4 may coordinate feeding as part of the egg laying behaviour.....	116
6.4. FUTURE RESEARCH	118
6.4.1. An alternative model of CGC nonsynaptic plasticity would be required based on the new experimental data	118
6.4.2. Other identified neurons could play a role in the Kamin effect	119
6.4.3. The neurotransmitter of PD4 is currently unknown.....	119
6.4.4. PD4 projects to an unknown cell type in the buccal ganglia.....	120
6.4.5. A stimulus that activates PD4 will need to be identified.....	120
6.5. CONCLUSION	121
REFERENCES	123

Abbreviations

5-HT	5-hydroxytryptamine (serotonin)
AA	Amyl acetate
ADC	Analogue-to-digital converter
ANOVA	Analysis of variance
B1-12	Buccal neuron (all motoneurons in <i>Lymnaea</i>)
CBC	Cerebral-buccal connective
CBI	Cerebral-buccal interneuron
CDCs	Caudodorsal cells
CGC	Cerebral giant cell
CNS	Central nervous system
CPG	Central Pattern generator
CS	Conditioned stimulus
CV	Cerebral ventral neuron
DLM	Dorsal longitudinal muscle motoneuron
EPSP	Excitatory postsynaptic potential
g_{\max}	maximum conductance
GNL	Gamma-nonalactone
HiDi	High divalent saline
I_A	Transient potassium current
I_{HVA}	High voltage activated calcium current
I_K	Delayed rectifier potassium current
I_{LVA}	Low voltage activated calcium current
I_{NaP}	Persistent sodium current
I_{NaT}	Transient sodium current
IP3	Input 3 neuron
IPSP	Inhibitory postsynaptic potential
ITM	Intermediate-term memory
LTM	Long-term memory
MLN	Median lip nerve
N1L	N1 lateral neuron
N1M	N1 medial neuron
N2d	N2 dorsal neuron
N2v	N2 ventral neuron
N3p	N3 phasic neuron
N3t	N3 tonic neuron
NO	Nitric oxide
NS	Normal saline
OC	Octopamine cell
PD	Parietal dorsal neuron
PeD	Pedal dorsal neuron
PIR	Post-inhibitory rebound
PKC	Protein kinase C

PKM	Protein kinase M
PIB	Pleural-buccal interneuron
RMP	Resting membrane potential
RN	Ring neuron
SEM	Standard error of the mean
SLN	Superior lip nerve
SN	Sensory neuron
SO	Slow oscillator neuron
STM	Short-term memory
TN	Tentacle nerve
US	Unconditioned stimulus
VD	Visceral dorsal neuron

Chapter 1: General Introduction

1.1. Outline

The work described in this thesis addresses important gaps in our understanding of the modulation of feeding and its role in appetitive memory consolidation. In order to appreciate this work, it is important to be aware of what constitutes behaviour and its alteration during learning and memory. It is also necessary to understand the behavioural classification of learning and memory, so that the category studied in this thesis, classical conditioning, can be placed within the broader framework. The concept of the engram will then be discussed, as this is crucial for understanding the neurophysiological basis for classical conditioning. Common features of associative conditioning, particularly relevant to this work will then be introduced. Following this the pond snail, *Lymnaea stagnalis*, will be introduced as an important model species for understanding the underlying features of associative memories. Important conceptual gaps in our current understanding of *Lymnaea* appetitive conditioning, relevant to the work of this thesis, will then be highlighted. Lastly, an outline of the results chapters of this thesis will be given.

1.2. The neural basis of behaviour

Behaviour can be defined as the interactions an animal has with its surroundings. The behaviour of an animal is often controlled by a central system of many neurons, each connected to one another and the periphery by synapses. Some behaviours are innately wired within the nervous system and do not change over time. Other behaviours are altered by experience; this is known as learning. The storage of learnt behaviours is known as memory. Learning and memory act to improve the animal's chances of survival and producing healthy offspring.

To understand behaviour, it is necessary to study the nervous system and its responses to environmental stimuli. In humans and mammals this is a difficult task due to the complexity of the brain. Therefore, many neuroscientists have turned to invertebrate species, whose brains are usually much smaller and simpler for study.

Often neural mechanisms identified in invertebrates can be translated to vertebrates, including humans. This is because many animal species have evolutionarily conserved traits at multiple biological levels including behaviour, electrophysiology and molecular cascades (Kandel *et al.*, 2014).

One of the most famous examples of the study of an invertebrate species with widely applicable findings was the veined squid (*Loligo forbesii*). Using recordings of a giant axon used for escape behaviours, Hodgkin and Huxley (1952) created a biophysical model for the action potential, which contained various voltage-gated ion channels. These mechanisms have since been found in other systems and generalised to excitable membranes in a wide variety of organisms (Hille, 2001).

In addition to basic neurophysiology, invertebrate species are also useful for studying learning and memory.

1.3 Classification of learning and memory

Throughout the thesis the research work will touch upon specific types of learning and memory. Learning and memory can broadly be divided into explicit and implicit forms (Squire & Zola-Morgan, 1988). Explicit memory consists of episodic and semantic memory whilst implicit memory consists of priming, procedural learning, associative learning and non-associative learning (**Figure 1.1**). Great progress has been made in the understanding of the neural basis of associative memory, as it can be easily studied in animal models including molluscs.

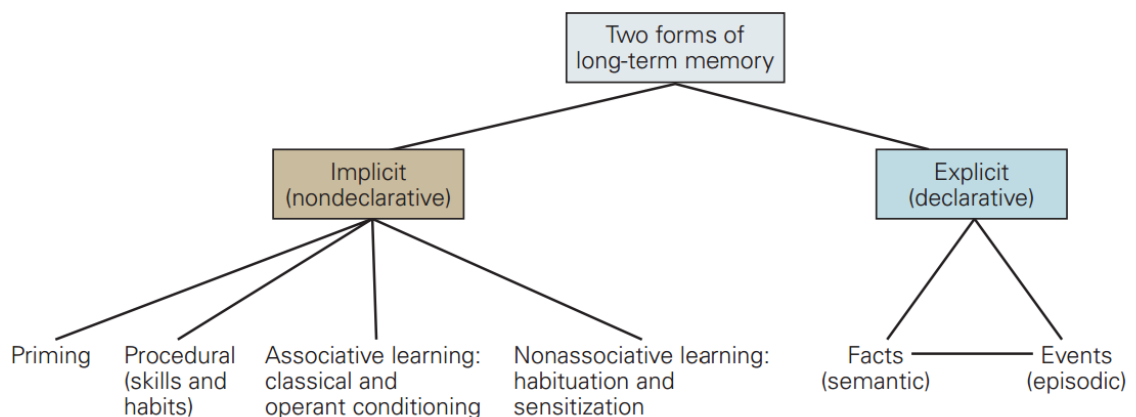


Figure 1.1. A diagram summarising the different forms of memory. Taken from Schacter and Wagner (2013).

1.4. Associative learning and memory

1.4.1. Operant conditioning

Operant conditioning is a form of simple associative learning in which an animal learns to associate a behavioural action with a reinforcing stimulus. This reinforcing stimulus can either be rewarding, and thus promote the behaviour, or aversive, and thus inhibit the behaviour (Thorndike, 1911). This form of learning can be observed using an operant conditioning chamber, where an animal is rewarded or punished in response to pressing a lever in its environment. At first this lever activation will be spontaneous (emitted), but the animal will soon predict the outcome of the behaviour and adapt it accordingly. The most well-known example of this is the use of hungry rats or pigeons which will learn to repeatedly press a lever in order to receive a food reward (Skinner, 1969).

1.4.2. Classical conditioning

One of the best-known examples of associative learning is Pavlov's experiment with dogs using classical conditioning (Pavlov, 1928). It was found that animals would salivate prior to feeding, suggesting that certain cues must allow them to anticipate food. To test this effect, a bell was rung before feeding. Over time the animals would learn this association and would salivate when the bell was rung, even if food was not present. Pairing of a stimulus which evokes a reliable behaviour (unconditioned stimulus, US) and a stimulus which is neutral, in respect to the behaviour (conditioned stimulus, CS) is now known as classical (Pavlovian) conditioning. This differs when compared to operant conditioning, because the animal responds to two stimuli within its environment whose occurrence it does not induce.

1.5. The neurophysiological basis of memory

1.5.1. The engram concept

Changes in behaviour, caused by learning, must have a physical basis in the nervous system. This idea of an alteration in the structure of networks within the brain, due to learning, is known as an engram, and was hypothesised long before there was experimental evidence (Semon, 1921; Konorski, 1948; Hebb, 1949).

1.5.2. Early evidence of the engram

Great progress in the search for the engram, was in the mollusc *Aplysia californica*, where it was shown that the lessening of an innate withdrawal response with repeated stimulation (habituation), can be correlated with the weakening of a single identified sensory-motor synapse (Castellucci *et al.*, 1970; Castellucci & Kandel, 1974). At a similar time, it was shown using cats that eyeblink classical conditioning resulted in nonsynaptic changes in neurons mediating sensory-motor facial circuits (Woody & Black-Cleworth, 1973). Therefore, it was clear that engrams could include sites of change both between neurons (synaptic plasticity) and within neurons (nonsynaptic plasticity).

1.5.3. The engram is often highly distributed

Early experimental work on studying the engram was often strongly focused on singular sites of change within the nervous system. However as understanding and observation of neural networks as a whole advanced, it became clear that the engram was often highly distributed. For example, classical conditioning of the mollusc *Hermissenda*, results in; nonsynaptic changes in photosensory neurons (Crow & Alkon, 1980; Fryszak & Crow, 1993), synaptic facilitation between photoreceptor types (Fryszak & Crow, 1994; 1997), synaptic facilitation between photoreceptors excitatory type I interneurons (Crow & Tian, 2002), and increased excitability of excitatory type I interneurons (Crow & Tian, 2003). All of these changes together contribute to a reduction in phototaxis and a shortening of the body as part of the conditioned response (Crow & Alkon, 1978).

A broader view of the engram has also been driven forward by recent technical advances that allow the monitoring, labelling and manipulation of large neuronal populations (ensembles) during learning (Tonegawa *et al.*, 2015). This has enabled researchers to selectively ablate or activate a given engram and causatively demonstrate a loss or activation of a conditioned response, respectively (Koya *et al.*, 2009; Liu *et al.*, 2012).

1.6. Features of associative conditioning

1.6.1. Coincidence detection

A core feature in a system capable of associative learning is a component, such as an enzyme or receptor, which can detect when two separate stimuli are temporally linked (coincident). The classical example of such a component is the NMDA receptor which will only conduct calcium inwards when there is both glutamate in the extracellular space and depolarisation of the postsynaptic membrane (Mayer *et al.*, 1984). If the NMDA receptor is blocked, for example in *Aplysia* during *in vitro* associative conditioning, preventing coincidence detection, then memory formation fails (Antonov *et al.*, 2003).

1.6.2. Consolidation and reconsolidation

Once an associative memory is acquired it is consolidated over time, with underlying changes in its anatomical, molecular and electrophysiological basis. As consolidation continues the engram should end up in a long-term crystallised state. For example, in *Lymnaea*, it can be possible to replace or erase an associative memory at early time points in consolidation, after weak conditioning, but not once LTM has formed (Marra *et al.*, 2013; Crossley *et al.*, 2019). In cases where the memory is updated by retrieval and still exists, this is known as reconsolidation.

An important part of understanding the consolidation process is identifying the underlying molecular cascades that are triggered by conditioning. Long-term memory (LTM) formation requires *de novo* mRNA synthesis (transcription) and can thus be blocked using actinomycin-D (Fulton *et al.*, 2005). Intermediate-term memory (ITM) requires protein synthesis only (translation), but can be blocked by anisomycin

(Kemenes *et al.*, 2002). Short-term memory (STM) is defined by its lack of reliance on transcription or translation (Marra *et al.*, 2013).

1.6.3. Synaptic plasticity

The ultimate site of change for all forms of memory is at the synapse, where a change in transmission within the neural network will result in a change in behavioural output. Two key types of synaptic plasticity have been identified due to conditioning; homosynaptic and heterosynaptic. Homosynaptic plasticity involves only the presynaptic and postsynaptic neuron. Heterosynaptic plasticity involves a presynaptic and postsynaptic neuron, but also a facilitatory neuron. The *Aplysia* gill withdrawal circuit shows examples of both of these forms of synaptic plasticity, at a single synapse following *in vitro* pavlovian conditioning (Antonov *et al.*, 2003). In terms of homosynaptic plasticity there is coincident activation of the LE sensory and LFS motor neuron during acquisition, causing activation of postsynaptic NMDA receptors and Hebbian long term potentiation. In terms of heterosynaptic plasticity there are facilitatory neurons activated by tail shock, (US) which release serotonin on to the presynaptic terminal, inducing sensory-motor synaptic facilitation.

1.6.4. Nonsynaptic plasticity

Although the synapse is always required as the ultimate effector of change following conditioning, it is also very common for plasticity to occur within neurons, through changes in their intrinsic properties (Mozzachiodi & Byrne, 2010). An excellent example of this is in the mollusc *Hermisenda* where light (CS) can be paired with rotation (US) to inhibit innate phototaxis (Crow & Alkon, 1978). Following conditioning, lateral type A and type B photoreceptors show an increase in membrane excitability (Crow & Alkon, 1980; Fryszak & Crow, 1993). This is due to a reduction in overall outward potassium conductance in type A cells (Farley & Han, 1997) and less $I_{K(Ca)}$ and I_A in type B cells (Alkon *et al.*, 1985). Additionally, the excitatory type I interneurons, that are secondary in the CS and US response pathway, show an increase in intrinsic excitability (Crow & Tian, 2003). The net result of these nonsynaptic changes, alongside other synaptic changes, is that there is increased inhibition of ventral pedal motoneurons, suppressing locomotion towards the light (CS).

1.7. *Lymnaea* as a model for associative learning

In this thesis I am using the model system of the pond snail, *Lymnaea stagnalis*. The pond snail has been an important species for the understanding of associative memory formation (Benjamin *et al.*, 2000). As a species of gastropod mollusc, it has large identifiable neurons, which form a relatively simple network, and can be recorded before, during and after associative conditioning (Marra *et al.*, 2013).

1.7.1. Operant conditioning of respiration

1.7.1.1 Behaviour

A useful operant conditioning paradigm for studying operant conditioning in *Lymnaea* has been developed. First the aquatic environment is made hypoxic, encouraging *Lymnaea* to approach the surface and attempt to carry out aerial respiration. Each time the animal tries to open its pneumostome to respire a tactile stimulus prevents it. After multiple spaced trials, this leads to a conditioned reduction in aerial respiration that can be detectable for several weeks (Lukowiak *et al.*, 1996; Lukowiak *et al.*, 1998; Lukowiak *et al.*, 2000).

1.7.1.2. Network

The neural network controlling aerial respiration is well characterised with three CPG neurons, each located in a different ganglion (Syed & Winlow, 1991b). The most commonly recorded is right pedal dorsal 1 (R PeD1), a giant dopaminergic cell that initiates rhythmic activity. R PeD1 is excited by osphradial cells, which are located in the periphery and detect changes in oxygen levels. Therefore when the environment becomes hypoxic, R PeD1 is excited, thus promoting aerial respiration (Bell *et al.*, 2007). In turn R PeD1 evokes spiking via post-inhibitory rebound in the input 3 cell (IP3). IP3 is a premotor CPG neuron located in the parietal ganglion which causes pneumostome opening. Through reciprocal inhibitory synapses, IP3 fires in alternation with visceral dorsal 4 (VD4), another premotor neuron, but which drives pneumostome closure. *In vitro* reconstruction of the CPG shows that this alternate bursting of IP3 and VD4 to open and close the pneumostome is dependent on the presence of dopamine from R PeD1 (Syed *et al.*, 1990). R PeD1 is multifunctional and

can also cause pneumostome opening directly through excitatory synapses with the pneumostome opener muscle (Haque *et al.*, 2006).

1.7.1.3. Plasticity

As one might expect the neural correlates of aversive operant conditioning can be identified as reductions in the excitability of the respiratory CPG neurons (Spencer *et al.*, 1999). R PeD1 which initiates respiration shows significantly less spontaneous activity following *in vivo* operant conditioning. Additionally, a fall in the spontaneous activity of IP3, monitored by recording motor neurons, can be found. Furthermore, if R PeD1 is artificially activated it shows a much weaker ability to drive respiration. The tactile stimulus during training causes inhibition of R PeD1, likely via the withdrawal neurons right pedal dorsal 11 (R PeD11) and right parietal dorsal 3 (R PD3) (Inoue *et al.*, 1996a; Inoue *et al.*, 1996b). Therefore, it was hypothesised by Lowe and Spencer (2006) that hyperpolarising R PeD1 between *in vitro* training trials might promote the formation of LTM. When this was carried out only two training sessions were required for LTM formation in a semi-intact preparation, rather than the usual four. Furthermore, surgical ablation of the R PeD1 soma has shown the cell body to be necessary for the formation of LTM, identifying this as a location of gene transcription during operant conditioning (Scheibenstock *et al.*, 2002).

1.7.2. Classical conditioning of feeding

1.7.2.1 Behaviour

Lymnaea can undergo appetitive conditioning with a variety of CS sensory modalities, usually following a few days starvation. Single trial visual conditioning is possible by pairing a black background (CS) with the presence of sucrose (US) (Andrew & Savage, 2000). Alternatively tactile stimuli applied to the lips or tentacle (CS) can be paired with sucrose (US) over multiple trials to elicit a conditioned response (Kemenes & Benjamin, 1989). Lastly, a single pairing of a neutral chemical stimulus, such as amyl acetate (CS), and sucrose (US) over two minutes, can elicit an appetitive memory which lasts for weeks (Alexander *et al.*, 1984).

1.7.2.2 Network

CPG and motoneurons

The core neuronal control of appetitive and consummatory bouts is by the same three premotor neurons; N1 medial (N1M), N2 ventral (N2v) and N3 tonic (N3t) (Benjamin, 2012). Together they form the central pattern generator (CPG) for feeding and are located in the buccal ganglia. Each neuron is sequentially active (N1->N2->N3), giving rise to a triphasic rhythm during feeding. This produces a behavioural pattern of three phases; protraction (N1), rasp (N2) and swallow (N3) (see **Figure 1.2**). During protraction, the buccal mass rotates outwards and the radula comes into contact with the substrate. Then the rasp phase occurs, with the buccal mass rotating backwards causing the radula to shear against the substrate. Lastly the swallow phase occurs when the buccal mass rotates fully backwards depositing food into the oesophagus. Note that in slower rhythms there can also be an additional rest phase.

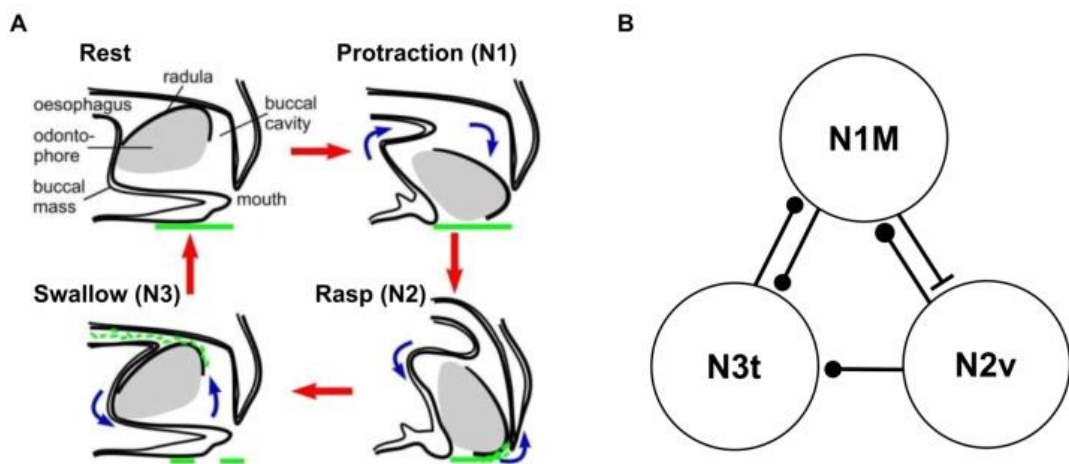


Figure 1.2. There are three phases of feeding activity in *Lymnaea*. **A.** Cartoon detailing the three sequential behavioural phases that constitute feeding in *Lymnaea*. In some cases, there is a rest phase between cycles. **B.** A network diagram of the core feeding CPG. Excitatory synapses are shown by bars and inhibitory synapses by dots. Adapted from (Benjamin, 2012).

A closer examination of each CPG neuron reveals key features required for pattern generation. When isolated in culture, N1M shows endogenous plateau potentials that outlast those seen in the intact nervous system (Straub *et al.*, 2002).

These plateau potentials are important for the generation of the rhythm and can provide the spontaneity seen with exploratory rasps. If N1M is stimulated then this is sufficient for feeding cycles to occur (Elliott & Benjamin, 1985a). N1M is also necessary for both slow oscillator and sucrose driven rhythms (Kemenes & Elliott, 1994; Kemenes *et al.*, 2001). When N1M is active it excites N2v, initiating a plateau potential which defines the rasp phase (Brierley *et al.*, 1997). In turn N2v inhibits N1M ending the protraction phase and preventing simultaneous activity. A computer model of the feeding system indicates N1M and N2v together maintain the rhythmicity of the system (Vavoulis *et al.*, 2007). Unlike N1M, N2v plateau potentials are dependent on the presence of acetylcholine (Straub *et al.*, 2002). Both N1M and N2v inhibit N3t when active, keeping the cell subthreshold during the protraction and rasp phase (Elliott & Benjamin, 1985a; Brierley *et al.*, 1997). When the N2v plateau potential ends (via an unknown endogenous mechanism) this allows post-inhibitory rebound to occur in N3t beginning the swallow phase and ending the protraction phase. In the quiescent state N3t fires continuously at a high rate and via its monosynaptic inhibitory connection with N1M, keeps the CPG silent.

The activity of the feeding CPG neurons drives activity in many different identified motor neurons, each of which innervates different structures. In terms of buccal mass neurons, there are B6, B7 which are active primarily during protraction, B10 during the rasp and B4, B4cl, B8 during the swallow phase (Rose & Benjamin, 1979). Many of these buccal mass motor neurons are electrically coupled with CPG neurons corresponding to their phase of activity (Staras *et al.*, 1998). This helps to maintain synchronicity and allows modulation of the activity of motor neurons to directly affect pattern generation. Some of the larger motoneurons of the buccal ganglia do not innervate the buccal mass. B1 and B3 are putative salivary gland neurons active during the protraction and rasp phase respectively (Benjamin *et al.*, 1979). B2 is not strongly entrained to the feeding rhythm but causes constriction of the foregut (Perry *et al.*, 1998). A number of rhythmically active small neurons have also been identified in the cerebral ganglia which project to the lip muscles, termed CV3, 5, 6, 7 (McCrohan, 1984b). Recently two buccal neurons, B11 and B12 have also been identified which switch activity phase depending on whether the animal is carrying out

ingestive or egestive feeding movements (Crossley, 2014). The fixed pattern of activity of many of these large motoneurons has been very useful for monitoring the motor output, without needing to record the significantly smaller CPG neurons (example shown in **Figure 1.3.**).

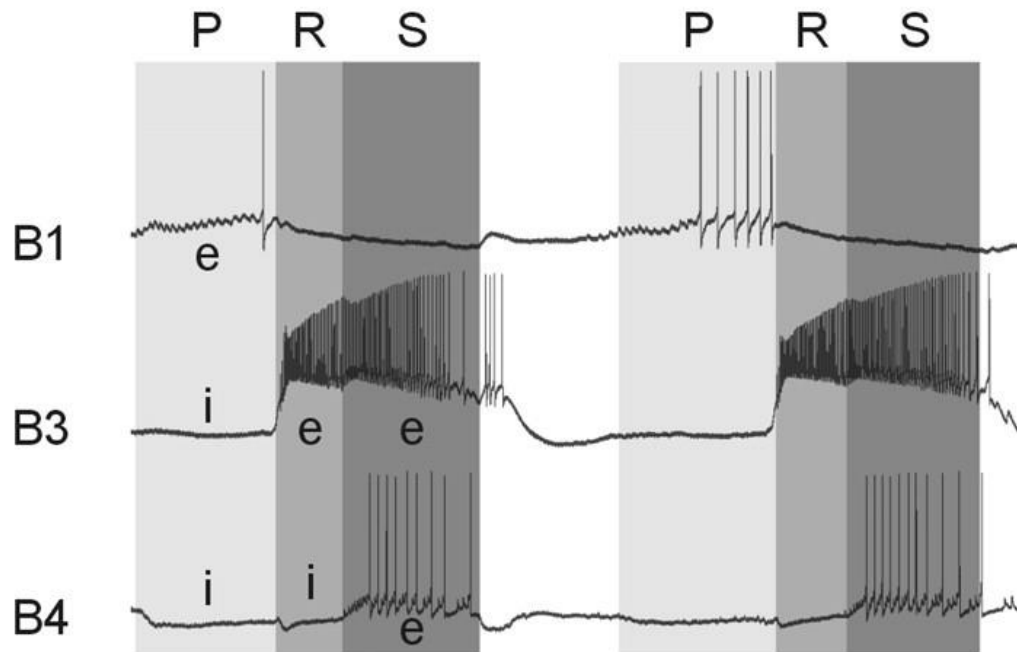


Figure 1.3. Electrophysiological recording showing the characteristic firing pattern of three large buccal motoneurons during fictive feeding. Taken from Straub *et al.* (2006).

Modulatory neurons

In addition to the CPG and motoneurons, there are neurons which modulate feeding activity by acting on endogenous and synaptic properties of other elements of the feeding system. In the past, some of these neurons were considered possible command neurons, as their stimulation was sufficient to evoke feeding. However further studies have shown them not to fulfil the strict criteria of being both sufficient and necessary for feeding, as defined by Kupfermann and Weiss (1978). Instead these neurons play more subtle roles such as being permissive (gating the behaviour), altering which neurons participate in the rhythm, and changing the frequency of feeding cycles. In many cases modulatory neurons have more than one function and can also be a component of the CPG or involved in initiation of rhythms. Modulation of the *Lymnaea* feeding system is summarised in **Figure 1.4.**

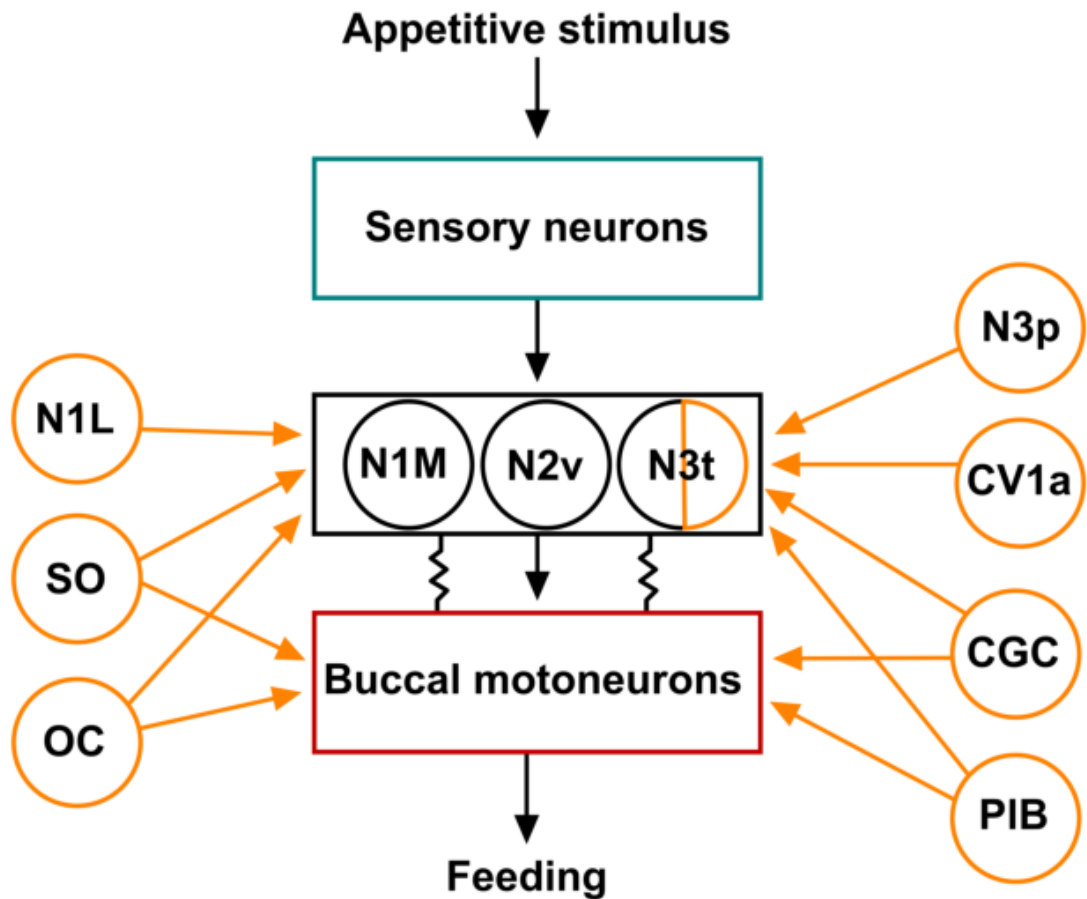


Figure 1.4. Simplified diagram summarising modulation of the feeding network in *Lymnaea*. Sensory neurons (SN) are shown in blue, modulatory neurons orange, CPG neurons black and motoneurons red.

A further classification divides modulatory neurons into two broad groups; extrinsic and intrinsic (Katz & Frost, 1996). Extrinsic neuromodulatory neurons are situated outside of the rhythm generating circuit and may not always be participating in feeding activity. Intrinsic neuromodulators are considered part of the rhythm generating circuit and thus will be contributing modulation during a particular phase of the behaviour.

Intrinsic modulation

Slow oscillator

The slow oscillator (SO) was one of the earliest identified neurons capable of initiating a feeding rhythm in *Lymnaea* (Rose & Benjamin, 1981). Despite its name, stimulation of SO can cause high frequency feeding rhythms in the isolated brain, through a facilitating excitatory connection with N1M and a biphasic connection with N2v (Elliott & Benjamin, 1985b; Brierley *et al.*, 1997). Unusually the cell only exists on one side of the buccal ganglia. Due to the ability of SO to drive strong feeding rhythms in the isolated CNS it was widely used in early studies of feeding. Later studies have used a more natural stimulus of sucrose to chemosensory structures and have shown that SO is not necessary for fictive feeding (Kemenes *et al.*, 2001).

Hybrid CPG neurons

Further examples of modulatory neurons that are considered intrinsic are the hybrid CPG neurons; N1 lateral (N1L), N3 phasic (N3p) and N3t. N1L is a protraction interneuron capable of driving fast rhythmic activity through a summing monosynaptic excitatory connection to N1M, along with electrical coupling to SO (Yeoman *et al.*, 1995). N3p is a swallow phase interneuron whose modulatory role has not been well characterised (Elliott & Benjamin, 1985a). It does not show the endogenous PIR that is seen in N3t (Straub *et al.*, 2002). N3t has been shown to play a very important modulatory role in satiety. When the animal is starved and in the quiescent state the cell fires more slowly than usual, making it more probable that N1M can become active (Staras *et al.*, 2003). The cell also shows a significant reduction in the firing frequency during the swallow phase in starved animals, increasing the probability of further feeding cycles (Crossley *et al.*, 2016).

Octopamine cells

The Octopamine cells (OC) are three swallow phase buccal interneurons, which were originally identified by staining for their neurotransmitter (Vehovszky *et al.*, 1998; Vehovszky *et al.*, 2000). Stimulation of the OC has significant long-term polycyclic effects. If the OC is activated by depolarisation beforehand, then when SO stimulation is carried out, a much higher frequency feeding rhythm is elicited (Elliott & Vehovszky,

2000). The basis of this high frequency rhythm includes heterosynaptic facilitation of the synapses of SO and N1L, and an increase in their endogenous excitability (Vehovszky & Elliott, 2002). The excitability of the motoneurons B1 and B4 is also raised and B2 lowered, which will enhance rhythmicity and buccal mass activity (Vehovszky *et al.*, 2005). Recruitment of neurons in the rhythm also changes, as the B3 motoneuron no longer participates if the OC are active (Vehovszky & Elliott, 2001). However, like many other intrinsic modulatory neurons in the isolated brain the cell is often subthreshold during sucrose driven rhythms (Vehovszky *et al.*, 2004).

Cerebral ventral 1 cells

The cerebral ventral cells are protraction phase neurons found in a small V shaped area at the entrance of the medial and superior lip nerves to the cerebral ganglion. They were originally identified due to their ability to drive feeding rhythms independently of the SO (McCrohan, 1984a). Further study has revealed multiple sub classifications of the CV1 cells. CV1a can reliably drive fictive feeding cycles through a monosynaptic connection with N1M (McCrohan & Kyriakides, 1989). However it is not necessary for sucrose driven feeding, only being active in 75% of induced rhythms (Kemenes *et al.*, 2001). CV1b can less reliably evoke fictive feeding and shows less rhythmicity (McCrohan & Kyriakides, 1989). A further sub classification of CV1b has also been carried out, based on the presence of the neuropeptide APGWamide, named the cerebral buccal white cell (CBWC) (McCrohan & Croll, 1997).

Extrinsic modulation

Cerebral giant cells

The cerebral giant cells are the most well studied modulatory neurons in *Lymnaea* with large (90µm diameter) soma located in the anterior lobes of the cerebral ganglion. They project up the cerebral buccal connective and provide the sole source of serotonin to the buccal ganglia (Straub & Benjamin, 2001). In the isolated brain, the cells fire continuously at around 0.7Hz, with one to one spikes, maintained by strong chemical and electrical synapses between the cells (McCrohan & Benjamin, 1980a; Goldschmeding *et al.*, 1981). Due to the long distance between the soma and buccal ganglia, where the synapses are located, the spikes are not perfectly synchronous, so

one cell leads and the other follows. This causes a difference in spike shape between the two, with the leader generally being more depolarised, with broader and lower amplitude action potentials.

The CGCs have a large number of excitatory, inhibitory and biphasic synapses with all types of feeding neurons, including the CPG neurons (Yeoman *et al.*, 1996), motoneurons (McCrohan & Benjamin, 1980b) and modulatory neurons (Vehovszky & Elliott, 2001). It is also possible that the CGC has effects on buccal muscle activity, similar to the metacerebral cell in *Aplysia*, but this has never been tested (Weiss *et al.*, 1978). Given the numerous connections of CGC with the network this means that the cell has a strong influence on feeding.

A detailed example of the modulatory effects of CGC is a study by Straub and Benjamin (2001) on the swallow phase motoneurons (B4, B4cl, B8). When isolated in culture, it was shown that serotonin, the main neurotransmitter of CGC, caused a prolonged depolarisation of the cells. Additionally, long-term changes in endogenous properties were found, with an increased amount of spontaneous bursting in B4/B4cl and an increase in PIR in all three motoneuron types. Furthermore, nitric oxide (NO), released consistently by an unidentified source, has been found to enhance the serotonergic synapse between CGC and B4, via a postsynaptic mechanism (Straub *et al.*, 2007).

Despite a predominance of excitatory synaptic connections formed by CGC there are also inhibitory and biphasic connections with the CPG neurons N2d and N3p, respectively (Yeoman *et al.*, 1996). The physiological basis for these effects may be due to the presynaptic corelease of the peptide myomodulin, which has been found to be present inside the CGC (Santama *et al.*, 1994). Alternatively, there are multiple types of serotonin receptor in the CNS of *Lymnaea*, which could cause differential effects in postsynaptic targets (Sugamori *et al.*, 1993; Gerhardt *et al.*, 1996). Interestingly there is evidence of a biphasic effect of serotonin on N2d and N3p in isolated cell culture, providing support for the latter explanation (Straub, 1998).

Despite most of the downstream CGC effects promoting feeding, there is a monosynaptic excitatory connection with N3t which in turn has a strong inhibitory

output (Yeoman *et al.*, 1996). At very high CGC firing frequencies this N3t pathway dominates and rapidly inhibits ongoing feeding. This makes it especially important to understand what the physiologically relevant firing rate of CGC is, to understand its normal modulatory role. Fine wire recordings of CGC *in vivo* were crucial in showing that the cell fires much more slowly in the intact animal compared to the isolated brain (Yeoman *et al.*, 1994). Even during natural feeding, CGC activity peaks at around 0.25Hz, compared to 0.7Hz *in vitro*. When the CGC was artificially controlled to fire at the normal physiological rate *in vitro* this does not stimulate fictive feeding. However, it is necessary for some spiking activity in CGC for an SO driven feeding rhythm to occur. Therefore, the cell plays a permissive (gating) role in the behaviour. In addition, a further rise in firing frequency within the physiological range, increases the frequency of SO elicited fictive feeding cycles. Therefore, the CGC plays a dual modulatory role in the intact snail, being both permissive and influencing the frequency of the rhythm. The influence of the CGC on N3t, is thought to be largely negligible to overall feeding output, within the physiological firing range of CGC (Yeoman *et al.*, 1996).

Pleural-Buccal interneuron

The pleural-buccal interneuron (PIB) was identified by its peptidergic neurotransmitter FMRFamide and is the only known example of direct inhibition of the feeding system from outside the CPG (Alania & Sakharov, 2000; Alania *et al.*, 2004). The cell has a relatively small soma (25µm), with a long ranging primary axon that branches extensively in both the cerebral and buccal ganglia. In the isolated brain PIB fires spontaneously at relatively high rates of around 4 Hz. Like the CGC, PIB synapses with its contralateral counterpart in the buccal ganglia. Also, similar to CGC, the cell has connections with all types of neurons in the feeding system. Most of the inhibitory connections between PIB and CPG neurons, motoneurons and modulatory neurons persist in HiDi, suggesting they are monosynaptic.

1.7.2.3 Plasticity

Tactile appetitive conditioning

Once long-term memories have been formed, multiple neurophysiological correlates have been identified in the brain.

B3 tactile response

In the CS response pathway, it has been shown that the B3 motoneuron has an EPSP of increased amplitude after conditioning of intact animals (Staras *et al.*, 1999a). The size of this EPSP has been shown to correlate with the strength of the fictive feeding response. The functional significance of this enhanced EPSP is unknown as B3 is not known to modulate feeding rhythms and is not electrically coupled to the CPG. It may indicate an enhanced CS response in other cells such as N1m which are crucial for rhythm generation and are known to respond to touch. If tentacle touch (CS) and sucrose (US) are paired, the B3 EPSP remains unchanged, despite a conditioned fictive feeding response. This demonstrates that different conditioning paradigms can result in different cellular correlates of memory (Jones *et al.*, 2001).

CV1a persistent depolarisation

In addition to synaptic enhancements, an important nonsynaptic mechanism for tactile appetitive memory has been identified. In unconditioned animals, CV1a responds to lip touch with a small depolarisation that does not reach threshold (Staras *et al.*, 1999b). Following tactile appetitive conditioning it was found by Jones *et al.* (2003) that lip touch does cause CV1a to reach threshold and remain active. Underlying this was a 11 mV depolarisation of the resting membrane potential of CV1a, that was concomitant with the expression of the memory. Despite this, there was no significant change in spike threshold, input resistance or spike frequency. There was also no change in the ability of CV1a to drive cycles when activated by current injection, indicating unchanged output synapses in the buccal ganglia. Therefore, when the CS was applied after conditioning CV1a was much more likely to reach threshold and begin firing, driving a fictive feeding response. Further experiments in the same study also showed that depolarisation of the CV1a resting potential was both sufficient and necessary for conditioned feeding in response to lip touch. In contrast, artificial depolarisation of CV1a did not cause fictive feeding in response to tentacle touch, demonstrating the stimulus specificity of this nonsynaptic plasticity.

Chemical appetitive conditioning

Chemical appetitive conditioning is a well-studied form of learning in *Lymnaea*. One important reason for this, is that it is possible to evoke a memory, detectable for several weeks, with a single pairing of a neutral chemical (CS) and food (US) (Alexander *et al.*, 1984). This has allowed detailed temporal analysis of memory consolidation.

N3t reduced firing frequency

In addition to a reduction in background activity following starvation, the CPG neuron N3t has also been found to have a further reduction in spontaneous firing frequency 1, 2, 3 and 4 hours after *in vitro* conditioning (Marra *et al.*, 2010). Similar to the starved animal this directly reduces inhibition on N1M making it much more likely for a feeding rhythm to be generated in response to the CS. This was supported by an observed negative correlation between the firing frequency of N3t and the strength of the conditioned feeding response.

CV1a CS response

Following formation of long-term memory Straub *et al.* (2004) recorded the lip/tentacle nerves and the cerebral-buccal connective (CBC) of semi-intact preparations, during CS application to the lips. This revealed no change in the response activity of the lip nerves, but a significant increase in CBC response activity. This suggested that there was an increase in the CS response activity of cerebral-buccal interneurons (CBIs) but not chemosensory fibres. Therefore, long-term plasticity must occur in the cerebral ganglia rather than in the periphery. This theory is supported by an early study using multi-trial conditioning, which provided a qualitative observation of CV1a depolarisation in response to CS application to the lips of trained preparations (Whelan & McCrohan, 1996). A quantitative analysis in a later study, using single trial training, also found a transient CS-induced depolarisation in CV1a, which precedes rhythm generation (Kemenes *et al.*, 2002).

CGC persistent depolarisation

Given that CV1a shows an enhanced CS response >24hr following tactile conditioning this suggested the existence of a similar mechanism of presynaptic facilitation after chemical conditioning, also within the cerebral ganglion. Recordings by Kemenes *et al.*

(2006) have revealed this mechanism to be a significant depolarisation of the CGC resting membrane potential, which emerges 16-24hr post conditioning and lasts for as long as the memory is detected. The same study found no significant change in CV1a resting membrane potential following chemical appetitive conditioning.

Persistent depolarisation of CGC increases baseline intracellular calcium concentrations, enhancing exocytosis and therefore increasing serotonin release (Awatramani *et al.*, 2005). This was observed by Kemenes *et al.* (2006) in cell culture as an enhanced EPSP between CGC and a nearby B1 motoneuron, when CGC is depolarised. In non-conditioned semi-intact preparations, a similar depolarisation of CGC, results in an increased CS response in both the CBC and motor output, identical to that seen in the conditioned response. This suggests that CGC depolarisation by 10 mV is sufficient for the expression of a conditioned feeding response.

Significantly, the depolarisation remains confined to the cerebral ganglia, affecting primarily the soma and axonal side branch of the CGC (Nikitin *et al.*, 2013). There is also no change in action potential shape or frequency (Kemenes *et al.*, 2006). This means that the CGC enhances its output proximally, within the cerebral ganglia (presynaptic to CBIs), without changing the modulatory effects in the distant buccal ganglia, where the CPG and motoneurons are located. It has not been directly tested whether depolarisation of CGC is necessary for conditioned feeding, as hyperpolarisation will not spread as readily as depolarisation down the axonal side branch (Kemenes *et al.*, 2006). Many other studies have also recorded persistent depolarisation of CGC following conditioning, with increases in membrane potential ranging from 2.5 to 10 mV (Nikitin *et al.*, 2008; Nikitin *et al.*, 2013; Ford *et al.*, 2015; Ford *et al.*, 2017; Crossley *et al.*, 2019).

All of the neuronal plasticity described above, for both types of classical conditioning of *Lymnaea*, are summarised in **Figure 1.5**.

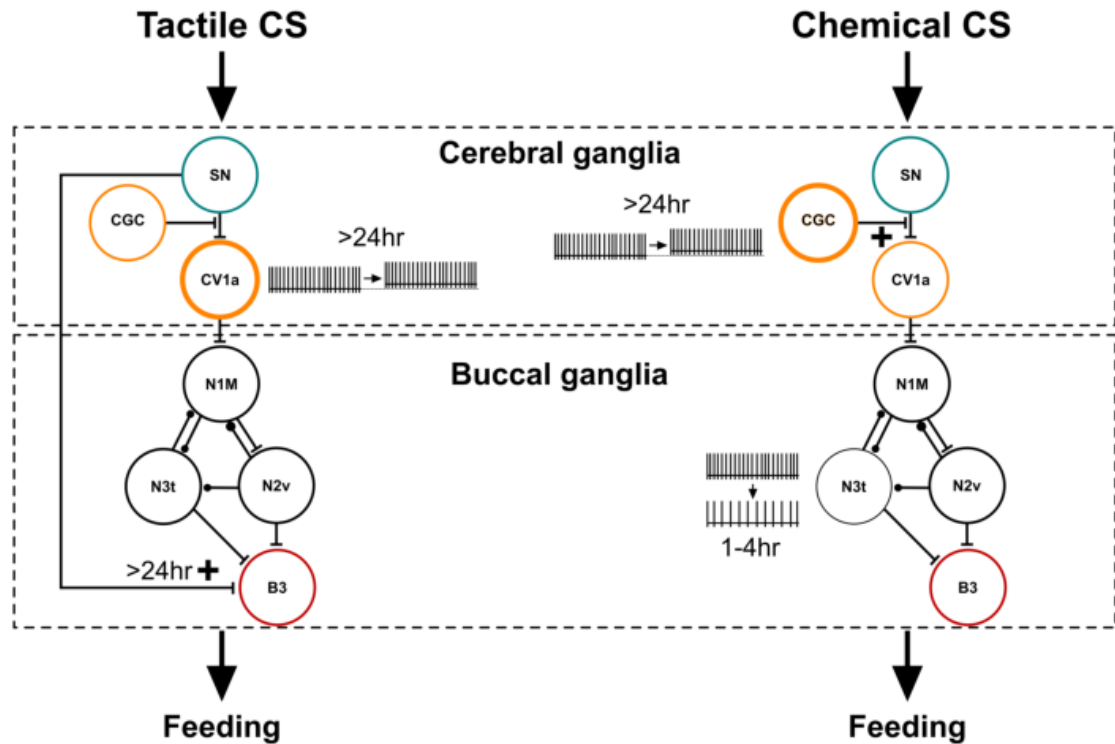


Figure 1.5. Network diagram summarising the synaptic and nonsynaptic changes that have been found at different time points following appetitive conditioning in *Lymnaea*. Sensory neurons (SN) are shown in blue, modulatory neurons orange, CPG neurons black and motoneurons red. Changes in cell membrane thickness indicate nonsynaptic changes. Strengthening of synapses is indicated by a plus symbol. Excitatory synapses are shown by bars and inhibitory synapses by dots. For clarity, some synapses have been omitted.

1.8. Conceptual gaps in the current understanding of chemical appetitive conditioning in *Lymnaea*

1.8.1. The ionic conductances responsible for nonsynaptic plasticity in CGC during LTM are theorised but not fully tested

As explained above the CGC develops a persistent depolarisation, following chemical appetitive conditioning of *Lymnaea*, that shows sufficiency for the conditioned feeding response (Kemenes *et al.*, 2006). However, the full ionic basis for this nonsynaptic

plasticity is currently unknown. Using voltage clamp and antibody staining Nikitin *et al.* (2008) have shown that there is an increase in the amount of persistent sodium current. Based on this voltage clamp data, alongside that of Staras *et al.* (2002), this has allowed the construction of a biophysical model of the CGC by Vavoulis *et al.* (2010). This model predicts that an increase in the persistent sodium current, delayed rectifier potassium current and high-voltage activated calcium current are necessary for the observed changes in endogenous CGC properties following chemical appetitive conditioning. However, this hypothesis remains to be tested in a living CGC, and thus will be the focus of the work described in chapter 3.

1.8.2. The monosynaptic connections of the lip and tentacle chemosensory neurons are uncharacterised

One of the biggest weaknesses of *Lymnaea* as a model system for understanding chemical appetitive conditioning, is that little is known about the chemosensory pathways of the lips and tentacles. This has made the understanding of the CS and US pathways very difficult. The reason for this is that the cell bodies of the lip/tentacle chemosensory neurons are located in the periphery, rather than the central nervous system, effectively preventing intracellular recording (Straub *et al.*, 2004). The issue is also further complicated by the fact that there are three nerves responsible for delivery of chemosensory information; the median lip nerve (MLN), the superior lip nerve (SLN) and the tentacle nerve (TN). As such, the only way to examine chemosensory input has been to make extracellular electrophysiological recordings from these three nerves (Straub *et al.*, 2004). While these nerve recordings have indicated no change in overall spiking activity in response to the CS, following conditioning, this does not discount possible endogenous changes in the chemosensory neurons, such as broadening of the action potential.

Given that the presynaptic neuron of the plastic synapse involved in chemical appetitive conditioning cannot be individually recorded, it has been difficult to identify clear direct monosynaptic targets of the CS/US pathways. For example, the CGC has been found to reliably become activated by sucrose (US), but it is unknown if this is a monosynaptic excitation from the chemosensory neurons or a polysynaptic pathway

(Kemenes *et al.*, 1986). Furthermore, no direct connections between chemosensory fibres of the lips/tentacles and the feeding CPG/motor neurons of the buccal ganglia have been characterised. Currently the best identified candidate for a monosynaptic chemosensory postsynaptic target is CV1a, which has been found to depolarise in response to the CS prior to rhythm generation, > 24 hours after chemical appetitive conditioning (Kemenes *et al.*, 2002; Kemenes *et al.*, 2006).

The lack of understanding of the CS pathway has made it difficult to decipher how stimulus specificity is achieved by the conditioned reflex. It has been found that the CGC will become persistently depolarised in LTM following training for either amyl acetate or gamma-nonalactone (Crossley *et al.*, 2019). How this nonsynaptic change can appear identical for either chemical CS, whilst preserving input specificity is unknown. One possibility is that the increased serotonin release in the cerebral ventral area by CGC, somehow preferentially activates presynaptic fibres of a particular CS pattern. A search for possible CS and US postsynaptic targets will be carried out in chapter 4.

1.8.3. The neural basis for memory lapses in *Lymnaea* is unknown

Single trial chemical appetitive conditioning has allowed for a detailed study of the temporal profile of memory consolidation in *Lymnaea* (summary shown in **Figure 1.6**). Marra *et al.* (2013) have also confirmed that the expression of memory is not always continuous during consolidation. Under normal circumstances, chemical appetitive conditioning uses a sucrose (US) concentration that is relatively high. However, it is still possible to condition the animals when 1/10 of this sucrose concentration is used. When this so called sub-optimal training is carried out memory can be detected at the 10 min, 1 hr, 2 hr, 4hr time points *in vivo*, but not at 30 minutes and 2 hours. Similarly, if the standard sucrose concentration (0.67 %) is used, but the conditioning is *in vitro* then this also causes lapses in memory recall at 30 minutes and 2 hours. Therefore, it appears that sub-optimal training reveals moments in consolidation when the memory trace is too weak to be detectable. The molecular basis for this weakness appears to be times of transition between the phases of memory consolidation (Marra *et al.*,

2013). The first lapse at 30 minutes coincides with the transition between STM and ITM. The second lapse at 2 hours, which is within ITM, suggests the existence of an early ITM and a late ITM. Indeed, further pharmacological blocking experiments in the same study have shown that early ITM and late ITM can be distinguished by a reliance on protein kinase M (PKM)/protein kinase C (PKC) together and PKM alone, respectively.

So far only the motor output for the *Lymnaea* CNS has been tested during memory lapses, so it is unknown what the upstream neural basis of this phenomenon is (Marra *et al.*, 2013). This question will be explored in chapter four. It seems plausible that the as yet unidentified cells involved in consolidation of strong memories in STM and ITM are the same as those for weak memories.

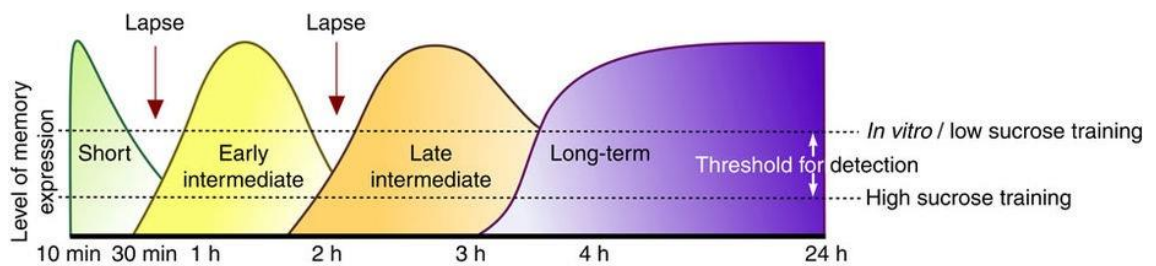


Figure 1.6. Diagram summarising the different phases of appetitive memory consolidation.

Adapted from Marra *et al.* (2013).

1.8.4. Presynaptic control of modulatory projection neurons is largely unexplored

Although modulatory neurons that project to the feeding system, such as CGC, CV1a and PIB, have been closely studied for their output effects, relatively little is known about their upstream control. As discussed earlier, it has not been possible to directly record chemosensory neurons that are theorised to be presynaptic to CV1a and CGC. The only unequivocal example of a modulatory projection neuron under presynaptic control is in the work of Pirger *et al.* (2014), who have shown that there is an asymmetric monosynaptic connection between the withdrawal system and the feeding system. More specifically, they have shown that the withdrawal neuron, pedal dorsal

12 (PeD12), has a monosynaptic excitatory connection with the PIB, such that an aversive touch will immediately shut down a feeding rhythm through the latter cell's extensive modulatory effects. This activation of PIB has been shown to be both sufficient and necessary for the cessation of feeding during withdrawal. Such presynaptic mechanisms of modulatory feeding control will be examined in chapter 5.

1.9. Thesis outline

As described above, modulation plays a very important role in feeding behaviour in *Lymnaea* and consequently the storage of appetitive memories. This thesis will focus on the control of identified modulatory neurons and how they represent appetitive memories at different time points following conditioning.

Previous work has demonstrated important nonsynaptic changes in the CGC that emerge during LTM. The first results chapter in this thesis will examine the biophysical basis of these changes, by testing whether they can be reproduced in untrained *Lymnaea*, via insertion of artificial channel conductances, using dynamic clamp. This is a very useful technique, as it allows the testing of a theoretical mathematical model directly on a living cell using simulated conductances. The ultimate aim will be to simulate the natural depolarised state of CGC during LTM, in order to revisit its effects on the conditioned feeding response and stimulus specificity. A second more simple electrophysiological technique, pattern clamp will also be applied, as this is useful for precise manipulation of cellular activity.

The second chapter will focus on the recently reported memory lapses that are found in *Lymnaea*, following sub-optimal single-trial conditioning. The neural basis of these lapses could be due to a reduction in the activity of an excitatory neuron, or an increase in activity of an inhibitory neuron. Therefore, both the CGC and the PIB neurons will be tested for nonsynaptic and synaptic plasticity at lapse and non-lapse time points, following sub-optimal training. This requires the use of semi-intact preparations, which allow for the intracellular recording of key identified modulatory neurons, whilst applying different chemosensory stimuli to the lips.

The final chapter involves identification of a new interneuron in the CNS of *Lymnaea*, termed parietal dorsal 4 (PD4). The morphology of this neuron will be determined using intracellular injection of fluorescent dyes and confocal imaging. Using intracellular recordings, connections with other cells of the feeding system will be examined, and their ability to elicit feeding will be tested in the isolated brain to limit movement. Utilising semi-intact preparations, PD4 will also be tested for a possible role in the acquisition of associative memory, by examining its response to sucrose (US) application to the lips. Lastly, in order to identify possible sensory inputs to PD4, the response of the neuron to the extracellular stimulation of different nerves will be examined.

Chapter 2: General Methods

2.1. Animal Maintenance

All data were collected from 4-5 month old *Lymnaea stagnalis* bred and housed at the University of Sussex and maintained by specialist technicians. Snails were kept in heated rooms (25 °C) in large holding tanks containing copper free water, in a 12/12 hr light/dark cycle. The animals were fed organic lettuce (Park Farm Shop, Falmer) three times a week, and TetraPhyll fish food (TETRA Werke) twice a week. In all cases where snails were conditioned or their sucrose (US) response tested the animals were isolated and food-deprived for 3 days prior to experimentation, in a heated room on an identical light/dark cycle.

2.2. Electrophysiological Preparations

Once collected from the animal unit, snails were transported in a small tub of copper free water to the electrophysiology laboratory. Dissection was initiated by removal of the shell using scissors, followed by a large cut below the mantle and across the body, removing the majority of the internal organs. The body was then placed in a small Sylgard dish filled with normal saline (NS). NS consisted of 50 mM NaCl, 1.6 mM KCl, 2.0 mM MgCl₂·6H₂O, 3.5 mM CaCl₂·2H₂O and 10 mM HEPES in reverse osmosis water at a PH of 7.9 reached using NaOH (Sigma-Aldrich). The Sylgard dish was then placed under a dissecting microscope and lit using a Schott KL 1500 cold light source. An incision was then made along the remaining anterior midline to the front of the animal using fine *Vannas* scissors. This forms skin flaps which can be pinned to either side of the animal, exposing the CNS, buccal mass and penis. A pin was also placed in the back of the foot to keep the animal fixed in position. The nerves between the buccal mass/penis and the CNS were then severed, allowing these two structures to be removed. This left only the CNS and its connections with the foot. If sensory stimuli were going to be applied then some of these connections were kept, forming a semi-intact preparation (see **Figure 2.1A/B**). If no sensory stimuli were going to be used then all connections were severed and the brain was completely isolated from the

periphery (see **Figure 2.1C/D**). For further details of different preparation types see individual chapter methods.

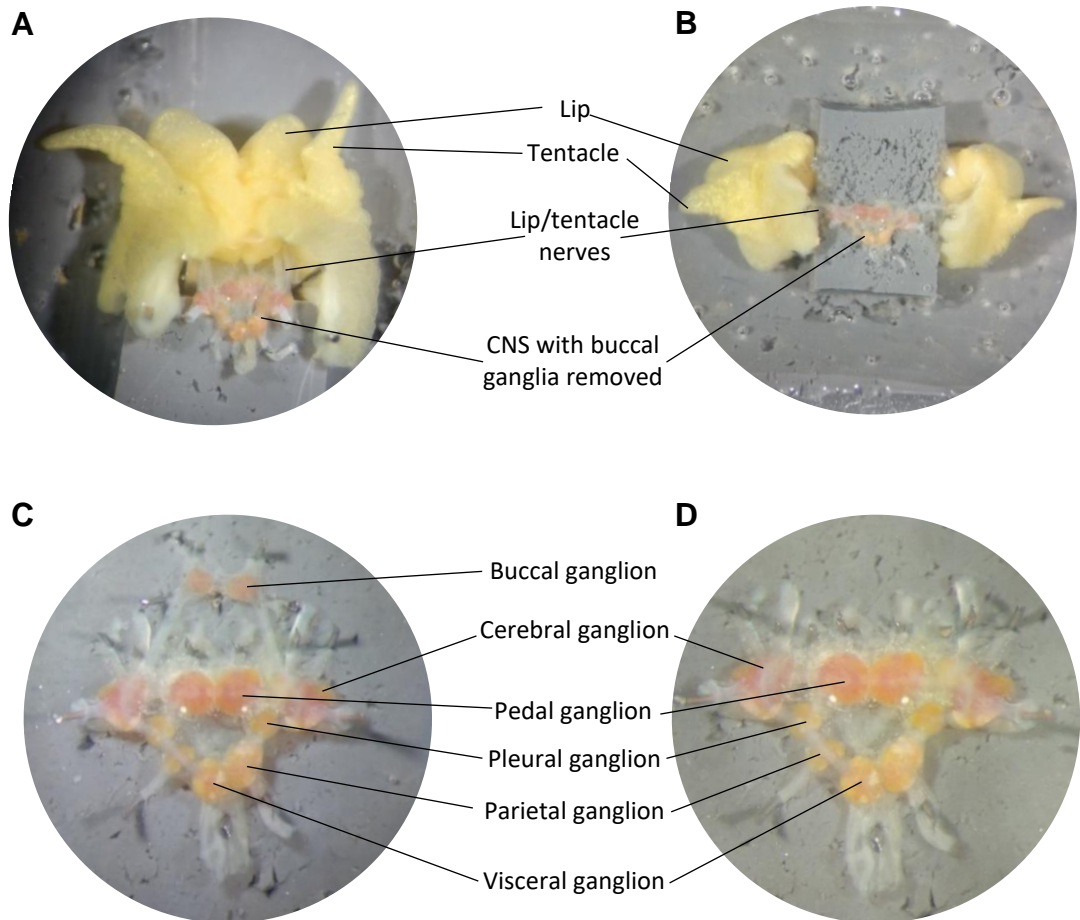


Figure 2.1. Preparations used for electrophysiology. A. Whole lip semi-intact preparation with the buccal ganglia removed. **B.** Split lip semi-intact preparation with the buccal ganglia removed. **C.** Isolated whole CNS preparation with all ganglia intact. **D.** CNS preparation with the buccal ganglia removed. The semi-intact preparations allowed stable recording of neurons whilst applying chemical and tactile stimuli. Removal of the buccal ganglia axotomised modulatory projection neurons and eliminated rhythmic feedback from the feeding CPG.

Once the dissection was finished and the preparation was stably pinned, the outer sheath surrounding the brain was removed using fine forceps. The inner sheath was then softened via the addition of type XIV protease crystals to the areas of interest. After one minute, the protease was removed by washing the preparation repeatedly with fresh NS. The dish was then moved to the recording setup.

2.3. Intracellular recording

The basic recording setup consisted of four Huxley micromanipulators placed on top of a recording table in a circle facing inwards. Each micromanipulator held a headstage preamplifier which was connected to either an Axoclamp 2B amplifier (Axon instruments) or a Neurolog NL 102 amplifier (Digitimer). Each amplifier was then connected to a Micro 1401-3 (additional ADC12 expansion, CED) analog-to-digital converter (ADC). Specifically, for headstage 2 (ME2) of the Axoclamp 2B, a 10x gain amplifier was situated between the amplifier and ADC to reduce noise. Measurement of current flow for each electrode was also passed to the ADC. The ADC then fed these signals to the PC via a USB cable.

The signal sent to the computer from each headstage, was the potential difference (mV) between the glass microelectrode and an inert reference electrode. The glass electrodes were formed from filamented borosillate glass capillaries (1.5 mm OD, 1.17 mm ID, 75 mm length, Biochrom) pulled using a P97 Flaming/Brown Micropipette Puller (Sutter Instrument) and filled with 4 M potassium acetate solution. The tip of each micropipette was dipped in T25 permanent black ink (Edding) to ensure visibility in the recording chamber. Once fixed in the headstage, placed in the bath and adjusted to 0 mV, these microelectrodes usually gave a resistance of 15-40 M Ω or were discarded otherwise.

Once a neuron of interest was identified, normally by its position, then it was impaled using a microelectrode. This was achieved using both mechanical pressure from the micromanipulators and overcompensation of capacitance in the circuit ('buzz'). Using this technique, it was possible to record from up to four neurons at once. A summary diagram of the recording setup is shown in **Figure 2.2**.

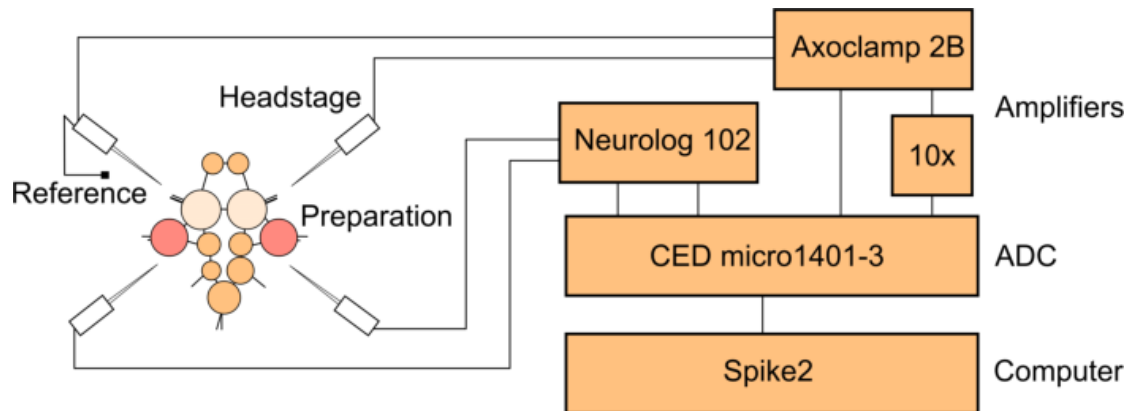


Figure 2.2. Schematic diagram of the basic setup for intracellular recordings. The preparation was placed in normal saline and pinned out in the Sylgard recording chamber. Up to four headstages, situated in Huxley manipulators, were connected to amplifiers and used to place microelectrodes into target cells. From the amplifiers the electrical signal was fed to an analogue to digital converter (ADC). The ADC was connected to a computer via a USB cable. The computer displayed and recorded electrophysiological activity detected by the 4 microelectrodes using Spike2 software.

2.4. Recording and data processing software

All electrophysiological recordings were made on a Precision T1700 compact desktop computer (Dell) using the program Spike2 (version 5.21, Cambridge Electronic Design) running on the Windows 7 operating system (Microsoft). Each voltage channel was sampled at 2 KHz and each current channel at 250 Hz. Both sampling and analysis were controlled by custom written scripts within Spike2, based on in built functions. For detailed analysis methods see individual chapters. Raw data was often transferred to Excel (versions 2013, 2016, Microsoft) or MATLAB (versions 2013-2017, Mathworks) before statistical analysis. Figures were created using Xara designer Pro (Version 7.1, Xara).

2.5. Statistical analysis of data

Graphs and statistical analysis were generated using GraphPad Prism (version 6, GraphPad software). Each sample in a data set was from a different snail to prevent nested data, unless otherwise stated. All charts and text report the mean of an experimental group \pm standard error of the mean (SEM). The distribution for

sufficiently large data sets was assessed using the D'Agostino and Pearson omnibus normality test and if normal a parametric analysis was used. Otherwise a non-parametric analysis was used. For statistical comparisons of two groups a paired t test was used. For statistical comparisons of more than two groups either an ANOVA followed by Dunnett's test or Kruskal-Wallis followed by Dunn's test was used. The significance level was set at $p < 0.05$. In cases where there were multiple comparisons, a Bonferroni correction was used to reduce type I errors. If the p value was below 0.05 it was reported with a comparison to the adjusted significance level (e.g. $p = 0.006 < 0.01$), according to the Bonferroni method. Statistical power was assessed *a priori* using G*Power (version 3.1) software (Faul *et al.*, 2007). Cohen's effect size was assumed to be large in all cases and statistical power was set at 0.8. For the two-way repeated measures ANOVA test used in chapter 3 it was found that a group sample size of at least 6 was necessary. For the paired t tests used in the chapter 3 pattern clamp section, a sample size of 8 was needed. The *in vivo* sub-optimal conditioning experiments described in chapter four required a sample size of 18 per group of animals for a one-way ANOVA. The Kruskal-Wallis test used to assess background firing frequency of CGC/PIB after sub-optimal conditioning required a group size of 20. The Wilcoxon matched pairs signed rank test used throughout chapter 4 requires a total sample size of 15 for sufficient statistical power.

Chapter 3: Electrophysiological basis for nonsynaptic plasticity in a key modulatory neuron of the feeding system

3.1. Introduction

A single pairing of a neutral chemical stimulus (CS) and an appetitive chemical stimulus (US) in the aquatic environment of *Lymnaea* is sufficient to elicit a long-term memory (LTM) that can be detected for weeks (Alexander *et al.*, 1984). This increase in CS-evoked feeding activity, following classical conditioning, is caused by plasticity in the CNS of *Lymnaea*, particularly in the cerebral ganglion (Straub *et al.*, 2004).

One important site of change is in the cerebral giant cell (CGC), where a persistent depolarisation of the cell membrane has been observed 16-24 hr and onwards, following classical conditioning (Kemenes *et al.*, 2006; Nikitin *et al.*, 2008; Nikitin *et al.*, 2013; Ford *et al.*, 2015; Ford *et al.*, 2017; Crossley *et al.*, 2019). This depolarisation ranges from 2.5-10 mV and persists indefinitely, for as long as the memory is detected.

The depolarisation measured at the CGC soma only spreads a short distance but includes an axonal side branch projecting to the area of CBI neurons within the cerebral ganglion (Kemenes *et al.*, 2006). Along this depolarised portion of membrane there is increased calcium entry and therefore increased exocytosis of serotonin. This causes presynaptic facilitation of the cerebral-buccal interneurons (CBIs) response to the CS, thus resulting in feeding. Interestingly this compartmentalised nonsynaptic plasticity acts to preserve the normal modulatory effects of CGC on the distant buccal ganglia, but increases serotonin release presynaptic to the CBIs (Nikitin *et al.*, 2013).

Despite the change in resting membrane potential (RMP) no change has been found in the firing frequency, spike characteristics or membrane resistance of the CGC. To understand the electrophysiological basis for these observations a mathematical model of the neuron was created by Vavoulis *et al.* (2010), based on fitting to previous voltage clamp and current clamp data (Staras *et al.*, 2002; Nikitin *et al.*, 2006). This

previous data including analysis of the kinetics and pharmacology of many of the different ion channels in CGC. Initially the two electrode voltage clamp data was used to estimate approximately half of the Hodgkin-Huxley model parameters and then fitting to current clamp data was used to estimate the remaining parameters (Vavoulis *et al.*, 2010). The effect of previously used modified salines and pharmacological blockers were also simulated to confirm that the model had a similar response to the real neuron. The final model included a total of 6 voltage-gated conductances: a transient sodium current (I_{NaT}), a persistent sodium current (I_{NaP}), a transient potassium current (I_A), a delayed rectifier potassium current (I_K), a low-voltage-activated calcium current (I_{LVA}) and a high-voltage-activated calcium current (I_{HVA}). These conductances together give a simulated cell with a spontaneous firing frequency of 0.7 Hz.

Using this model a prediction was made by Vavoulis *et al.* (2010) for the change in the voltage-gated conductances necessary for the observed nonsynaptic plasticity. Specifically, an increased maximum conductance (g_{max}) by 50% of I_{NaP} and 50% of I_K is predicted to give a depolarisation of 3.1 mV, without changing spike frequency (Vavoulis *et al.*, 2010). An increase of 20% g_{max} of I_{HVA} was also predicted to be necessary, to reduce change in the spike halfwidth and spike amplitude.

These predictions were tested here using dynamic clamp, a technique that was originally developed simultaneously by Robinson and Kawai (1993) and Sharp *et al.* (1993), which allows the experimenter to introduce artificial conductances in a living neuron. These artificial conductances can model either synapses or ion channels. In this case the model ion channels I_{NaP} , I_K and I_{HVA} as defined by Vavoulis *et al.* (2010) will be used. Similar manipulation of ionic conductances to examine the electrophysiological activity has been used in the *Aplysia* R20 neuron (Ma & Koester, 1996).

The overall aim of this chapter was to examine the ionic basis for nonsynaptic plasticity in *Lymnaea* and if possible to simulate a conditioned (persistently depolarised) state in CGC, in order to confirm that is indeed sufficient for the conditioned feeding response (Kemenes *et al.*, 2006)

3.2. Methods

3.2.1. Preparation

The brain was completely isolated from the periphery by severing all nerves. Once transferred to the recording chamber, the CNS was laid flat, dorsal surface facing up, with the cerebral commissure severed. In all recordings, except when stated, the buccal ganglia were removed and pins were placed in the cerebral-buccal connective, close to the cerebral ganglion, as in Staras *et al.* (2002). This axotomises the CGC and removes the connection with the contralateral CGC, preventing synchronised activity (McCrohan & Benjamin, 1980a; Goldschmeding *et al.*, 1981).

3.2.2. Cell surface estimation

The model conductances given by Vavoulis *et al.* (2010) provide g_{\max} per unit area. Therefore, the surface area of the CGC was important in determining the overall amount of current injection. Initially the cell was assumed to be a perfect sphere and the visual radius of the cell was used to calculate the surface area (S):

$$S = 4\pi r^2$$

If the radius is assumed to be 50 μm then this gives a surface area of $3.14 \times 10^{-4} \text{ cm}^2$. This results in a total g_{\max} of 138 nS for I_{NaP} , 376 nS for I_{K} and 323 nS for I_{HVA} . Vavoulis *et al.* (2010) predict g_{\max} increases of 50% in I_{NaP} , 50% in I_{K} and 20% in I_{HVA} are necessary for persistent depolarisation. Therefore, the injected artificial conductances used a g_{\max} of 69 nS for I_{NaP} (50%), 188 nS for I_{K} (50%) and 64 nS for I_{HVA} (20%), in addition to what naturally occurs in the cell.

Assuming the CGC to be adequately described as a sphere turned out to be an oversimplification. Therefore it was necessary to calculate the surface area using the total capacitance of the membrane (Lindau & Neher, 1988). To determine total capacitance the cell was first hyperpolarised to prevent it from firing action potentials at the beginning of each recording. Repeated sine wave currents of 1 nA amplitude, with frequencies ranging from 5-9.5 Hz (0.5 Hz intervals), were then injected into the cell, each with a 3 s duration. Based on the response of the cell the total capacitance could be calculated:

$$C = \frac{I}{2 \times \pi \times A} \times \sin \phi \times \frac{1}{f}$$

where I is the current injection amplitude (baseline to peak), A is the maximum voltage change (baseline to peak), ϕ is the phase difference between injected current and voltage response in radians, and f is the frequency of the driving signal (current). These measurements are shown in **Figure 3.1**. The total capacitance was then averaged over all sine wave injections in each individual cell. Assuming a specific membrane capacitance of $1 \mu\text{F}/\text{cm}^2$, as in Vavoulis *et al.* (2010), it is possible to calculate the total surface area of the cell. Once the total surface area was known, the g_{max} for each of the three conductances was scaled up to a unique value for each cell, and dynamic clamp was carried out.

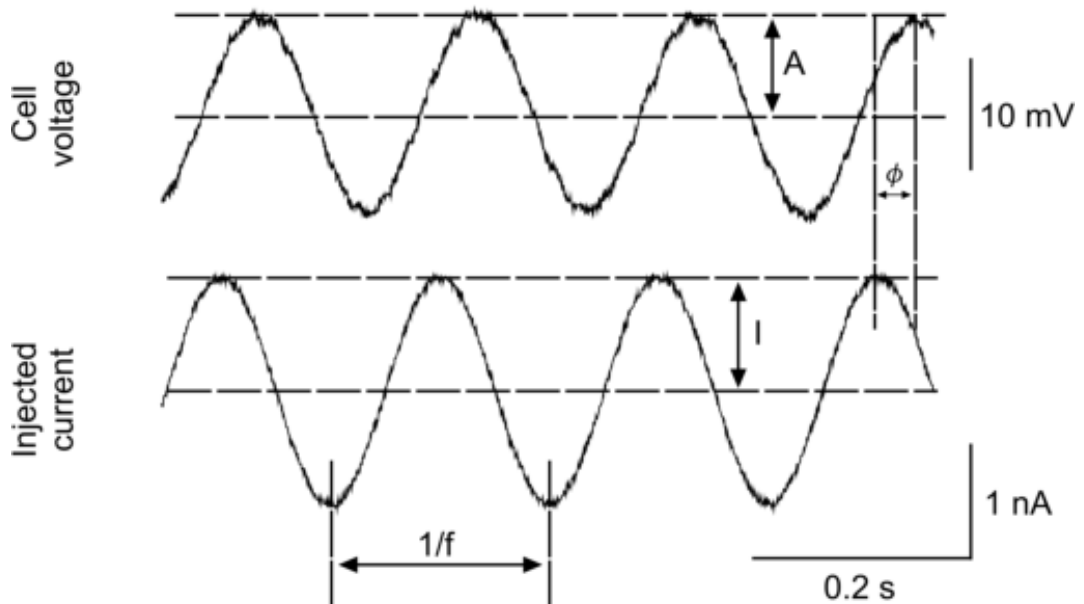


Figure 3.1. An example recording showing the response of the cell voltage to the injection of a sine wave current. From this data, the injection cycle period ($1/f$), the amplitude of each sine wave (current and voltage) and the phase difference between the waves can be measured.

3.2.3. Insertion of artificial conductances using dynamic clamp

Due to the large size of the CGC soma it was possible to impale with two electrodes, one for voltage recording and one for current injection. An additional ADC (BNC-2110, National Instruments) connected to another non-recording computer was used to

carry out the dynamic clamp. The National Instruments ADC received voltage signals from headstage 1 (ME1) of the Axoclamp2B. Once the computer had calculated the appropriate current injection, a command was sent from the ADC to a 10x gain headstage 2 (ME2), attached to the Axoclamp 2B. Calculating current injection based on measured voltage is the basis for the dynamic clamp, and is illustrated in **Figure 3.2**, along with an overview of the setup

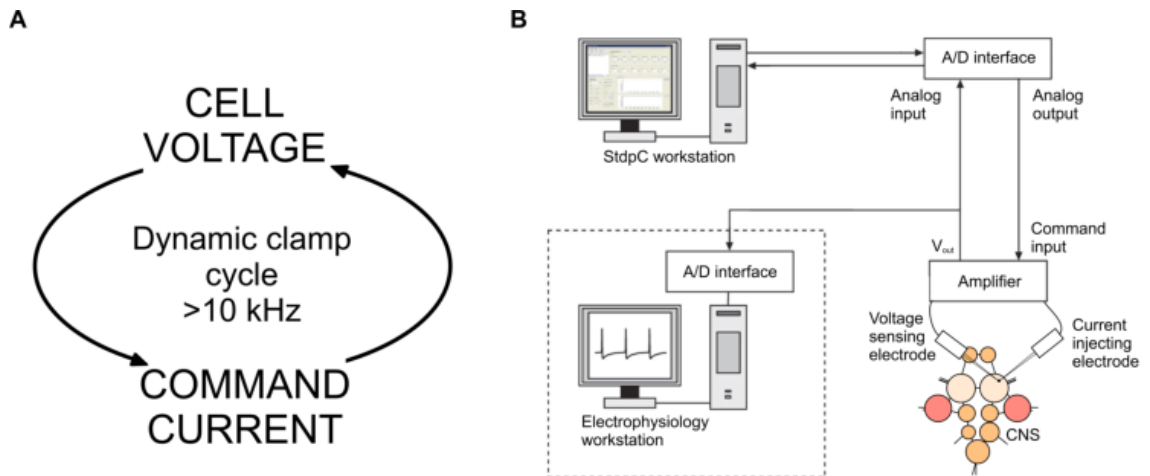


Figure 3.2. Overview of the dynamic clamp. A. The technique can be thought of as a continuous cycle of voltage measurement determining current injection, which acts back on the membrane at high frequency. **B.** A simplified diagram showing the major components of the recording setup, note the use of two computers and two ADCs. Adapted from Kemenes *et al.* (2011).

Calculation on the non-recording computer were carried out by the program StdpC (custom version) running on Windows 7 (Nowotny *et al.*, 2006; Kemenes *et al.*, 2011). Each artificial current used (I_{NaP} , I_K , I_{HVA}) was modelled as in Vavoulis *et al.* (2010):

$$I_{NaP} = g_{NaP} \times r^3 \times (V - E_{Na})$$

$$I_D = g_D \times n^4 \times (V - E_K)$$

$$I_{HVA} = g_{HVA} \times e^3 \times f \times (V - E_{Ca})$$

where g is maximum conductance and E is the reversal potential specific to each ion channel ($E_{Na} = 55$ mV, $E_K = -90$ mV, $E_{Ca} = 80$ mV). V is the membrane potential

measured at that moment in time. The dynamic variables r , n , e (activation) and f (inactivation) obey first order kinetics:

$$\frac{dx}{dt} = \frac{x_{\infty} - x}{\tau_x}$$

where x represents the dynamic variable (i.e. r , n , e , f). Both the steady state of the dynamic variable (x_{∞}) and time scale (τ_x) are dependent on the voltage through sigmoid functions:

$$x_{\infty} = \left(1 + \exp\left(\frac{V_H^x - V}{V_S^x}\right) \right)^{-1}$$

$$\tau_x = \tau_0^x \times \exp\left(\delta^x \frac{V_H^x - V}{V_S^x}\right) \times \left(1 + \exp\left(\frac{V_H^x - V}{V_S^x}\right) \right)^{-1} + \tau_{\min}$$

where V_H^x is the mid-point for the sigmoid (in)activation function for dynamic variable x , and V_S^x is the inverse slope of the (in)activation function (positive if activation, negative if inactivation). τ_0^x sets the overall scale (the maximal) time scale. A minimum tau of $\tau_{\min} = 0.001$ ms, not present in the original model, was added to reduce current instability.

3.2.4. Collection and analysis of dynamic clamp data

Once the the CGC was impaled and the artificial conductances were appropriately set up, then both +50% $g_{\max} I_{\text{NaP}}$ and I_K were injected into the cell through headstage 2 for 100 s. The cell was then permitted to rest for 100 s before injection of +50% $g_{\max} I_{\text{NaP}}$, I_K , +20% $g_{\max} I_{\text{HVA}}$ for another 100 s. Provided that the recording remained stable for both electrodes during this time, the data was used for analysis.

Analysis was carried out using a custom written Spike2 script which allowed for designated times in the recording to be analysed. These regions of interest ranged from 50 s to 5 s before the change in a recording period (either passive recording or dynamic clamp). Therefore a comparison could be made between the time period before and during current injection.

Once regions of interest were specified the analysis script identified the peak of all action potentials that occurred. The resting membrane potential (RMP) was then obtained by taking a voltage measurement at the distance halfway between the two peaks. The amplitude was calculated as the difference between the peak and resting membrane potential. The spike halfwidth was measured as the width of the action potential taken halfway from the RMP to the peak. The afterhyperpolarisation was taken as the maximum change in voltage between the resting membrane potential and the trough after the peak. All four of these spike characteristics (summarised in **Figure 3.3**) were averaged over the total number of spikes in the region of interest. Spike frequency was calculated as the total number of spikes divided by the time length of the region of interest.

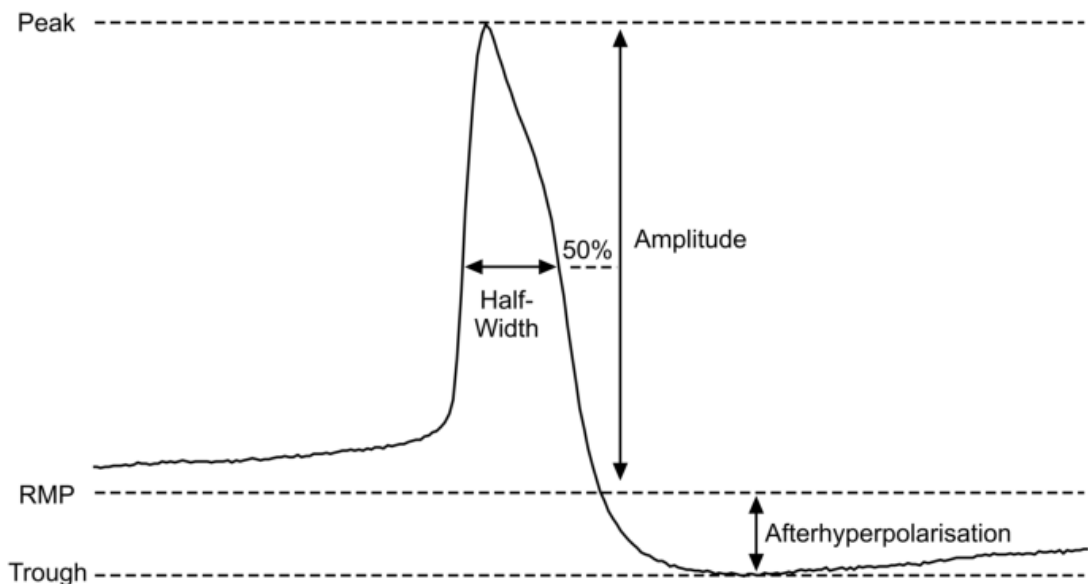


Figure 3.3. An example CGC action potential showing the spike characteristics that were measured. Note that the RMP is not visible due to the large delay between action potentials.

3.2.5. Pattern Clamp

The use of pattern clamp as a simpler alternative to using model conductances was explored. At the beginning of a CGC recording, a small section of the recording was extracted as a voltage vector and saved as a text file. This vector was loaded into MATLAB and 5 mV was added to each voltage element. The depolarised voltage

waveform was then saved as a text file and loaded into the spike generator of STDPC. By creating a strong artificial electrical synapse (10 μ S) between the spike generator and the cell it was attempted to force a +5 mV depolarised pattern of electrical activity on to the cell.

3.3. Results

3.3.1. Addition of model conductances has little effect when CGC is assumed to be a sphere

Based on the assumption that the CGC could be considered a sphere, artificial conductances were introduced in 10 untrained preparations using two electrode dynamic clamp. In one condition I_{NaP} and I_K were increased by 50% g_{max} of what should already be present in the cell. In the other condition I_{NaP} and I_K were increased by 50% g_{max} and I_{HVA} was also increased by 20% g_{max} . This resulted in little obvious difference in the electrophysiological activity of the cell for either condition, as can be seen in **Figure 3.4**. To quantify these electrophysiological results an analysis script was used to determine RMP, firing frequency and spike characteristics both before and during application of the dynamic clamp (see methods section for more details).

Statistical analysis of the RMP using a two-way ANOVA revealed that there was no significant interaction between the conductances simulated (I_{NaP} and I_K or I_{NaP} , I_K and I_{HVA}) and dynamic clamp activation ($F_{1,9} = 0.63$, $p = 0.45$, $n=10$). A post hoc Fisher LSD multiple comparisons test confirmed no significance difference in the mean RMP before or during dynamic clamp for either condition (-57.6 ± 0.8 mV before, -58.1 ± 0.8 mV during I_{NaP} and I_K , $p = 0.1553$; -57.48 ± 0.48 mV before vs -57.62 ± 0.62 mV during I_{NaP} , I_K and I_{HVA} , $p = 0.67$, Bonferroni correction, $n=10$, **Figure 3.5A**).

Analysis of action potential amplitude using a two-way ANOVA revealed a significant interaction between the conductances applied (I_{NaP} and I_K or I_{NaP} , I_K and I_{HVA}) and dynamic clamp activation ($F_{1,9} = 63.48$, $p < 0.0001$, $n=10$). Post hoc Fisher LSD comparisons showed that there was a significant difference in the mean amplitude caused by application of two of the conductances (94.53 ± 0.83 mV before vs 92.58 ± 0.70 mV during I_{NaP} and I_K , $p \leq 0.0001 < 0.005$, $n=10$) but not for all three conductances

(94.49 ± 0.64 mV before vs 94.47 ± 0.61 mV during I_{NaP} , I_K and I_{HVA} , $p = 0.91$, Bonferroni correction, $n=10$, **Figure 3.5B**).

A further two-way ANOVA test was carried out on the afterhyperpolarisation and showed that there was no significant interaction between the conductances applied (I_{NaP} and I_K or I_{NaP} , I_K and I_{HVA}) and activation of the dynamic clamp ($F_{1,9} = 1.00$, $p = 0.34$, $n=10$). A post hoc Fisher LSD comparison determined no significant difference in the mean afterhyperpolarisation caused by the simultaneous application of I_{NaP} and I_K (-14.41 ± 0.51 mV before vs -14.78 ± 0.43 mV during, $p = 0.08$, Bonferroni correction, $n=10$, **Figure 3.5C**). There was also no significant change in the mean afterhyperpolarisation magnitude caused by simultaneous injection of all three conductances (-15.04 ± 0.23 mV before vs -15.68 ± 0.29 mV during I_{NaP} , I_K and I_{HVA} , $p = 0.008 > 0.005$, Bonferroni correction, $n=10$).

Analysis of the spike halfwidth using a two-way ANOVA revealed no significant interaction between conductances applied (I_{NaP} and I_K or I_{NaP} , I_K and I_{HVA}) and activation of the dynamic clamp ($F_{1,9} = 0.36$, $p = 0.56$, $n=10$). There was a significant reduction in the mean halfwidth caused by insertion of artificial conductances in both cases (14.64 ± 1.04 ms before, 13.03 ± 0.89 ms during I_{NaP} and I_K , $p = 0.0007 < 0.005$; 15.85 ± 1.20 ms before vs 13.96 ± 0.87 ms during I_{NaP} , I_K and I_{HVA} , $p = 0.0007 < 0.005$, Bonferroni correction, $n=10$, **Figure 3.5D**).

The last electrophysiological characteristic analysed was the spike frequency of the CGC. A two-way ANOVA showed that there was no significant interaction between the conductances applied (I_{NaP} and I_K or I_{NaP} , I_K and I_{HVA}) and activation of the dynamic clamp ($F_{1,9} = 1.46$, $p = 0.25$, $n=10$). A post hoc Fisher LSD comparison also showed no significant change in the mean frequency by introduction of either simulated conductance sets (0.77 ± 0.08 Hz before, 0.75 ± 0.07 Hz during I_{NaP} and I_K , $p = 0.46$; 0.82 ± 0.05 Hz before vs 0.77 ± 0.05 Hz during I_{NaP} , I_K and I_{HVA} , $p = 0.358 > 0.005$, Bonferroni correction, $n=10$, **Figure 3.5E**).

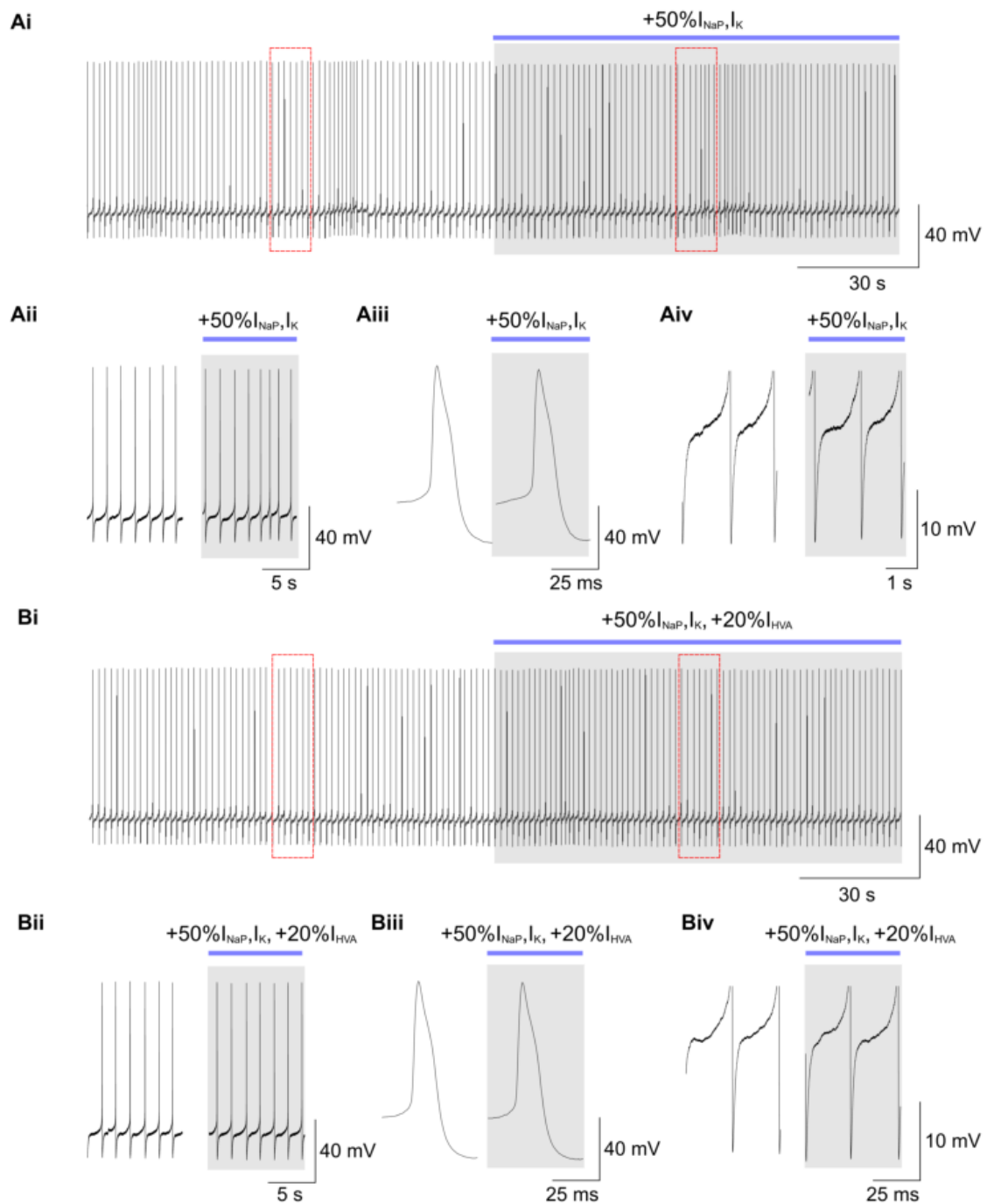


Figure 3.4. Electrophysiological traces of CGC during spontaneous activity and dynamic clamp show little difference, when the soma is assumed to be a sphere. Ai. Representative trace showing the long-term activity of the CGC before and during injection of I_{NaP} and I_K . The red dashed boxes indicate areas which are shown in more detail in **Aii**, **Aiii** and **Aiv**. A small drop in spike amplitude and spike halfwidth can be seen. **Bi.** Representative trace showing the long-term activity of the CGC before and during injection of I_{NaP} , I_K and I_{HVA} . The red dashed boxes indicate areas which are shown in more detail in **Bii**, **Biii** and **Biv**. A small drop in spike halfwidth can be seen.

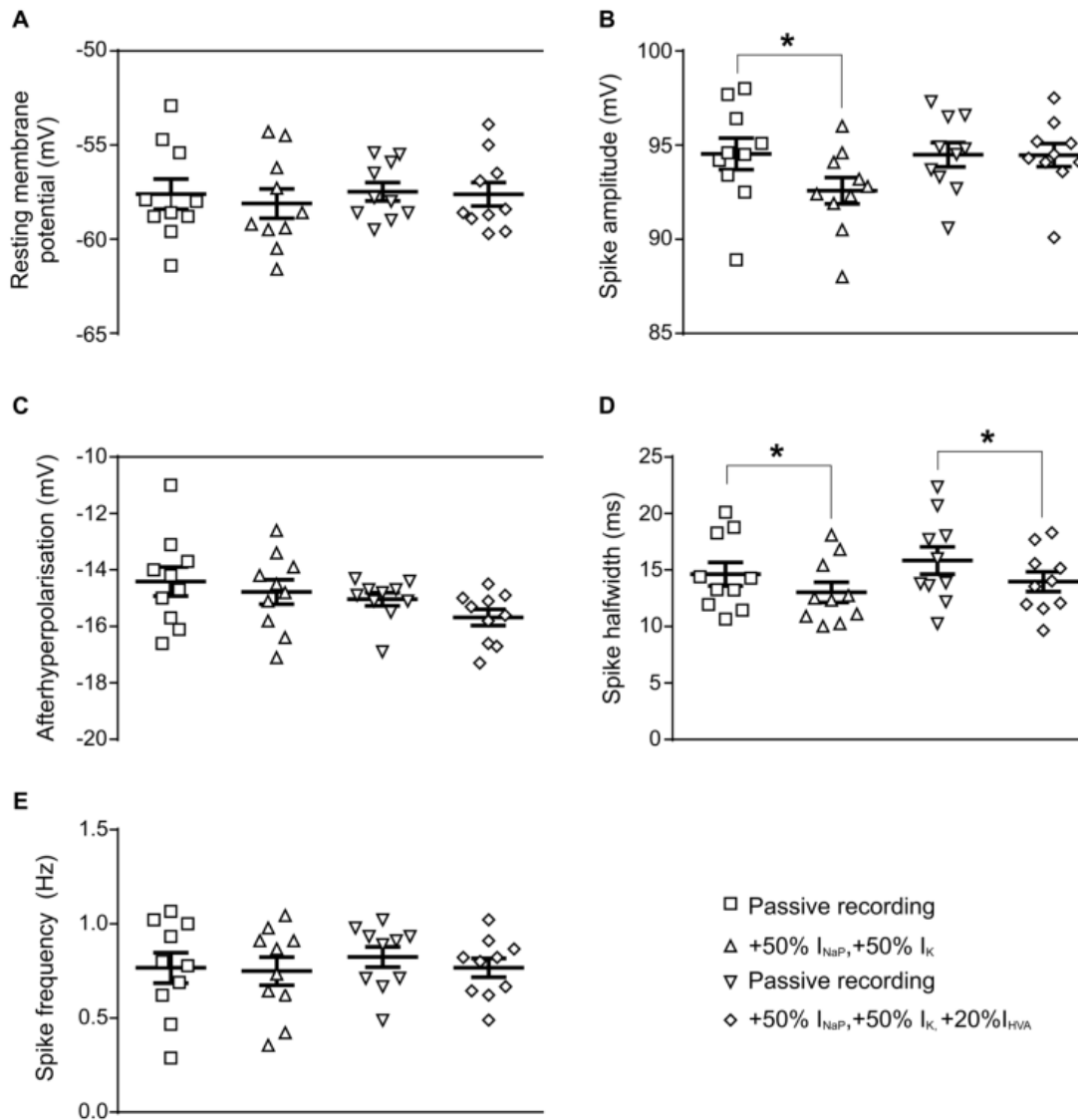


Figure 3.5. Introduction of artificial conductances does not depolarise CGC when the soma is assumed to be a sphere. Averaging 45s of cellular activity before and during dynamic clamp over 10 preparations reveals no significant changes in RMP (**A**). **B**. Spike amplitude was significantly increased by introduction of I_{NaP} and I_K simultaneously but not I_{NaP} , I_K and I_{HVA} . **C**. No significant change in spike afterhyperpolarisation was observed when simulated conductances were added to the membrane. **D**. Introduction of both conductance sets caused a significant reduction in spike halfwidth during dynamic clamp compared to before. **E**. Spike frequency remained unchanged in all conditions.

3.3.2. The surface area of CGC is much larger than a sphere

Due to the lack of response of the cell to addition of the model currents it was suspected that the sphere assumption might be invalid, and therefore that the g_{\max} parameters for each conductance might have been underestimated. To test this a protocol was developed where a sine wave current was injected at the start of each recording. Based on the voltage response of the cell during this injection the total capacitance could be calculated (see methods section). For 10 cells, the average capacitance was found to be 2.86 ± 0.08 nF. Given the specific membrane capacitance ($1\mu\text{F}/\text{cm}^2$) this allows an average surface area of $2.85 \times 10^{-3} \text{ cm}^2$ to be calculated. This value is approximately 9 times larger than what would be expected for a perfect sphere of $100 \mu\text{m}$ diameter (**Figure 3.6A**). There are two probable explanations for this discrepancy. One is that the cell has many axonal arborisations within the cerebral ganglion that survive the axotomisation. The other is that the cell membrane is highly folded. A simple cartoon is shown in **Figure 3.6B** which demonstrates both possibilities.

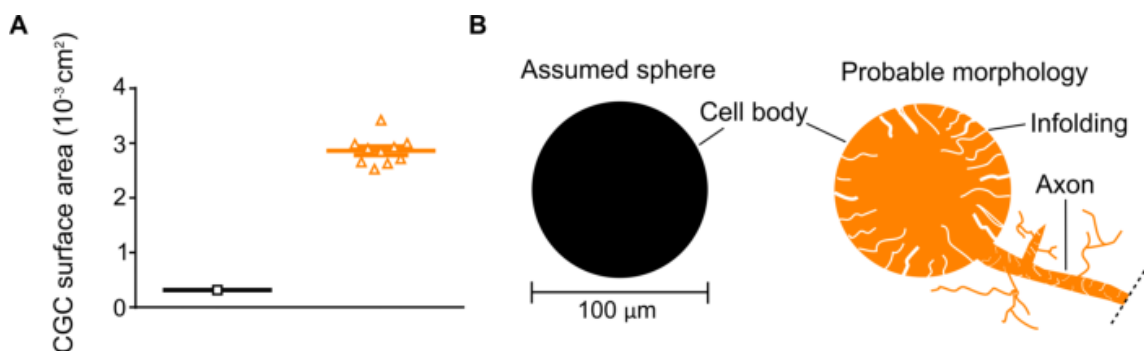


Figure 3.6. The CGC has a surface area much larger than a sphere. **A.** Comparison of the surface area between a sphere ($100 \mu\text{m}$ diameter) and the measured surface area ($n = 10$). **B.** Cartoon demonstrating the possible morphological differences between a perfect sphere and the living cell.

3.3.3. Addition of modelled conductances still does not depolarise CGC, when based on measured cell surface area

Using sine wave current injection, the surface area of each CGC was now calculated at the beginning of each recording (see methods section) and g_{\max} for each conductance was scaled up accordingly. Now when the artificial conductances were added, a much stronger response from the cell was seen, as shown in **Figure 3.7**.

When this was quantified (n=10) the results looked similar to those of **Figure 3.4**, but with larger changes invoked by the dynamic clamp. A two-way ANOVA of the RMP revealed no significant interaction between the conductances simulated (I_{NaP} and I_{K} or I_{NaP} , I_{K} and I_{HVA}) and dynamic clamp activation ($F_{1,9} = 0.40$, $p = 0.54$, $n=10$). A post hoc Fisher LSD analysis also revealed no significant change in the mean RMP before versus during dynamic clamp activation for either conductance combination (-59.98 ± 0.68 mV before, -58.29 ± 0.72 mV during I_{NaP} and I_{K} , $p = 0.03 > 0.005$; -58.76 ± 0.56 mV before vs -57.82 ± 0.69 mV during I_{NaP} , I_{K} and I_{HVA} , $p = 0.008 > 0.005$, Bonferroni correction, $n=10$, **Figure 3.8A**).

A two-way ANOVA analysis of spike amplitude revealed a significant interaction between the conductance combination used and dynamic clamp activation ($F_{1,9} = 313.6$, $p < 0.0001$, $n=10$). A post hoc Fisher LSD comparison of the mean values also revealed significant change caused by simulation of either current combinations (89.39 ± 0.56 mV before, 80.81 ± 0.63 mV during I_{NaP} and I_{K} , $p \leq 0.0001$; 89.47 ± 0.57 mV before vs -91.09 ± 0.75 mV during I_{NaP} , I_{K} and I_{HVA} , $p = 0.0032 < 0.005$, Bonferroni correction, $n=10$, **Figure 3.8B**).

Analysis of afterhyperpolarisation using a two-way ANOVA revealed no significant interaction between the conductance combination and dynamic clamp activation ($F_{1,9} = 1.26$, $p = 0.29$, $n=10$). Furthermore, a post hoc Fisher LSD comparison showed no significant change in the mean afterhyperpolarisation caused by injection of either combination of modelled conductances (-13.71 ± 0.40 mV before, -13.56 ± 0.89 mV during I_{NaP} and I_{K} , $p = 0.88$; -13.49 ± 0.36 mV before vs -14.89 ± 1.15 mV during I_{NaP} , I_{K} and I_{HVA} , $p = 0.18$, Bonferroni correction, $n=10$, **Figure 3.8C**).

A two-way ANOVA of spike halfwidth demonstrated that there was a significant interaction between the conductance types used and dynamic clamp activation ($F_{1,9} = 11.51$, $p = 0.008$, $n=10$). A post hoc Fisher LSD test also found that there was a significant difference in the mean halfwidth before versus during dynamic clamp for both conductance sets (13.42 ± 0.71 ms before, 9.06 ± 0.26 ms during I_{NaP} and I_K , $p \leq 0.0001$; 14.05 ± 0.78 ms before vs 10.69 ± 0.37 ms during I_{NaP} , I_K and I_{HVA} , $p \leq 0.0001$, Bonferroni correction, $n=10$, **Figure 3.8D**).

Analysis of spike frequency using a two-ANOVA revealed no significant interaction between conductance combination and dynamic clamp activation ($F_{1,9} = 0.010$, $p = 0.76$, $n=10$). A post hoc Fisher LSD comparison of the mean frequency before and during dynamic clamp did show a significant difference for both conductance sets (0.80 ± 0.07 Hz before, 0.63 ± 0.10 Hz during I_{NaP} and I_K , $p \leq 0.0001$; 0.84 ± 0.07 Hz before vs 0.66 ± 0.10 Hz during I_{NaP} , I_K and I_{HVA} , $p \leq 0.0001$, Bonferroni correction, $n=10$, **Figure 3.8E**).

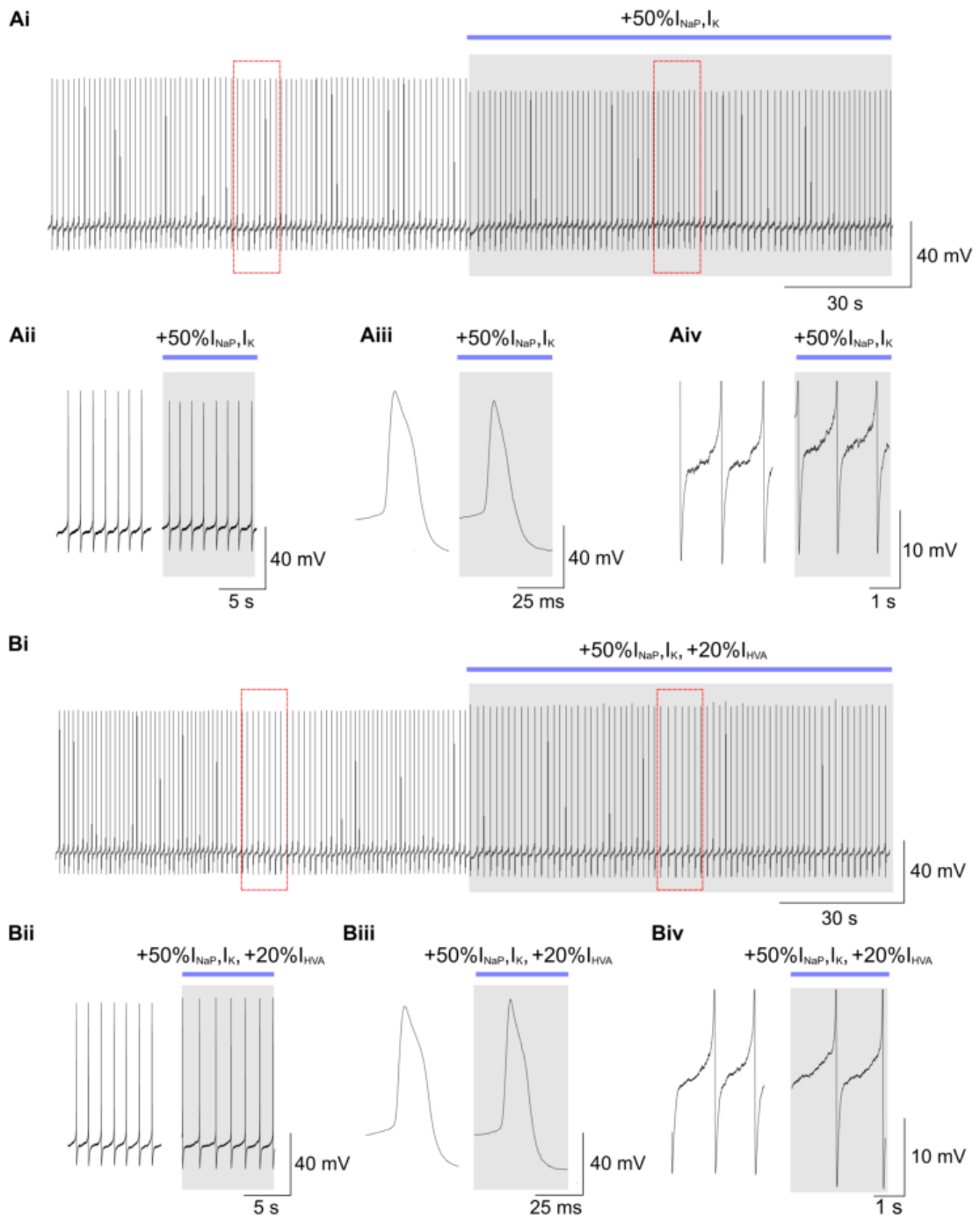


Figure 3.7. Electrophysiological traces of CGC during spontaneous activity and dynamic clamp show more obvious difference, when based on measured surface area. Ai.

Representative trace showing the long-term activity of the CGC before and during injection of I_{NaP} and I_K . The red dashed boxes indicate areas which are shown in more detail in **Aii**, **Aiii** and **Aiv**. A large drop in spike amplitude and spike halfwidth can be seen. **Bi**. Representative trace showing the long-term activity of the CGC before and during injection of I_{NaP} , I_K and I_{HVA} . The red dashed boxes indicate areas which are shown in more detail in **Bii**, **Biii** and **Biv**.

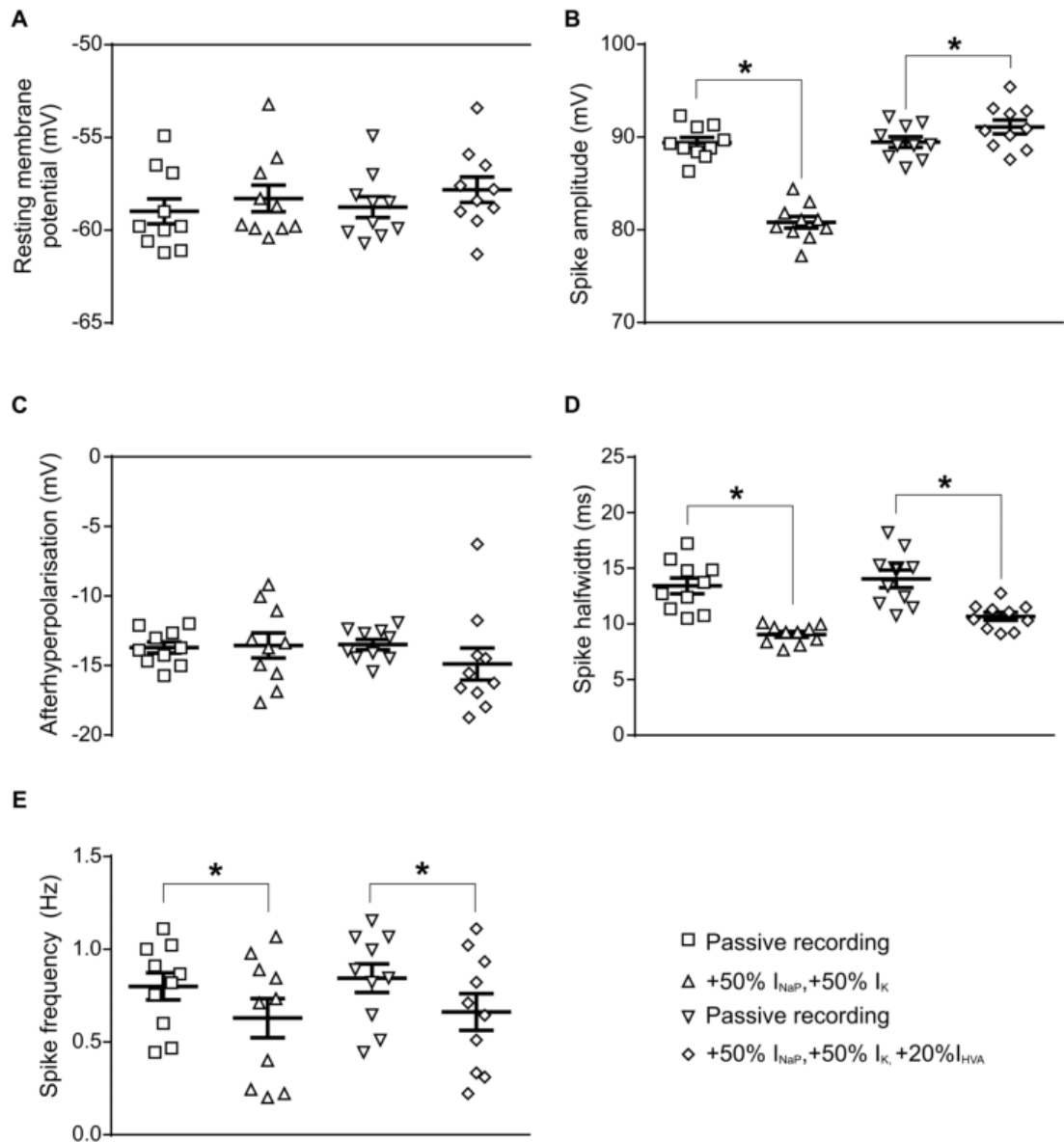


Figure 3.8. Introduction of artificial conductances still does not depolarise CGC, even when based on measured surface area. Averaging 45s of cellular activity before and during dynamic clamp over 10 preparations reveals no significant changes in RMP for either condition (**A**). **B**. Spike amplitude was significantly decreased in both conditions compared to prior passive activity. **C**. No significant change in spike afterhyperpolarisation was observed when simulated conductances were added to the membrane. **D**. Introduction of both conductance sets caused a significant reduction in spike halfwidth during dynamic clamp compared to before. **E**. Spike frequency remained unchanged in all conditions.

3.3.4. Pattern clamp can depolarise the CGC soma, but induces irrepressible action potentials elsewhere in the cell

The underlying hypothesis for the pattern clamp experiments was that the previous attempt of transforming the electrical activity of a naïve CGC into activity that closely resembles the activity of a CGC in a trained animal may have failed because our knowledge of the ionic currents was incomplete or imprecise. I, therefore, decided to use a more direct approach to mimicking the electrical activity of a CGC in a trained snail using so-called pattern clamp. In pattern clamp, a cell is clamped to a target form of electrical activity, that it may not naturally show. For the purposes of mimicking the activity of a CGC from a trained animal, we took the view that this activity is essentially the same spiking activity as of a CGC from a naïve snail but shifted upwards by 5mV. In order to generate the voltage template for the pattern clamp, we therefore extracted at the beginning of each CGC recording and 5 mV was added to every element. This depolarised vector was then used as the target voltage for pattern clamp of CGCs taken from untrained snails (see methods for more details).

Pattern clamp was effective in raising the resting membrane potential by approximately 5 mV. However, it also regularly caused ectopic mini spikes to be recorded in the CGC soma, normally as the cell was approaching spike threshold (n= 9, **Figure 3.9Ai-ii**). By recording the other CGC, with the buccal ganglia intact, it was confirmed that the suppressed spikelet seen in the leader soma CGC, was a full action potential elsewhere in the cell. This ectopic spike can initiate a 1:1 action potential in the follower (**Figure 3.9B**). Additionally, ectopic spikes were still present when the CGC was axotomised (n = 8, **Figure 3.9C**). This indicates that they were being initiated outside of the CGC soma but in the portion of axon contained within the cerebral ganglion.

Quantitative analysis of the data from both leader (paired) and axotomised (unpaired) CGC in untrained preparations confirmed that there was a significant depolarisation caused by activation of the pattern clamp (-57.33 ± 0.6 mV before vs -52.19 ± 0.90 mV during, for leader CGC, $p < 0.0001$, $n = 9$; -56.55 ± 1.80 mV before vs -

51.14 ± 1.78 mV during, for axotomised CGC, $p < 0.0001$, $n = 8$; paired t tests, Bonferroni correction, **Figure 3.10A**).

In addition to the depolarisation there was also a significant decrease in the average spike amplitude from 97.93 ± 0.84 mV before to 95.86 ± 0.74 mV during pattern clamp in leader (paired) CGCs ($p = 0.0001 < 0.01$, $n = 9$, paired t test, Bonferroni correction). This was also seen in axotomised CGCs with a drop from 95.68 ± 1.10 mV during passive recording to 93.96 ± 1.09 mV during pattern clamp ($p = 0.0023 < 0.01$, $n = 8$, paired t test, Bonferroni correction). These decreases can be seen in **Figure 3.10B**.

As in the dynamic clamp there was no significant change in the afterhyperpolarisation before versus during pattern clamp, for either preparation type (-15.16 ± 0.42 before vs -15.46 ± 0.34 mV during, for leader CGC, $p = 0.23$, $n = 9$; -16.29 ± 0.43 mV before vs -16.43 ± 0.45 during, for axotomised CGC, $p = 0.27$, $n = 8$; paired t tests, Bonferroni correction, **Figure 3.10C**).

The mean spike halfwidth was also unchanged by pattern clamp in both preparation types (17.14 ± 0.92 ms before vs 17.08 ± 0.95 ms during, for leader CGC, $p = 0.52$, $n = 9$; 18.17 ± 1.66 ms before vs 18.91 ± 1.89 ms during, for axotomised CGC, $p = 0.17$, $n = 8$; paired t tests, Bonferroni correction, **Figure 3.10D**).

Importantly, the frequency of full-sized action potentials was also not significantly different before compared to during application of pattern clamp, in both preparation types (0.74 ± 0.02 Hz before vs 0.71 ± 0.02 Hz during, for leader CGC, $p = 0.04 > 0.01$, $n = 9$; 0.71 ± 0.04 Hz before vs 0.70 ± 0.04 ms during, for axotomised CGC, $p = 0.80$, $n = 8$; paired t tests, Bonferroni correction, **Figure 3.10E**).

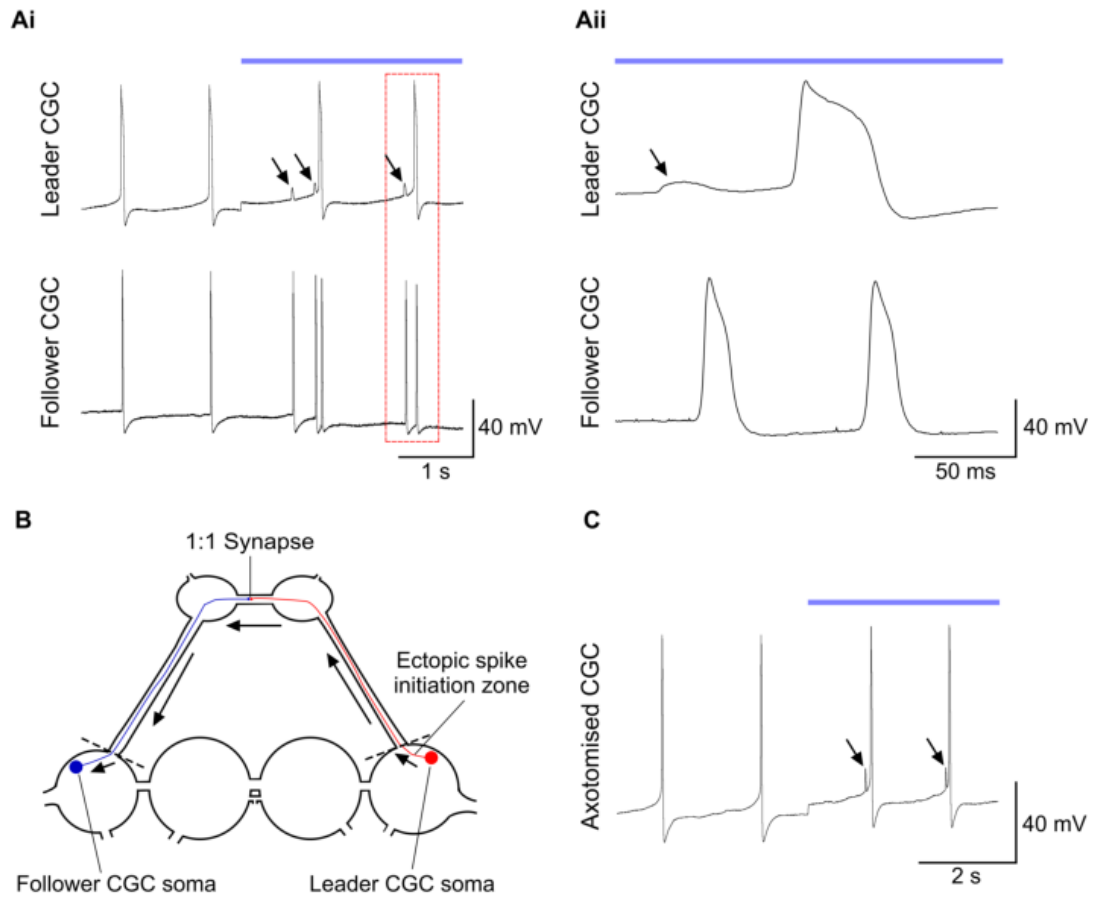


Figure 3.9. Depolarising the CGC using pattern clamp causes uncontrollable spike initiation. **Ai.** Recording of both CGCs showing that depolarisation of one CGC causes ectopic spikes within the same cell (marked by black arrows). The red dashed boxes indicate an area shown in more detail in **Aii**. Here it can be clearly seen that the ectopic mini spike precedes a full action potential in the follower CGC. **B.** A simple diagram showing the anatomical basis for what is observed in the recordings. An uncontrollable spike must be initiated from within the leader CGC that then causes a full action potential to be recorded in the follower CGC. **C.** Axotomisation of the CGC does not prevent the ectopic spike, suggesting that initiation must take place within the cerebral ganglion.

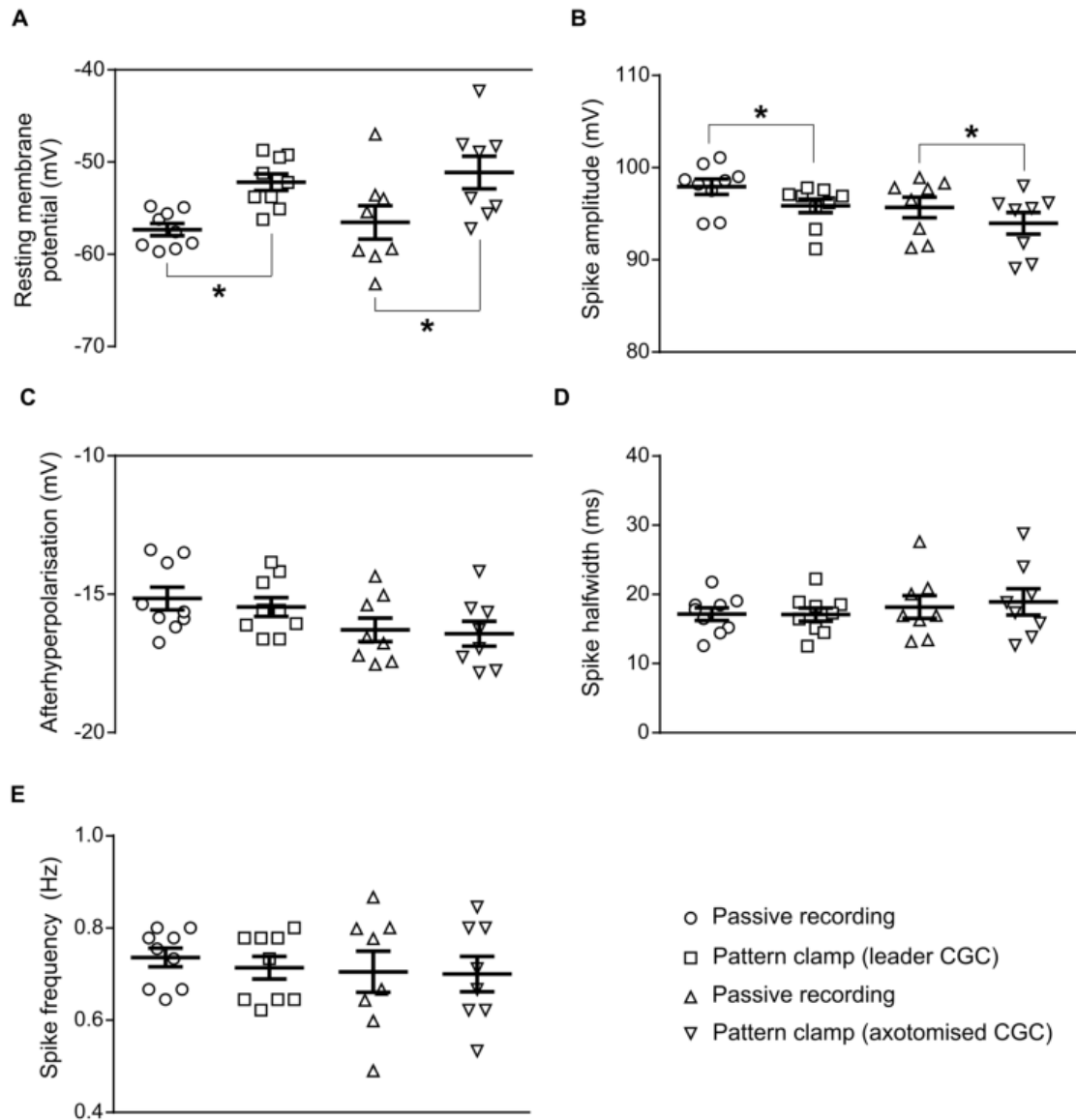


Figure 3.10. Despite ectopic spikes pattern clamp can achieve significant depolarisation of the CGC. Pattern clamp was applied to two types of preparation; one in which the CGC remained paired to the follower ($n=9$) and the other in which the CGC was axotomised ($n=8$). **A.** In both cases activation of pattern clamp caused a significant depolarisation of the CGC RMP. **B.** However there was also a significant decrease in spike amplitude for both types of preparation. The remaining spike characteristics of afterhyperpolarisation (**C**), spike halfwidth (**D**) and full-sized spike frequency (**E**) remained unchanged.

3.4. Discussion

It was important to identify the electrophysiological parameters underlying LTM in *Lymnaea* as it is currently unknown how nonsynaptic plasticity of the CGC occurs. This is a particularly complex problem as the neuron becomes persistently depolarised with no change in action potential frequency, characteristics or input resistance (Kemenes *et al.*, 2006).

3.4.1. Neuronal surface area

An important initial finding was that injection of artificial conductances initially had very little effect on CGC RMP or activity. This was due to a gross, approximately 9-fold, underestimation of the total surface area of the cell that was only revealed by measuring total capacitance. There are two plausible explanations for this underestimation based on the morphology of the cell. The first explanation is that there were still substantial neuronal processes intact after axotomisation. This would include the part of the main axon within the cerebral ganglion, before it enters the CBC. It also includes the axonal side branch of the CGC, which also remains confined to the cerebral ganglion, and is thought to release serotonin presynaptic to the CBIs (Kemenes *et al.*, 2006; Nikitin *et al.*, 2013). The second possibility is that the soma and its processes do not have a smooth surface area, and instead contain many folds. Such infolding has been reported in other identified giant molluscan neurons from *Anisodoris* (Mirolli & Talbott, 1972), *Aplysia* (Coggeshall, 1967; Graubard, 1975; Pinsker *et al.*, 1976; Fejtl *et al.*, 1995) and *Tritonia* (Longley, 1984). It has also been observed in cultured populations of unidentified neurons, taken from the circumesophageal ganglia of *Lymnaea*, and may be important in expansion and shrinking of the cell with changes in osmotic pressure (Dai *et al.*, 1998). It seems that axons of greater diameter show a larger amount of infolding in gastropod molluscs (Graubard, 1975; Longley, 1984). If the same holds true in *Lymnaea* then infolding of the CGC cellular membrane would be relatively high compared to smaller cells. Overall, despite the morphological cause of the discrepancy, capacitance measurements meant g_{\max} for artificial conductances could be scaled correctly.

3.4.2. The ionic basis of nonsynaptic plasticity

Even with corrected g_{\max} , application of artificial I_{NaP} and I_{K} to the CGC did not cause a significantly depolarised state, as predicted by Vavoulis *et al.* (2010). A prediction that was met, was that an increase in these two currents would cause a significant drop in spike amplitude and spike halfwidth. This was partially rescued by the additional 20 % increase in g_{\max} of I_{HVA} , which made the change in amplitude non-significant and slightly reduced the change in spike halfwidth. Once all three conductances (I_{NaP} , I_{K} , I_{HVA}) were artificially increased simultaneously then RMP still remained the same. There was also significant change in spike frequency and spike halfwidth. Overall these results suggest that the current biophysical model created by Vavoulis *et al.* (2010) is not sufficient to explain the large depolarisation seen in CGC following classical conditioning.

There are many possible explanations for the failure of the model to explain the observed nonsynaptic plasticity. The first is that the parameters of the model were too finely tuned to previous electrophysiological data resulting in an unrealistic representation. The simulated CGC is very unstable, such that increases in I_{NaP} and I_{K} must be very closely matched to prevent the cell firing at impossibly high rates (15 Hz) or not at all (Vavoulis *et al.*, 2010). This demonstrates the difficulty in modelling a giant neuron such as CGC, where there are many voltage-gated ion channels, which may not be uniformly distributed. It also seems unlikely that the increase in the g_{\max} of I_{K} is as large as 50 %, given that the observed increase, following classical conditioning, did not reach statistical significance during a step from -60 mV to 30 mV (Nikitin *et al.*, 2008). Inactivation of I_{NaP} also occurs in CGC, as Nikitin *et al.* (2006) showed, but this was not included in the model, likely as the time scale (τ) of this process is not known. It may be that there is an unidentified conductance which counteracts the depolarising effect of I_{NaP} . For example, Staras *et al.* (2002) reported a small number of CGCs showing a possible S_{K} -type Ca^{2+} -sensitive outward potassium current, which could be upregulated following conditioning.

There can also be significant variation in the ionic conductances of the same identified neuron between individuals of the same species (Schulz *et al.*, 2006). Inter-individual variation is common in biology and is normally addressed by averaging over

the population. In most cases this is sufficient, but it has been found that under certain conditions this will not work for conductance based-models (Golowasch *et al.*, 2002). This failure occurs as the average does not account for non-linear relationships between the different conductances of the cell. This could explain the difficulty of the simulated CGC in accurately representing the conductances of each living neuron.

3.4.3. Spike initiation outside the soma

To overcome the failure of artificial current injection, a simpler approach was tested where the CGC was pattern clamped to a depolarised state at the natural firing rate. This was intended as a more sophisticated method of simulating LTM compared to the 1 Hz suprathreshold pulsing alongside 10 mV depolarisation used by Kemenes *et al.* (2006). However, this technique failed as the space clamp was not strong enough to prevent the occurrence of ectopic spikes. This means it was not possible to apply pattern clamp in a semi-intact preparation, and examine its effects on the conditioned feeding response.

The unwanted spikes occurred as the membrane potential was ramping upwards, slightly before the occurrence of the commanded spike. This suggests that the difficulty is caused by a spreading depolarisation causing early action potential initiation outside of the soma. Indeed, it is a difficult task for the pattern clamp, as it must keep the CGC firing at the same low frequency, whilst also depolarising RMP by several mV, with slow ramping potentials between action potentials.

Using different preparations, it was possible to determine the source of the ectopic spikes. When the buccal ganglia were kept, and the connection between the CGCs preserved, then an ectopic spike in the leader CGC invoked a full-sized action potential in the follower CGC. This suggests that spike initiation is occurring in the artificially depolarised CGC, outside of the soma, and propagating up to the buccal ganglia, where it initiates an antidromic action potential in the follower CGC. Furthermore, if the pattern clamped CGC was axotomised then ectopic spikes still occurred. This provides strong evidence that the spike initiation zone is located within the cerebral ganglion itself and away from the soma. This is a finding that is consistent with the original studies of CGC spike initiation in *Lymnaea* which identified a site

equidistant between the soma and proximal CBC (McCrohan & Benjamin, 1980a; Goldschmeding *et al.*, 1981).

Chapter 4: The role of modulatory neurons in memory lapses

4.1. Introduction

Despite the ability of some conditioning paradigms to produce a stable LTM, in many cases there is fluctuation of the expression of memory over time. In some cases, these fluctuations can temporarily prevent the detection of a conditioned response, and can be termed memory lapses.

An early example of a memory lapse during consolidation was revealed by aversive multi-trial training in rats, where learned avoidance was lost at 1 hr, but returned at later time points (Kamin, 1957). If rats were divided into fast and slow learners, then the latter group had a prolonged memory lapse (1-6 hr post training), suggesting that weaker learning shows a greater propensity for memory loss during consolidation (Kamin, 1963). Such lapses in conditioned responses due to weak training have since been termed the Kamin effect.

A well-known example of the Kamin effect in insects was identified in behavioural experiments on the honey bee. Following single trial classical conditioning of the proboscis extension reflex with 1-hexanol, memory expression is present at 30 s, 1 min and 10 min, but is absent at 3 min post training (Gerber & Menzel, 2000). Similar but weaker trends are also observed with three other CS compounds; limonene, 1-octanol and geraniol, suggesting a common yet unidentified physiological mechanism in this species.

A further example of the Kamin effect in insects is found in the cockroach, where multi-trial classical conditioning of the olfactory system initiates a rapid consolidation process that culminates in LTM at 1 hour (Hosono *et al.*, 2016). If a weak single trial training paradigm is used memory expression is stable in the first 5 minutes, disappears from 7-10 minutes, reappears at 30 minutes, then disappears permanently. This single trial training paradigm is too weak to elicit LTM but does show lapses in the early/intermediate stages of memory formation.

The Kamin effect has also been identified in *Lymnaea*, when the US concentration used during conditioning is a tenth of its normal (optimal) value or *in vitro* training is used (Marra *et al.*, 2013). In both cases the training paradigm is weak enough that memory lapses are observed at 30 minutes and 2 hours. Furthermore, it has been found that the memory lapses correspond to two transitions in the molecular phases of memory. The first lapse corresponds to the transition between STM and early ITM (30 min), and the second lapse corresponds to the transition between early ITM and late ITM (2 hr). These are moments of lability in the memory trace, as secondary training, during a lapse point, will replace the primary memory and reinitiate the consolidation process (Crossley *et al.*, 2019). If secondary training is applied at a non-lapse point (10 mins or 1 hr) then replacement does not occur.

Despite a detailed understanding of memory lapses at the behavioural level, nothing is known about the underlying neuronal mechanisms. Therefore, to address this question, two modulatory projection neurons, the CGC and PIB, were targeted during this work. The CGC is a large serotonergic neuron which promotes feeding through numerous synaptic connections with the feeding system (McCrohan & Benjamin, 1980b; Yeoman *et al.*, 1996). The PIB is an inhibitory peptidergic neuron that projects to the buccal ganglia and inhibits feeding cells by releasing FMRFamide (Alania & Sakharov, 2000; Alania *et al.*, 2004).

The CGC and PIB neurons were targeted because appetitive memory has previously been shown to be stored by modulatory feeding neurons in *Lymnaea* (Kemenes *et al.*, 2006; Marra *et al.*, 2010). The CGC has also been shown to respond to an appetitive stimulus, sucrose, applied to the lips in untrained animals (Kemenes *et al.*, 1986). Examining these two identified neurons also covered two major conceptual mechanisms by which memory lapses could occur, shown in **Figure 4.1**. The first possibility being an excitatory neuron (CGC) which forms part of the memory trace but loses its activity during a lapse. This drop in activity could be due to a reduction in background firing or CS-evoked firing. This would be the simplest mechanism and therefore seems to be the most plausible. The second mechanism could be active inhibition by a neuron, such as PIB, which could decrease its activity following conditioning but then return to an 'untrained' state during the memory lapse. This

increased inhibitory activity would prevent the occurrence of the conditioned feeding response. A similar disinhibition mechanism has already been identified in another inhibitory neuron, N3t, at 1-4 hours following conditioning (Marra *et al.*, 2010).

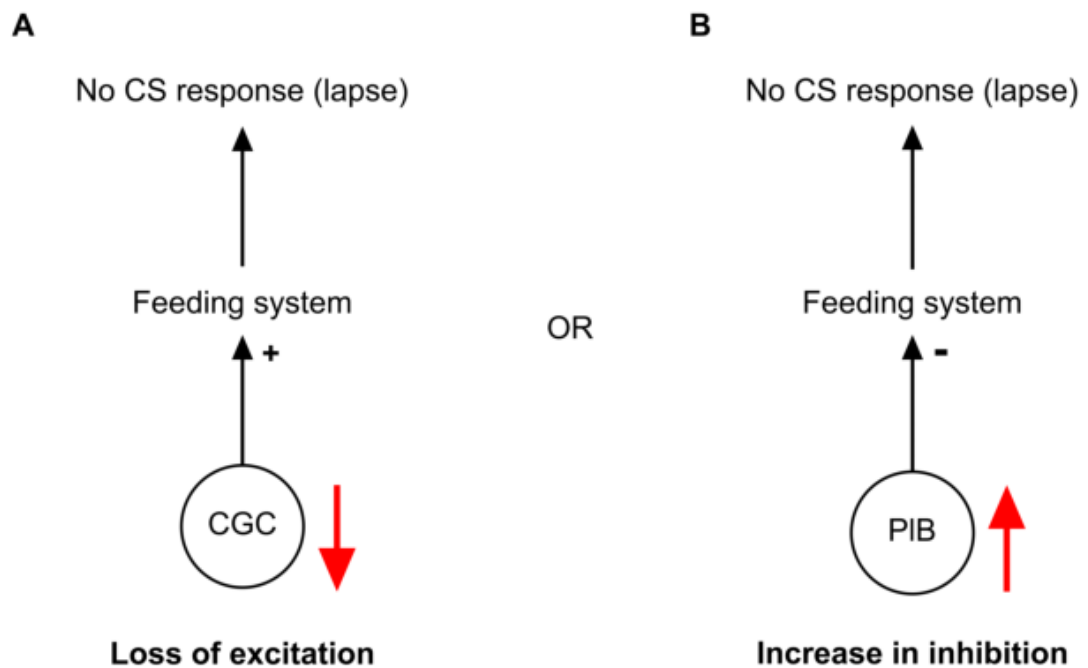


Figure 4.1. Two possible neural mechanisms that could be responsible for lapses in appetitive memory consolidation. A. An excitatory neuron, such as CGC, could have temporarily reduced activity at lapse points, preventing a CS response (feeding). **B.** An inhibitory neuron could increase its activity temporarily and actively prevent the feeding system responding to the CS.

4.2. Methods

4.2.1. Sub-optimal behavioural conditioning

Conditioning of *Lymnaea* was carried out in the animal unit and consisted of a single pairing of a chemical CS, gamma-nonalactone (GNL)/amyl acetate (AA) (Sigma-Aldrich), and a chemical US, sucrose (Fisher Scientific). This took place in a small 14 cm diameter transparent petri dish. For training to be sub-optimal when pairing with GNL, 0.168 % sucrose was used (weight/volume concentration). This is a quarter of the concentration used generally (0.67%), which produces optimal training and doesn't

reveal memory lapses (Kemenes *et al.*, 2006). When using AA as the CS, 0.067 % (1/10th usual) sucrose was used, as in Marra *et al.* (2013). Twenty animals were trained and tested per experimental group, at 1 hr, 2 hr and 4 hr post training. Often the final group size would be slightly smaller due to death of an animal, or lack of response to the US. To avoid overcrowding stress, a maximum of ten snails were kept in each tank.

Pairing took place in plastic petri dishes where the snails had already been acclimatised for 10 minutes in 90 ml of copper-free water. Both the CS and US were added by squirting 5 ml of solution from 10 ml plastic syringes, into the petri dish, away from the body of the snail. This caused a 20-fold dilution of the CS and US such that the final concentrations were as described above. The CS was added first, followed by the US 30 s later. The snails were then left exposed to both chemicals simultaneously for two minutes. After this time, each snail was gently removed, briefly rinsed in a washing tub, and then returned to their home tank until testing.

For behavioural testing, each animal was acclimatised for 10 minutes in a transparent petri dish containing 90 ml copper-free water. 5 ml of copper-free water was then squirted into the dish using a plastic syringe. Using a clicker, the number of rasps was manually counted for 2 minutes and noted down. This was aided by mirrors, allowing the experimenter to see from below and behind the petri dish. Lastly 5 ml of CS was added to the dish using another plastic syringe to bring the total volume to 100 ml (final concentration 0.004 % CS). For 2 further minutes the number of rasps was counted. The snails were then removed from the dish ending the experiment. If a snail did not rasp at all during these two minutes, then it was tested for a US response over a further two minutes. If there were none, then the animal was removed from the data set. As the rasping of only four snails could be counted at once, it was necessary to stagger the experiments around each time point, by dividing each experimental group into 5 subgroups. Once all subgroups had been tested a feeding score was calculated for each snail, by subtracting the number of rasps in the presence of the CS from the number of rasps in water alone. A mean feeding score was calculated by averaging over all the snails in that experimental group. The same process was repeated for each conditioned time point; 1 hr, 2 hr and 4 hr. An untrained experimental group was also tested as a control. This group did not receive any pairing, but was starved for the

same amount of time in the same environment as the conditioned experimental groups.

4.2.2. Semi-intact preparations

To test the CS-evoked responses of PIB and CGC it was necessary to use semi-intact preparations where the lip, containing chemosensory neurons, is kept attached to the brain via the lip and tentacle nerves. The rest of the foot posterior to the lip was removed. When recording the PIB, the lip was severed down the midline, forming a split lip preparation. For CGC recordings a whole lip preparation was used.

One data set was collected for CGC analysis and another data set was collected for PIB analysis. This was because PIB impalement/instability increased the firing rate of the cell and could cause monosynaptic inhibition on CGC (Alania *et al.*, 2004). Additionally, CGC was found to be depolarised by the CS GNL, even when the lips were not present, necessitating the use of a different CS.

Like the first results chapter, the CGC and PIB were also axotomised by removal of the buccal ganglia and pinning the CBC close to the cerebral ganglia. This was done to reduce the rhythmic feedback the cells receive from the CPG, especially during the rasp phase, which could have masked changes in firing rate. It also disconnected each cell from its contralateral partner, as their synaptic connections are in the buccal ganglia (McCrohan & Benjamin, 1980a; Goldschmeding *et al.*, 1981; Alania & Sakharov, 2000).

4.2.3. Time course of the electrophysiology experiments

During the semi-intact experiments, the same conditioning sequence was used as in the earlier behavioural experiments where the CS was added for 30 s followed by the US for 120 seconds. Dissection began 50 minutes before each time point being tested. Once complete the preparation was perfused with normal saline using a gravity fed perfusion system. Excess saline was removed using a Gilson peristaltic pump.

Ten minutes prior to the time point for testing the cells of interest were impaled. Neurons were identified based on their position and characteristic firing activity. The CGCs are found in the anterior lobe of the cerebral ganglion and usually

show a low firing rate (≈ 0.4 Hz) with large amplitude action potentials (≈ 95 mV). The PIB neuron was found on the dorsal surface of the pleural ganglion slightly towards the centre of the circumesophageal ring and pedal ganglia. It typically showed a high firing rate (≈ 4 Hz) with small amplitude action potentials (≈ 50 mV).

After ten minutes of recording, a custom Spike2 script was used to send a TTL voltage pulse from the ADC to a valve controller and on to pinch valves (Cole-Parmer) which cut off NS flow and allowed CS flow for 2 minutes, before reverting to NS. After 5 minutes, another TTL pulse was sent causing sucrose to be perfused over the preparation lasting for 2 minutes. If the CGC increased its firing rate by more than 5 % then this confirmed the preparation had intact chemosensory pathways, and was therefore valid for analysis (Kemenes *et al.*, 1986). Both the CS and US were dissolved in NS. A summary of the time course for each experimental group is shown in **Figure 4.2**.

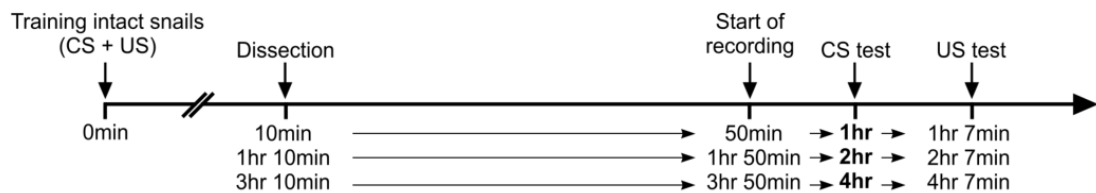


Figure 4.2. Diagram summarising the time course of the electrophysiological experiments in this chapter.

4.2.4. Analysis of electrophysiological recordings

Both the CS and US response were analysed using Spike2. Regions of interest were taken from the two minutes before and the two minutes during both the CS and US. Analysis was carried out using the same script as in the previous chapter. The script gives the average spike frequency, RMP, spike amplitude, spike halfwidth and afterhyperpolarisation during each region of interest. For a detailed definition of each spike characteristic see the previous chapter methods (section 3). An additional script was also used on the same regions of interest, which binned the spikes before and during CS/US application and generated a text file. This was exported to Microsoft Excel where it was used to create spike histograms.

4.3. Results

4.3.1. Sub-optimal conditioning using GNL as the CS shows memory lapses

The first step was to confirm that a lowered concentration of sucrose, paired with GNL, was sufficient to form a memory, but which also lapsed (Marra *et al.*, 2013; Crossley *et al.*, 2019). Pairing of 0.004 % GNL with 0.168 % sucrose resulted in feeding scores at 1 hr (14 ± 2 rasps, $n = 16$) and 4 hr (13 ± 2 rasps, $n = 18$) that were significantly higher than untrained (5 ± 2 rasps, $n = 18$) (one-way ANOVA, $F_{3,68} = 5.526$, $p = 0.0019$; Holm-Sidak multiple comparison post hoc tests; untrained vs 1 hr $p = 0.0071$; untrained vs 4 hr $p = 0.0151$). Further post hoc Holm-Sidak comparisons also showed that there was a significant difference in the mean feeding score between the 2 hr (6 ± 2 rasps, $n = 20$) group and 1 hr and 4 hr groups (1 hr vs 2 hr, $p = 0.0153$; 2hr vs 4hr, $p = 0.0170$). This data is shown in **Figure 4.3** and confirms the presence of memory lapses at 2 hours following this training paradigm.

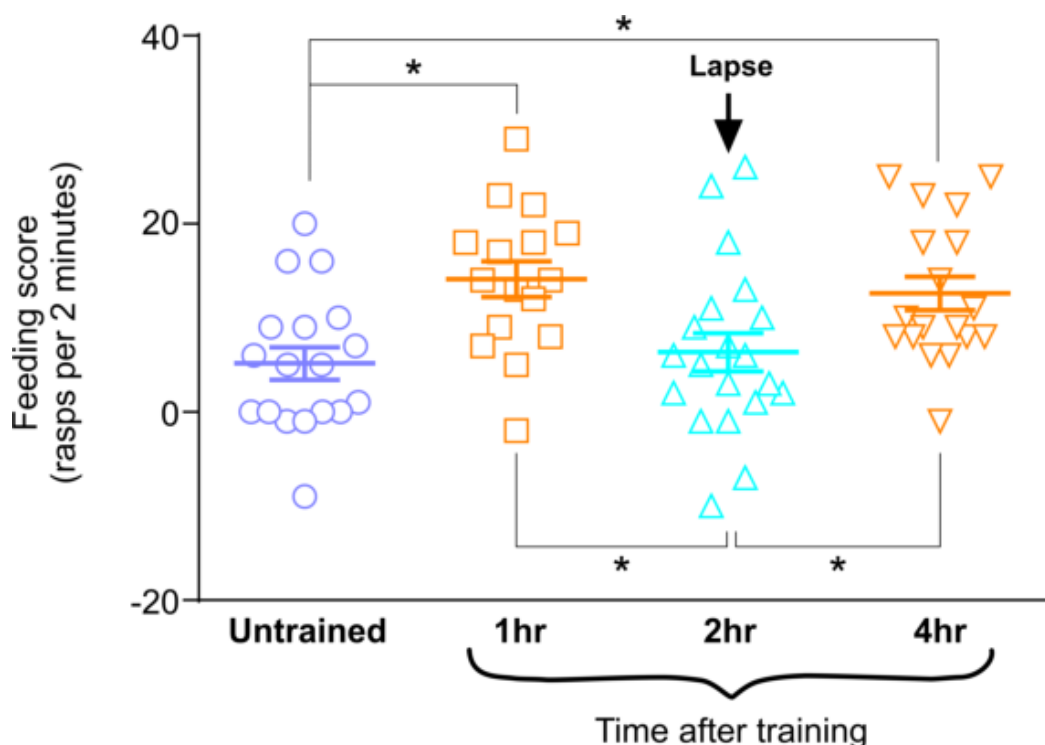


Figure 4.3. Sub-optimal training, using GNL as the CS, evokes a memory trace that lapses at the 2hr time point. Chart showing feeding scores for untrained ($n=18$), 1 hour post-training ($n=16$), 2 hours post-training ($n=20$) and 4 hours post-training ($n=18$) snails.

4.3.2. Sub-optimal conditioning did not reveal significant change in spontaneous or CS-evoked PIB firing rates

Once the behavioural paradigm was established as showing memory lapses, intact animals were again conditioned, but were then dissected before the CS test (as described above). Analysis of this data revealed no significant change in CS induced firing rate compared to the spontaneous (background) firing rate (i.e. pre CS application) of PIB at any time point after training (Kruskal-Wallis test, $p = 0.2819$).

There was also no significant change in firing rate caused by CS application, in either trained or untrained animals (Wilcoxon matched pairs signed rank test (referred to hereafter as Wilcoxon test), Bonferroni correction, before vs during; untrained, $p = 0.25$, $n = 4$; 1 hr, $p = 0.81$, $n = 5$; 2 hr, $p = 0.31$, $n = 5$; 4 hr, $p = 0.99$, $n=4$).

Representative traces of PIB activity and bar charts for the different experimental groups are shown in **Figure 4.4**. Additional temporal detail of firing activity is shown by spike histograms in **Figure 4.5**.

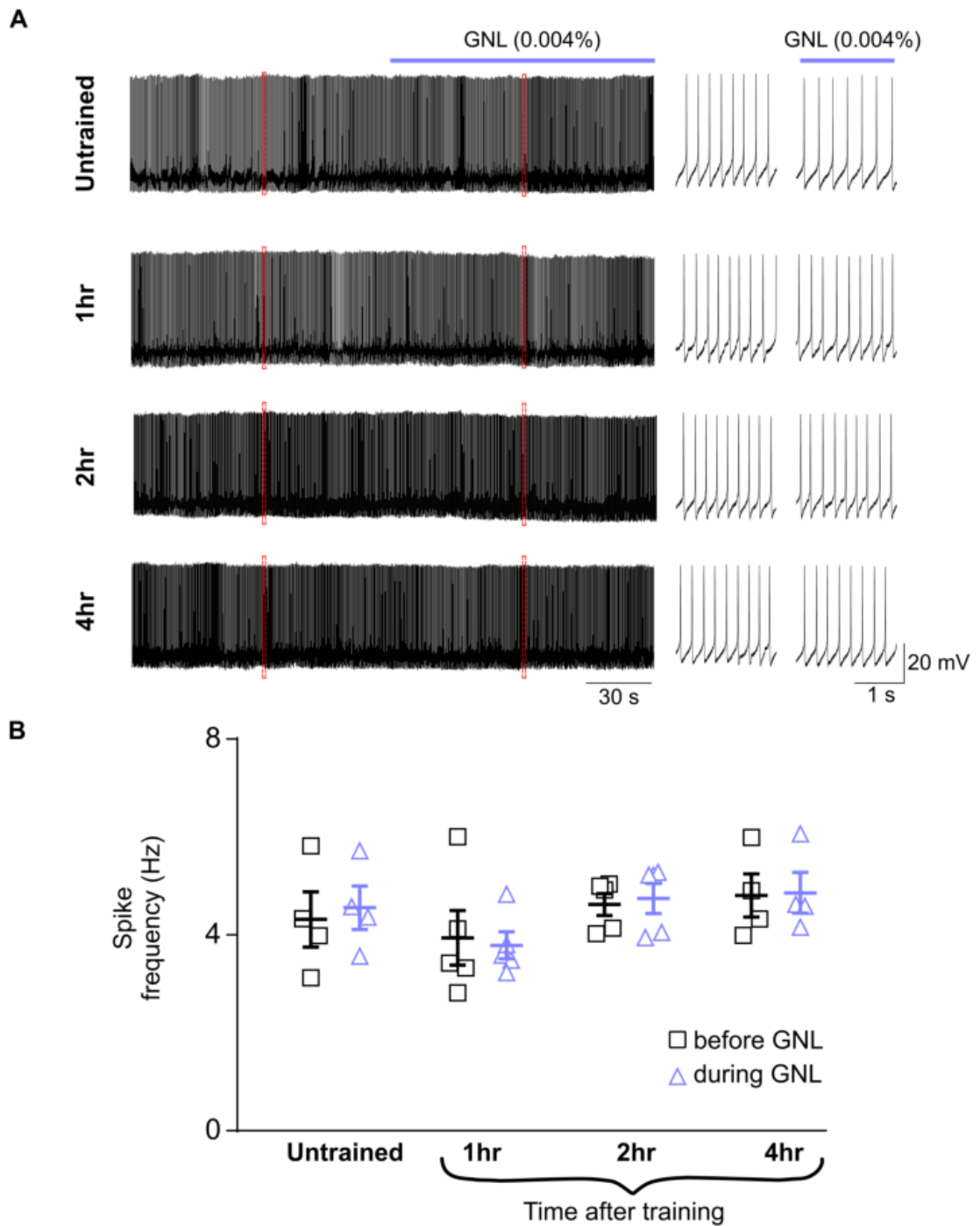


Figure 4.4. GNL has little effect on PIB firing rate before or after conditioning. A.

Representative traces showing the firing activity of PIB before and during GNL perfusion of the lips. Expanded traces taken from the red segregated boxes are shown to the right. **B.** Chart showing the firing frequency of PIB for untrained ($n = 4$), 1 hr post-training ($n = 5$), 2 hr post-training ($n = 5$) and 4 hr post-training ($n = 4$) individuals.

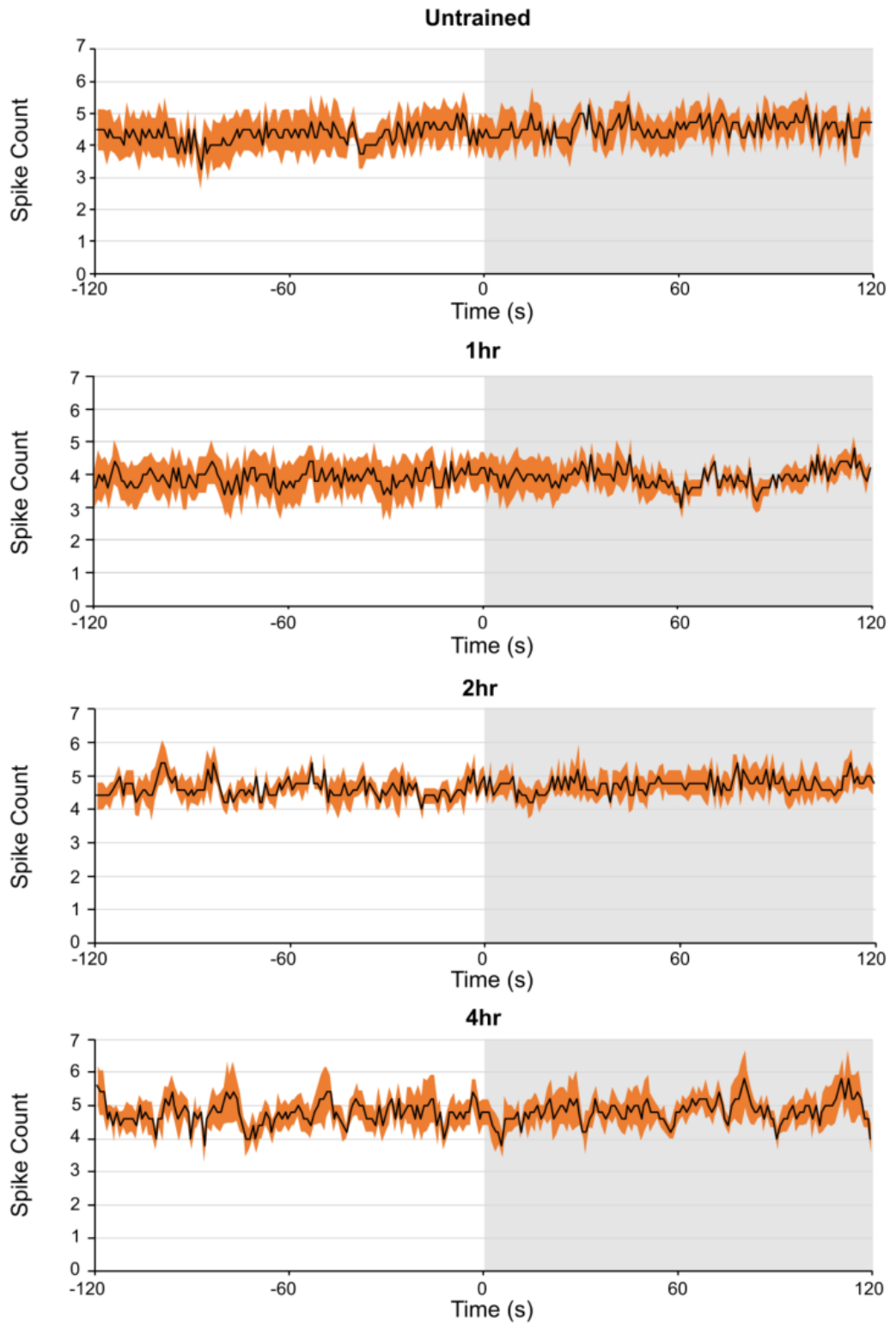


Figure 4.5. A more detailed temporal view of PIB spike activity during GNL application.

Average spike counts taken from 1 s bins are shown for untrained ($n = 4$), 1 hr post-training ($n = 5$), 2 hr post-training ($n = 5$) and 4 hr post-training ($n = 4$) groups. SEM is shown in orange.

4.3.3. No significant changes were found in PIB spike characteristics following sub-optimal conditioning

In addition to firing frequency, PIB spike characteristics were also analysed in all experimental groups (untrained $n = 4$, 1 hr $n = 5$, 2hr $n = 5$, 4hr $n = 4$). As before there was no significant change in background spike characteristics, prior to CS application, caused by conditioning, for any of the features examined (Kruskal-Wallis test; RMP $p = 0.99$; afterhyperpolarisation $p = 0.30$; spike amplitude $p = 0.44$; spike halfwidth $p = 0.49$). There was also no significant change in RMP during GNL application in untrained snail or at any time points following conditioning (Wilcoxon test, Bonferroni correction, before vs during; untrained, $p = 0.25$; 1 hr $p = 0.63$; 2 hr $p = 0.99$; 4hr $p = 0.99$). Afterhyperpolarisation was also not significantly different during CS application compared to before CS application for any group (Wilcoxon test, Bonferroni correction, before vs during; untrained, $p = 0.13$; 1 hr, $p = 0.99$; 2 hr, $p = 0.81$; 4 hr, $p = 0.88$). Analysis of spike amplitude for untrained and trained snails also revealed no change from before compared to during CS application (Wilcoxon test, Bonferroni correction, before vs during; untrained, $p = 0.88$; 1 hr, $p = 0.06$; 2 hr, $p = 0.99$; 4 hr, $p = 0.63$). Lastly, spike halfwidth did not change significantly when the CS was applied to the lips, in any experimental group (Wilcoxon test, Bonferroni correction, before vs during; untrained, $p = 0.38$; 1 hr, $p = 0.63$; 2 hr, $p = 0.44$; 4 hr, $p = 0.99$). This data is summarised in **Figure 4.6**.

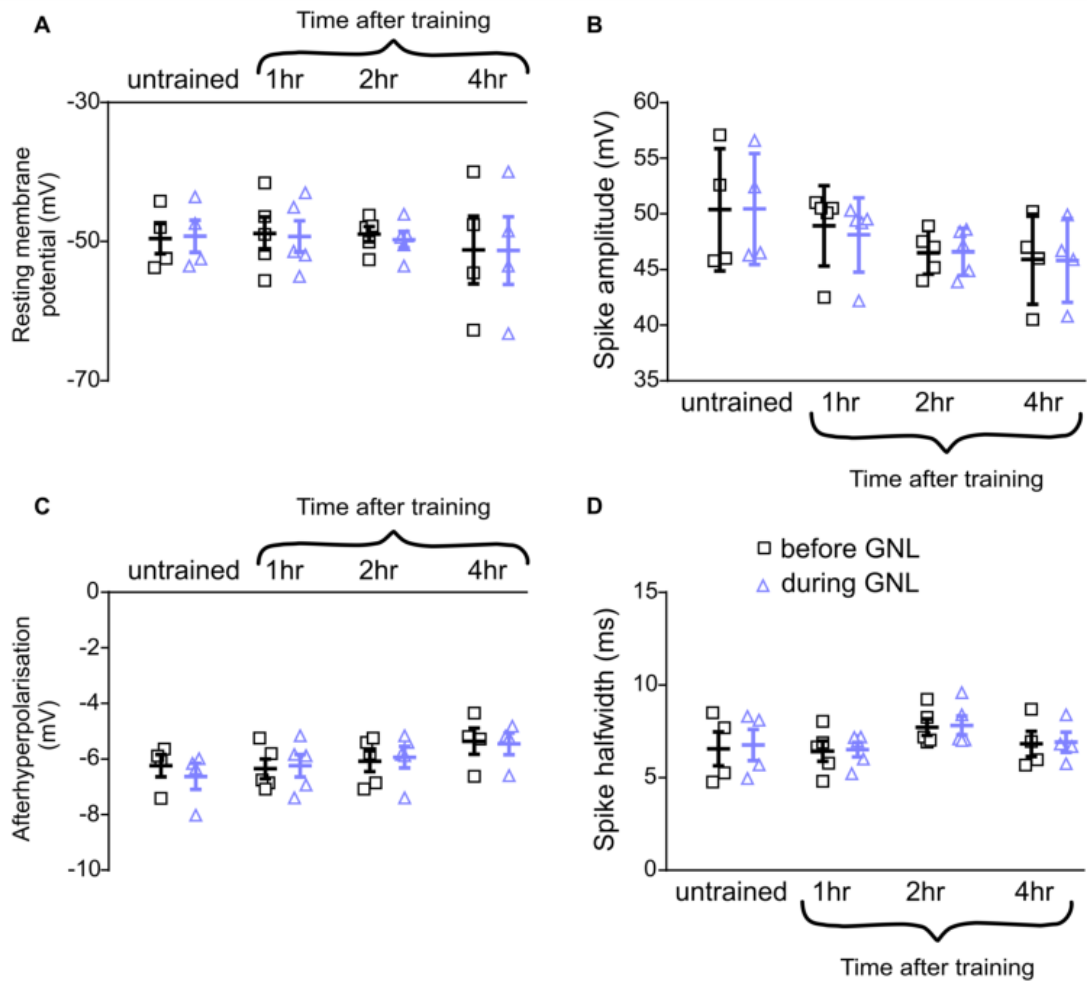


Figure 4.6. PIB spike characteristics reveal no change following GNL application in trained or untrained snails. Data is shown for RMP (A), spike amplitude (B), afterhyperpolarisation (C) and spike halfwidth (D). Sample sizes were $n = 4$, untrained, $n = 5$, 1 hr post-training, $n = 5$, 2 hr post-training and $n = 4$, 4 hr post-training.

4.3.4. No change in PIB firing rate was found by application of the US before or after sub-optimal conditioning

In addition to analysing the CS response, the US response of PIB was also analysed. Due to the difficulty in holding this cell for the entirety of the experiment the sample numbers are smaller. Despite a small tendency for the firing frequency to fall slightly during sucrose application, in conditioned animals, the difference was not significant in any group (Wilcoxon test, before vs during; untrained, $p = 0.63$, $n = 4$; 1 hr, $p = 0.50$, $n = 3$; 2hr, $p = 0.13$, $n = 4$; 4 hr, $p = 0.25$, $n = 3$). This data can be seen in a summary form in **Figure 4.7** and in a more temporally detailed spike histogram in **Figure 4.8**.

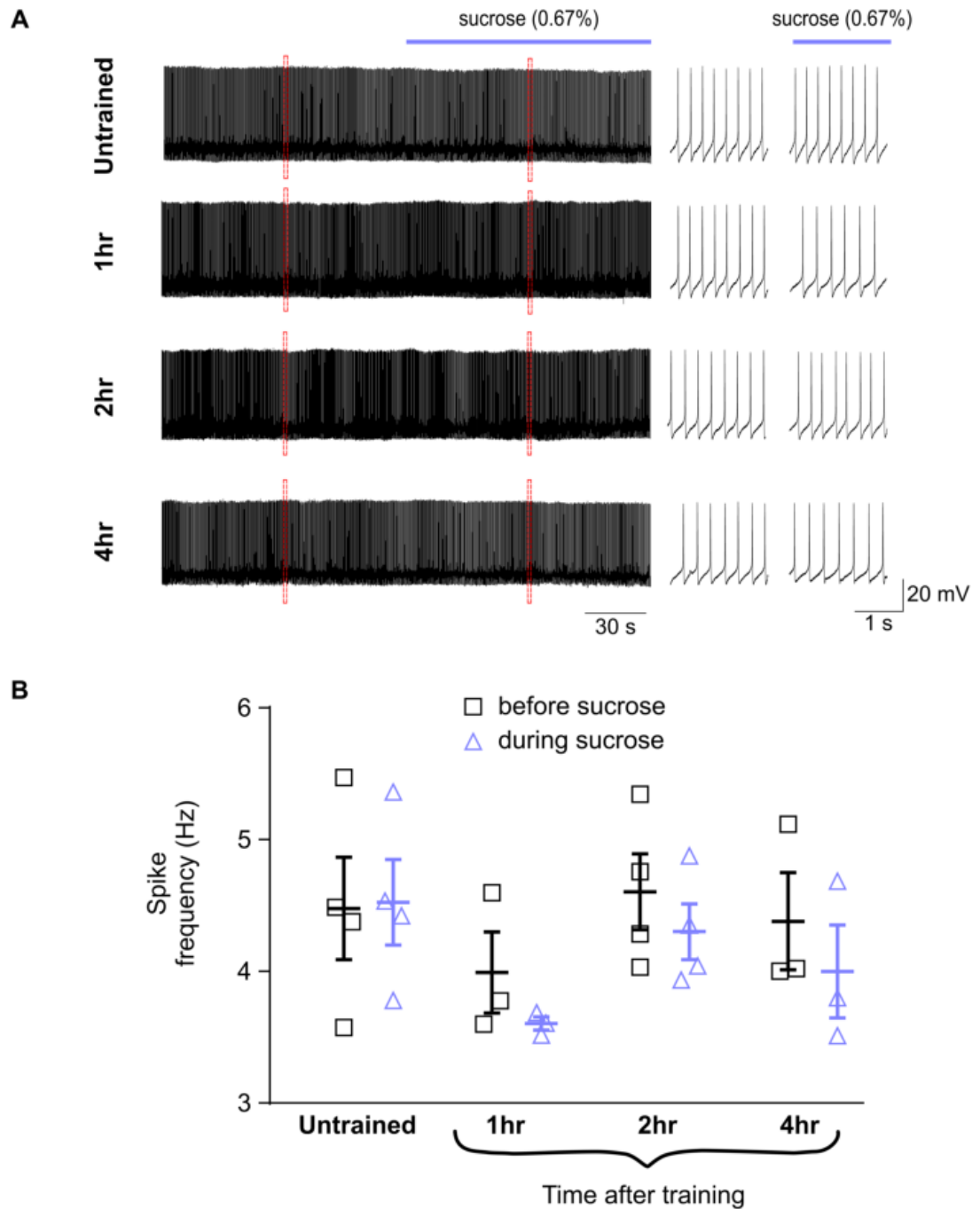


Figure 4.7. Sucrose has little effect on PIB firing rate before or after conditioning. A.

Representative traces showing the firing activity of PIB before and during sucrose perfusion of the lips. Expanded traces taken from the red segregated boxes are shown to the right. **B.**

Chart showing the firing frequency of PIB for untrained ($n = 4$), 1 hr post-training ($n = 3$), 2 hr post-training ($n = 4$) and 4 hr post-training ($n = 3$) individuals.

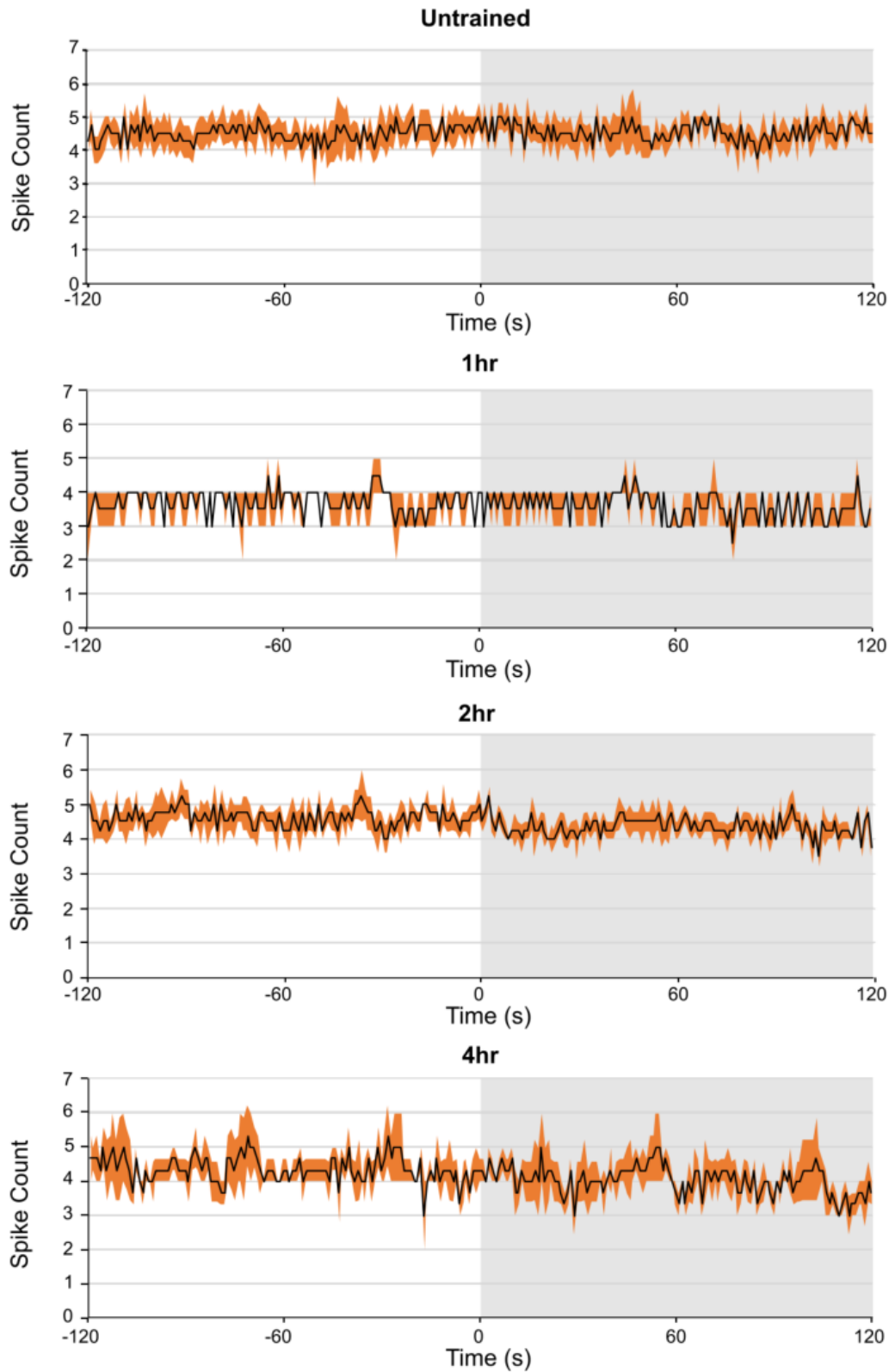


Figure 4.8. A more detailed temporal view of PIB spike activity during sucrose application. Average spike counts taken from 1 s bins are shown for untrained ($n = 4$), 1 hr ($n = 3$), 2 hr ($n = 4$) and 4 hr ($n = 3$) groups. SEM is shown in orange.

4.3.5. GNL causes a direct depolarisation of CGC without the lips

An unexpected finding of this work was that GNL seemed to cause an increase in CGC firing, regardless of whether the animal had been conditioned. Importantly, this response persisted even in preparations without the lips ($n = 5$), suggesting that GNL may be acting directly on the cell. Hyperpolarising CGC, with a second electrode, revealed a slow but constant depolarisation of the cell, caused by GNL release into the bath. This nonspecific effect prevented the examination of the conditioned responses of CGC using GNL. Instead a different CS was used (amyl acetate), which has no effect on CGC, as can be seen in **Figure 4.9**.

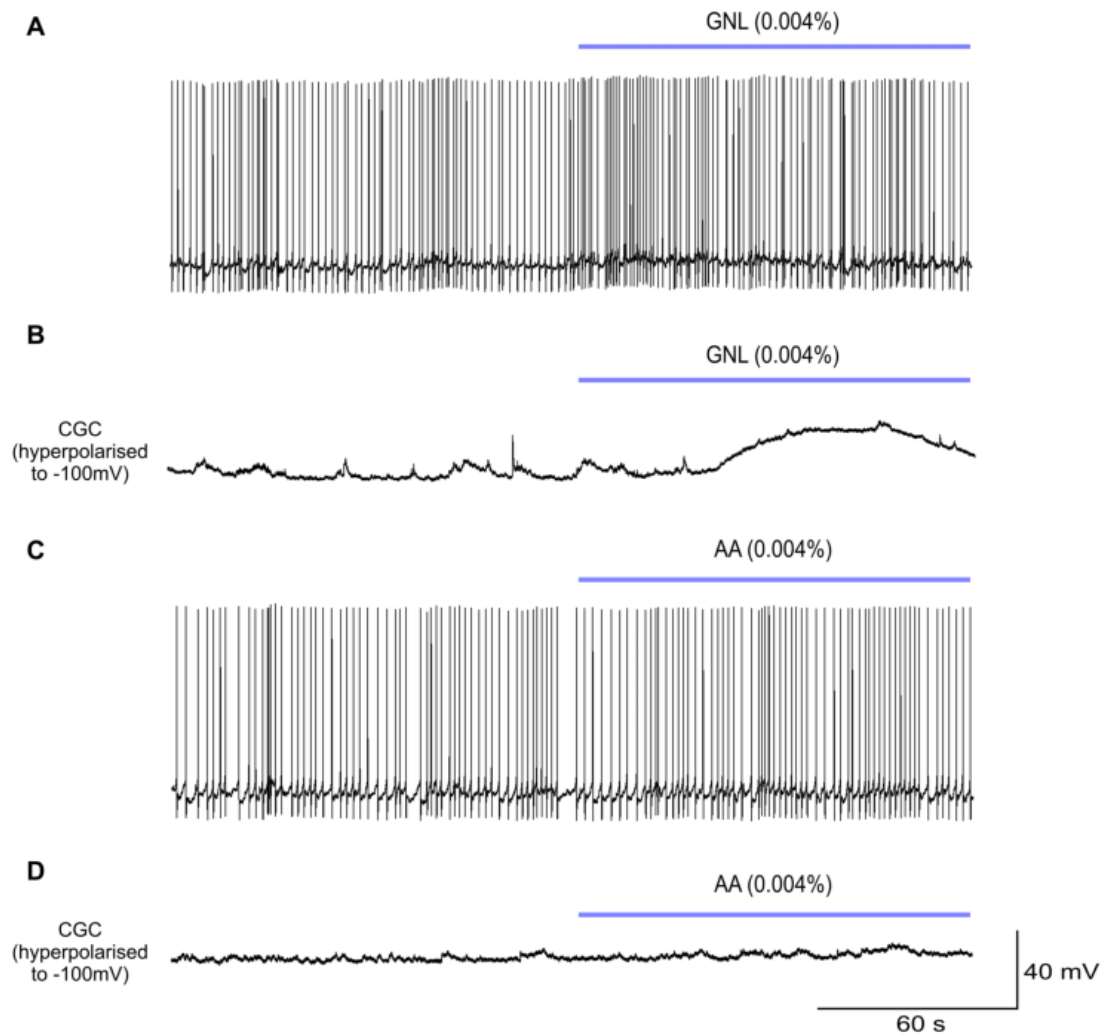


Figure 4.9. GNL causes depolarisation of CGC even when the lips are not present. A. A small increase in the spike frequency can be seen in the presence of GNL. **B.** Enhanced effect of depolarization by application of GNL while CGC firing was prevented by hyperpolarization of the cell. **C.** Amyl acetate does not change the firing rate of CGC. **D.** When the cell is hyperpolarised by a second electrode (not shown) no depolarisation is visible in the presence of amyl acetate. All traces were taken from a whole CNS preparation without the lips.

4.3.6. Sub-optimal conditioning using AA as the CS shows memory lapses

Once AA was confirmed to have no direct effect on the CGC, conditioning of intact snails was carried out, using the same sub-optimal concentration of sucrose (0.067%) as in Marra *et al.* (2013). In behavioural experiments this reproduced previous findings, with feeding scores that were significantly higher than untrained (-1 ± 1 rasp, $n = 17$), at 1 hr (5 ± 1 rasps, $n = 8$) and 4 hr (3 ± 1 rasps) after conditioning (one-way ANOVA, $F_{3,68} = 5.417$, $p = 0.0021$; Holm-Sidak post hoc comparisons; untrained vs 1hr, $p = 0.0036$; untrained vs 4 hr $p = 0.0195$). Further Holm-Sidak post hoc comparisons between trained groups also showed that there was a significant difference in the mean feeding response between the 2 hr group (0 ± 1 rasp, $n = 18$) and 1/4 hr groups (1 hr vs 2 hr, $p = 0.0195$; 2hr vs 4hr, $p = 0.0450$). Therefore, the memory lapse was occurring at 2 hours, as previously shown by Marra *et al.* (2013) (Figure 4.10).

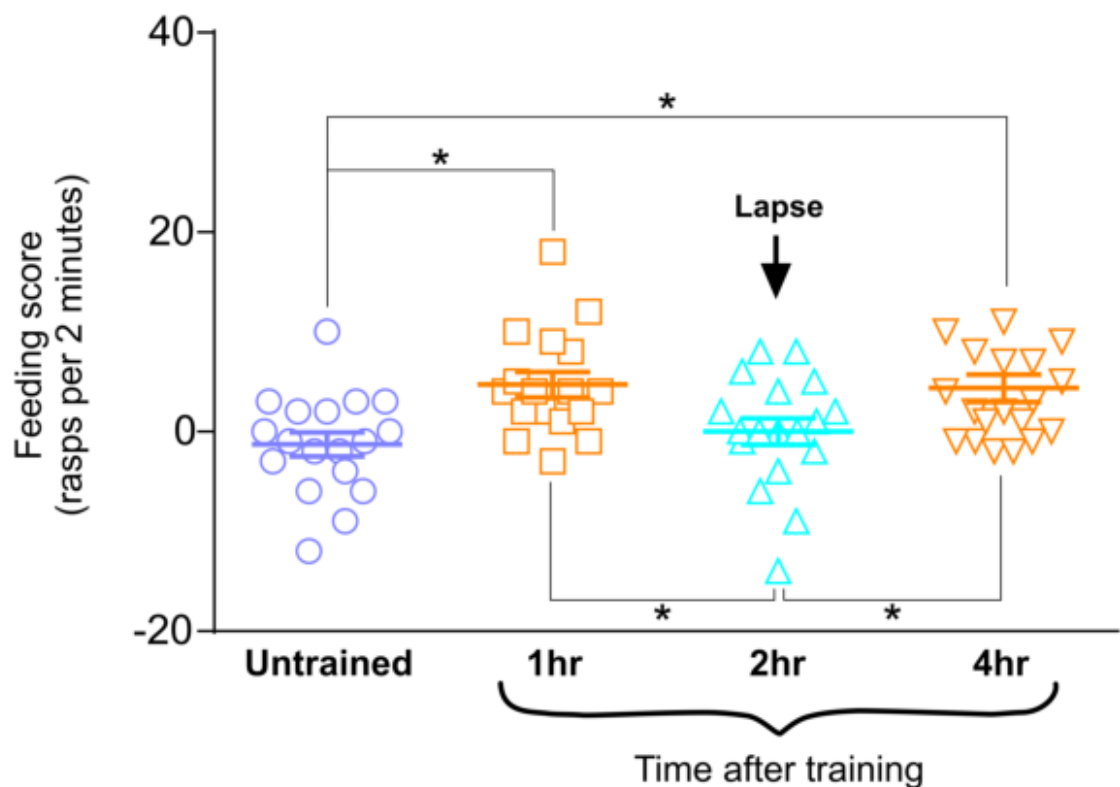


Figure 4.10. Sub-optimal training using AA as the CS evokes a memory trace that lapses at the 2 hr time point. Chart showing feeding scores for untrained ($n = 18$), 1 hour post-training ($n = 17$), 2 hours post-training ($n = 18$) and 4 hours post-training ($n = 19$) snails

4.3.7. Sub-optimal conditioning did not reveal significant change in spontaneous or CS-evoked CGC firing rates

Comparison of spontaneous CGC firing frequency, prior to CS application, between experimental groups revealed no significant difference following sub-optimal conditioning (Kruskal-Wallis test, $p = 0.87$). This suggests there is no change in the background firing rate of CGC at 1 hr ($n = 7$), 2 hr ($n = 6$) and 4 hr ($n = 6$) following suboptimal conditioning compared to untrained snails ($n = 7$). There was also no significant change in the firing frequency of CGC during AA perfusion of the lips in any group of snails, either before or after training (Wilcoxon test, Bonferroni correction, before vs during; untrained, $p = 0.44$; 1 hr, $p = 0.94$; 2 hr, $p = 0.31$; 4 hr, $p = 0.09$). This data is summarised in **Figure 4.11** and shown in greater temporal detail in **Figure 4.12**.

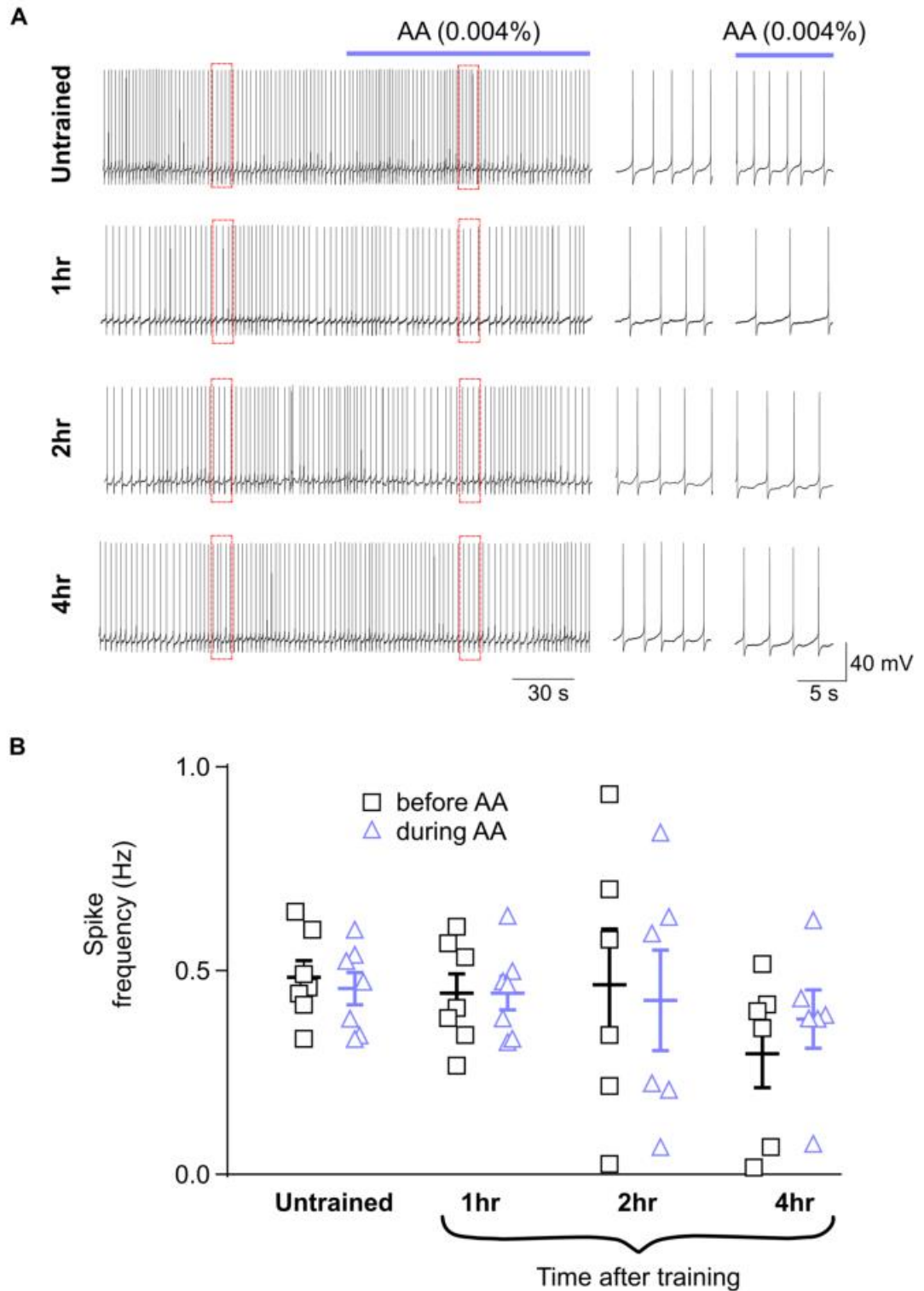


Figure 4.11. AA has little effect on CGC firing rate before or after conditioning. A.

Representative traces showing the firing activity of CGC before and during AA perfusion of the lips. Expanded traces taken from the red segregated boxes are shown to the right. **B.**

Chart showing the firing frequency of CGC for untrained ($n = 7$), 1 hour post-training ($n = 7$), 2 hours post-training ($n = 6$) and 4 hours post-training ($n = 6$) individuals.

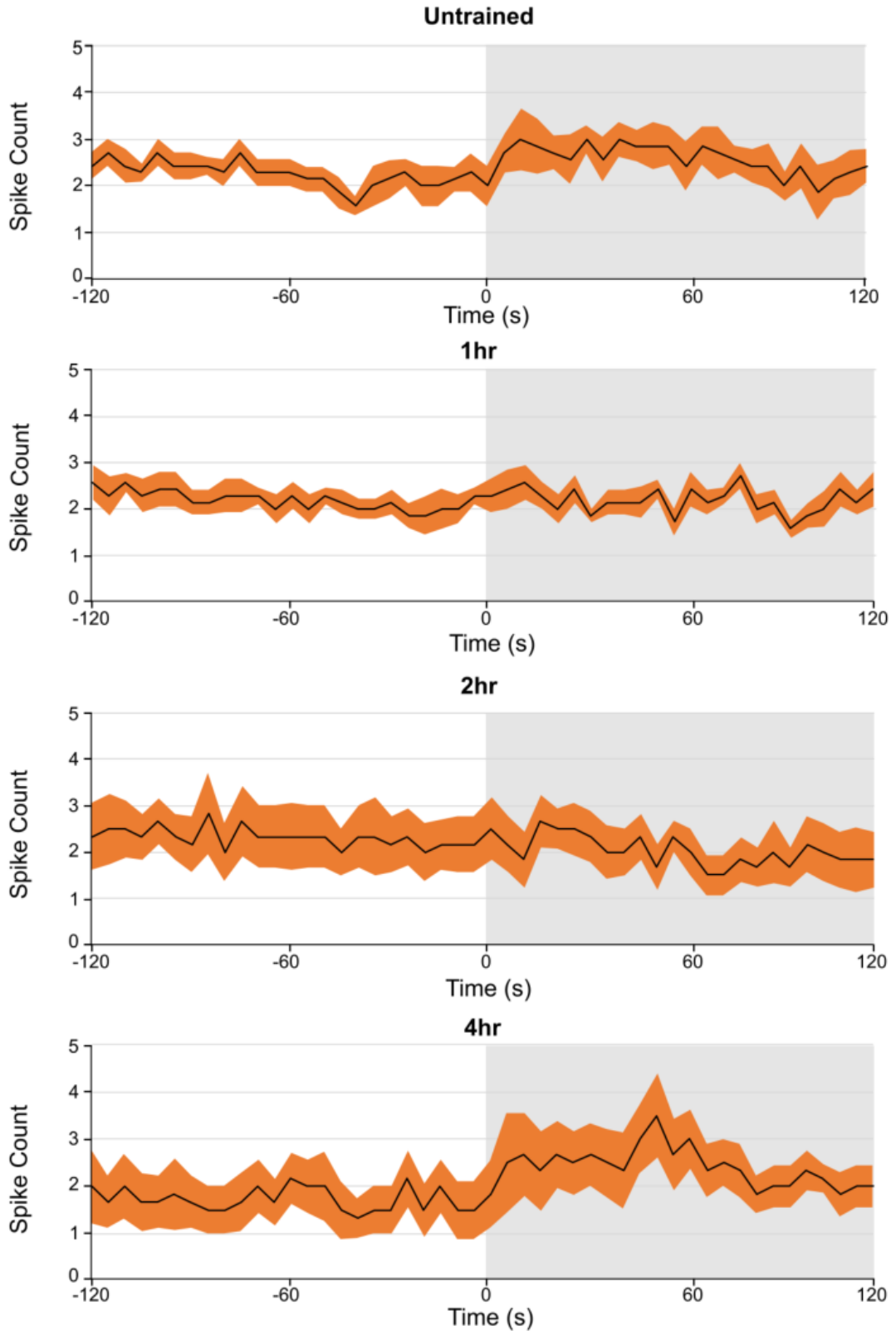


Figure 4.12. A more detailed temporal view of CGC spike activity during AA application.

Average spike counts taken from 5 s bins are shown for untrained ($n = 7$), 1 hr ($n = 7$), 2 hr ($n = 6$) and 4 hr ($n = 6$) groups. SEM is shown in orange.

4.3.8. No significant changes were found in CGC spike characteristics following sub-optimal conditioning

Analysis of the spike characteristics of CGC prior to the application of amyl acetate showed no significant difference between experimental groups for any parameter (Kruskal-Wallis test, RMP $p = 0.84$, afterhyperpolarisation $p = 0.81$, spike amplitude $p = 0.76$, spike halfwidth $p = 0.19$). Comparison of the RMP for each experimental group revealed no significant change caused by perfusion of the CS compared to prior activity (Wilcoxon test, Bonferroni correction, before vs during; untrained, $p = 0.56$ $n = 7$; 1hr, $p = 0.94$, $n = 7$; 2 hr, $p = 0.99$ $n = 6$; 4 hr, $p = 0.03 > 0.01$, $n = 6$). Afterhyperpolarisation also remained constant when comparing before versus during amyl acetate perfusion for conditioned and unconditioned groups (Wilcoxon test, Bonferroni correction, before vs during; untrained, $p = 0.69$; 1hr, $p = 0.58$; 2 hr, $p = 0.99$; 4 hr, $p = 0.16$). Spike amplitude showed no significant change during CS perfusion compared to preceding activity for any group (Wilcoxon test, Bonferroni correction, before vs during; untrained, $p = 0.16$; 1hr, $p = 0.58$; 2 hr, $p = 0.40$; 4 hr, $p = 0.31$). Lastly the difference in halfwidth caused by AA perfusion to the lips was nonsignificant for all experimental groups (Wilcoxon test, Bonferroni correction, before vs during; untrained, $p = 0.04 > 0.01$; 1hr, $p = 0.58$; 2 hr, $p = 0.22$; 4 hr, $p = 0.56$). This spike characteristic data is summarised in **Figure 4.13**.

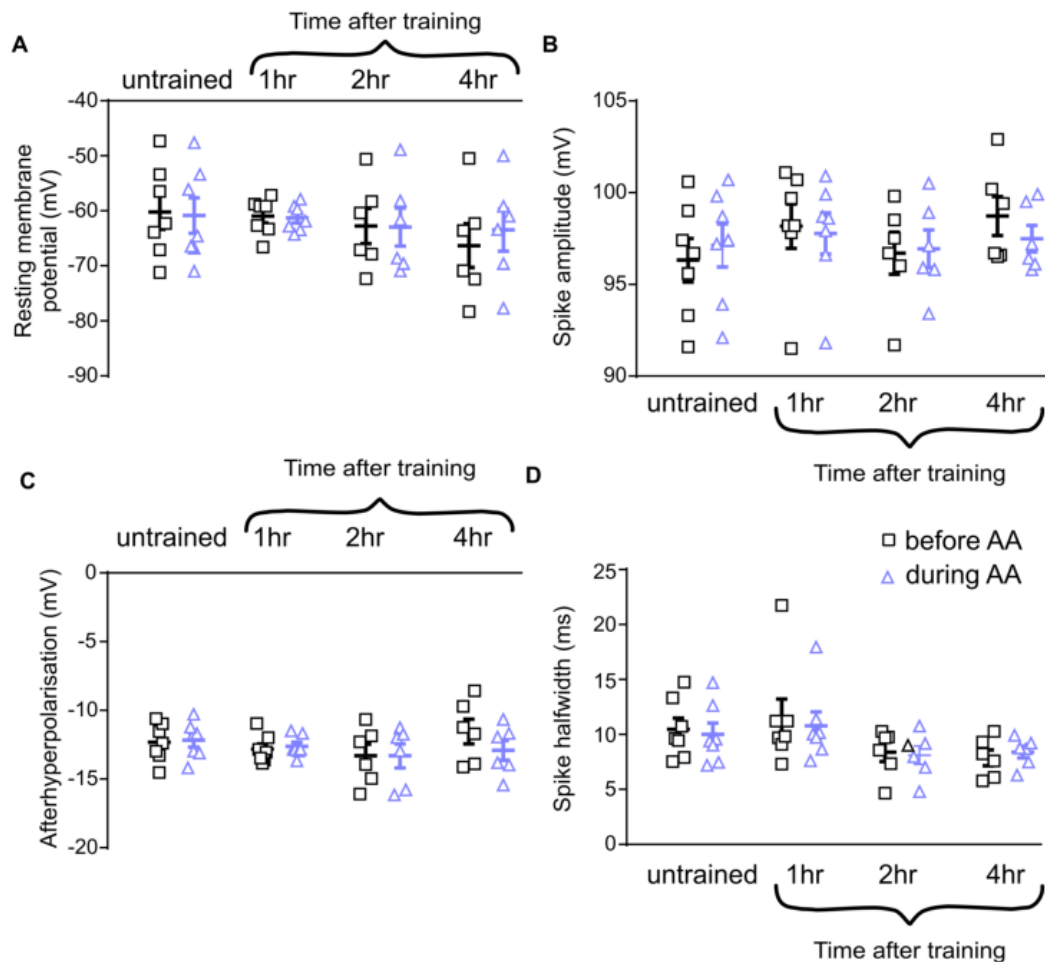


Figure 4.13. CGC spike characteristics reveal no change following AA application in trained or untrained snails. Data is shown for RMP (A), spike amplitude (B) afterhyperpolarisation (C) and spike halfwidth (D). Sample size were $n = 7$, untrained, $n = 7$, 1 hr post-training, $n = 6$, 2 hr post-training and $n = 6$, 4 hr post-training.

4.3.9. Sucrose caused significant increases in CGC firing frequency both in conditioned and unconditioned preparations

The response of CGC to sucrose was also analysed in both trained and untrained animals. As reported previously, administering sucrose causes an increase in CGC firing rate that is sustained throughout application (Kemenes *et al.*, 1986). Statistical analysis found that this increase was significant in all experimental groups, regardless of conditioning (Wilcoxon test, before vs during; untrained, $p = 0.01$, $n = 7$; 1 hr, $p = 0.01$, $n = 7$; 2 hr, $p = 0.03$, $n = 6$; 4 hr, $p = 0.03$, $n = 6$). This data is shown in **Figure 4.14** with representative traces and bar charts, and in more temporal detail in spike histograms in **Figure 4.15**.

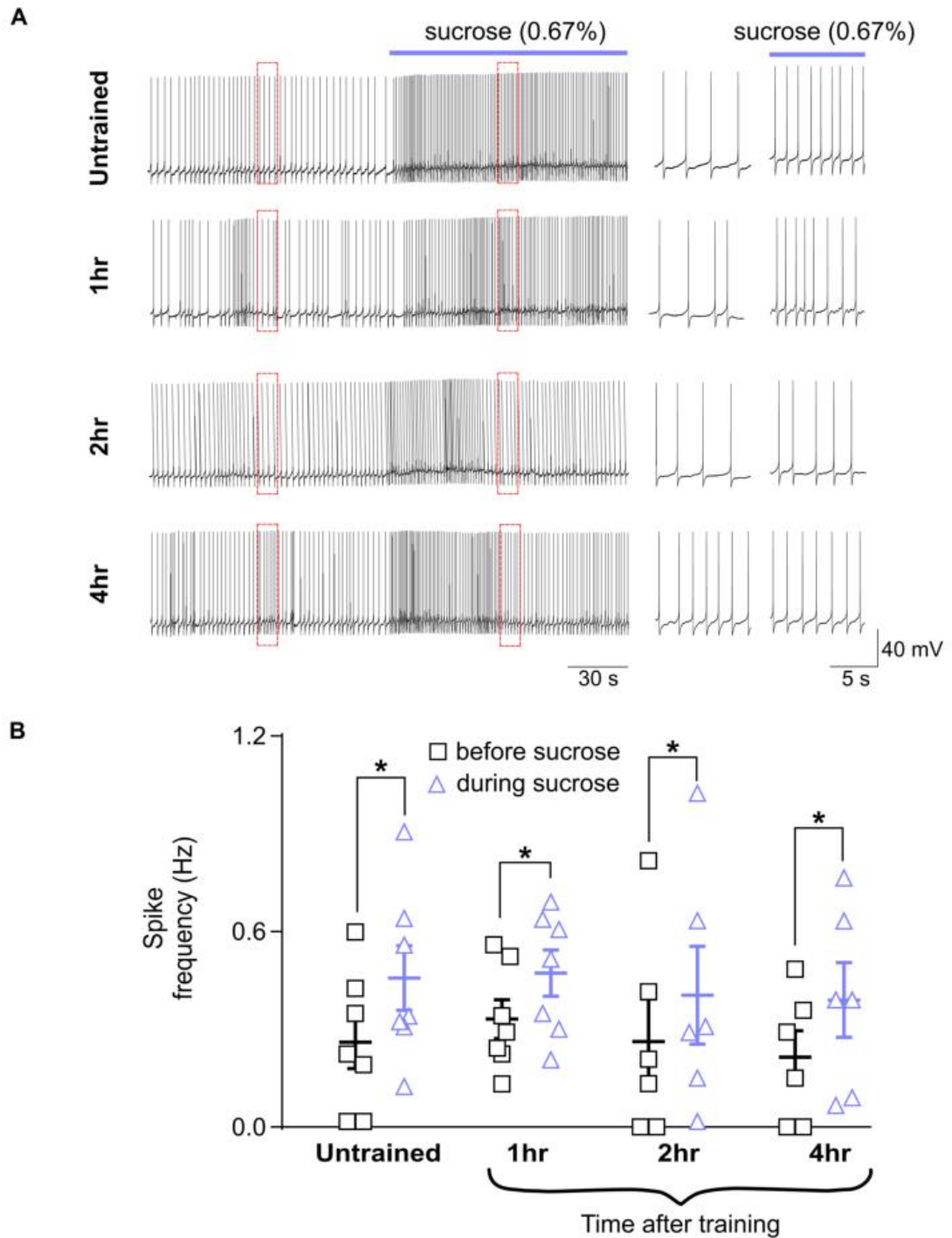


Figure 4.14. Sucrose causes a significant increase in CGC firing rate in both trained and untrained snails. A. Representative traces showing the firing activity of CGC before and during sucrose perfusion of the lips. Expanded traces taken from the red segregated boxes are shown to the right. **B.** Chart showing the firing frequency of CGC for untrained ($n=7$), 1 hour post-training ($n=7$), 2 hours post-training ($n=6$) and 4 hours post-training ($n=6$) individuals.

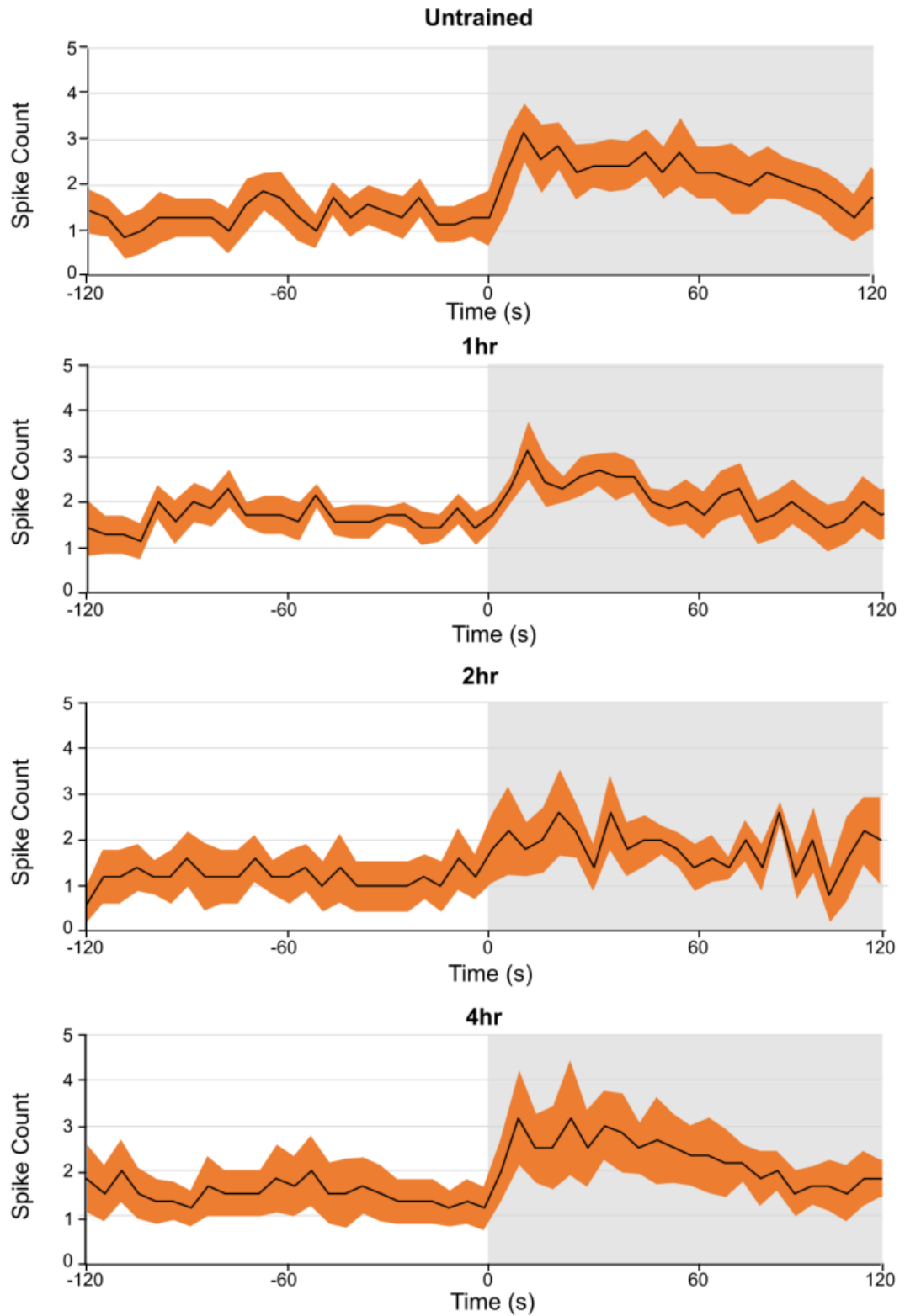


Figure 4.15. A more detailed temporal view of CGC spike activity during sucrose application. Average spike counts taken from 5 s bins are shown for untrained ($n = 7$), 1 hr ($n = 7$), 2 hr ($n = 6$) and 4 hr ($n = 6$) groups. SEM is shown in orange.

4.4. Discussion

Fluctuation in memory expression during consolidation of memory is a widespread phenomenon. However, it is unknown whether fluctuations are a by-product relating to the storage of memories, or whether they have adaptive value. Moreover, nothing is known about the neural basis for these memory lapses. The recent description of the Kamin effect in *Lymnaea* by Marra *et al.* (2013) has provided the opportunity to study identified neurons that may underlie this phenomenon. Single trial conditioning means that the stages of memory formation are temporally accurate, as it is known precisely when the consolidation process has begun. Two modulatory projection neurons were targeted in this study, CGC and PIB, as they have strong control over feeding activity which allows them to prevent or promote a feeding response at different times.

4.4.1. Nonsynaptic plasticity in the CGS and PIB neurons was not detected within either the lapse or non-lapse periods during memory consolidation

Cellular studies of appetitive memory in *Lymnaea* have revealed that neural plasticity often occurs in the background and lasts for prolonged periods of time. For example during ITM and early LTM it has been found that the inhibitory CPG neuron N3t shows a reduction in tonic firing rate, that reduces inhibition of N1M, and makes it more likely that a conditioned feeding response will occur (Marra *et al.*, 2010). This effect appears at both lapse (2 hr) and non-lapse (1 hr, 3 hr, 4 hr) time points suggesting that N3t is not responsible for any Kamin effect. For LTM of 24 hours or more it has been shown that CGC has a persistent depolarisation that facilitates the CS response (Kemenes *et al.*, 2006). Therefore, it was important to analyse the spontaneous firing rate and electrophysiological characteristics of the two target cells both in untrained and trained preparations.

For both CGC and PIB no significant changes were observed in RMP at 1 hr, 2 hr and 4 hr, compared to untrained. We, therefore, have no evidence for an effect of membrane potential at these time points after sub-optimal training. This is consistent with previous work recording CGC at 2 hr and 4 hr following optimal appetitive conditioning (Kemenes *et al.*, 2006). We also did not observe a significant change in

spike characteristics, such as spike halfwidth, which have shown plasticity in some other molluscan species following conditioning (Gandhi & Matzel, 2000). Lastly we did not observe a significant change in tonic firing rate for either modulatory neuron, which would have been a plausible mechanism based on the previously described N3t plasticity in *Lymnaea* (Marra *et al.*, 2010).

4.4.2. No response to the CS was detected in either the CGC or the PIB neurons after conditioning

In addition to persistent endogenous changes some neurons show a CS response that is either enhanced or appears only after conditioning. Examples of this in *Lymnaea* include a transient depolarisation in CV1a caused by amyl acetate application to the lips, that precedes rhythmic activity (Kemenes *et al.*, 2002). Another example is an EPSP in the B3 motoneuron, caused by lip touch, that is increased following tactile appetitive conditioning (Staras *et al.*, 1999a). Based on these findings it seemed possible that a similar mechanism could occur with CGC and PIB, so this was tested using CS application to the lips of semi-intact preparations. We did not observe any significant effects caused by CS application either before or after training, for both CGC and PIB. This cannot be attributed to unresponsive preparations as the CGC sucrose response served as a positive control, confirming that the chemosensory pathways were intact.

4.4.3. Low statistical power makes interpretation of the electrophysiological results of this chapter inconclusive

Power calculations were run based on the assumption of the presence of a strong statistical effect, and suggested group sample sizes of 20 would be necessary for strong statistical power in the sub-optimal conditioning results, that were analysed using a Kruskal-Wallis test in this chapter. Furthermore, analyses of before vs during electrophysiological activity, using the Wilcoxon matched pairs signed rank test, were calculated to require total sample sizes of 15, for a statistical power of 0.8.

Due to time constraints and the technical difficulty of these experiments the electrophysiological sample sizes were often much lower than was necessary. This makes the interpretation of these results difficult as low statistical power can prevent

the presence of real biological effects from reaching statistical significance. In the worst-case of section 4.3.4. where a total sample size of only 14 was reached, for the PIB sucrose response, the resultant statistical power was only 0.16, meaning that there can be little definitive conclusion reached. In the best-case example of section 4.3.9., examining the CGC sucrose response, a total sample size of 14 was reached, equivalent to a statistical power of 0.76. Although this experiment is more statistically robust than the previous example it is still possible that the unsatisfactory statistical power could have resulted in a false positive. Future experiments would require much larger n numbers in order to provide more robust data of effects.

4.4.4. Other possible loci underlying memory lapses

CV1a

Given that none of the data suggests a role for CGC or PIB in the 2 hr memory lapse, other cells within the feeding network will need to be studied. One probable candidate cell is CV1a, which has previously been found to show a CS response during LTM for chemical appetitive conditioning and has also been shown to be persistently depolarised in LTM following tactile appetitive conditioning (Kemenes *et al.*, 2002; Jones *et al.*, 2003). This cell can be considered downstream of CGC and PIB and is well situated anatomically to play an important role in chemosensory responses. It can also initiate feeding rhythms through strong connections with buccal feeding neurons (McCrohan & Kyriakides, 1989).

N1M

It is possible that during STM and ITM there is presynaptic facilitation from lip chemosensory neurons directly on to N1M. This facilitation could temporarily fail at 30 mins and 2 hr following sub-optimal conditioning, resulting in the observed memory lapses at these time points. This would be difficult to test as N1M is relatively inaccessible, small in size and shows complex electrophysiological activity.

4.4.5. Alternative experimental approaches

Nerve stimulation

In other molluscan species extracellular stimulation of the lip nerve (AT₄) and oesophageal nerve (EN₂) has been used as a substitute for the CS and the US,

respectively (Mozzachiodi *et al.*, 2003). This can be very useful as it negates the presence of chemosensory structures such as the lips, which cause lots of movement in the preparation and make the collection of stable recordings very difficult. An additional advantage of nerve stimulation is that it avoids unintentional interaction between perfused substances and the CNS, such as that observed with GNL. So far nerve stimulation has been underutilised in *Lymnaea* and it is possible that stimulation of the lip and oesophageal nerves could substitute for the CS and US, respectively. Indeed it has been shown that sucrose activation of the oesophagus is necessary for *in vitro* chemical appetitive conditioning in *Lymnaea* (Marra, 2009). One problem to overcome would be the possibility that lip nerve stimulation is aversive to feeding, rather than mildly appetitive, as this nerve carries many different processes. By calibrating the strength of extracellular stimulation, it may be possible to modify activation, so that it is perceived as relatively neutral by the feeding system, prior to CS-US pairing.

***In vitro* conditioning**

Another alternative experimental technique would be to use chemical *in vitro* training of semi-intact preparations, as in Marra *et al.* (2010). This is useful, as there is no delay between conditioning of the animal and recording of neurons, which normally occurs by the need to carry out a dissection. It also gives a direct recording of the state of feeding neurons during acquisition of the memory, as well as its later expression. However, it is worth noting that this technique is relatively difficult, as the semi-intact preparation moves due to chemosensory structures, and learns less readily than the intact animal, resulting in weak memory formation (Marra, 2009).

Chapter 5: A novel parietal neuron that controls feeding modulation

5.1. Introduction

The previous chapters have examined the role of modulatory projection neurons in the consolidation of appetitive memory. This chapter will focus on expanding the known feeding modulation circuitry, in order to aid the understanding of appetitive memory storage. The output effects of modulatory projection neurons have been extensively studied. Currently there are three major identified cells that project to the buccal ganglia and whose activity influences feeding. The first, CGC, a tonically active cell, is known to gate feeding activity by increasing its release of serotonin in the presence of food (Yeoman *et al.*, 1994). Through this release CGC has both immediate synaptic effects and long term endogenous effects on buccal neurons that act to promote feeding (McCrohan & Benjamin, 1980b; Yeoman *et al.*, 1996; Straub & Benjamin, 2001). CV1a is a smaller modulatory projection neuron, which is also located in the cerebral ganglion, but with a cell body found at the intersection between the superior/medial lip nerve (McCrohan & Kyriakides, 1989). CV1a is often rhythmically active during sucrose driven feeding rhythms, and when artificially stimulated can reliably drive feeding, via N1M (McCrohan & Kyriakides, 1989; Kemenes *et al.*, 2001). Another modulatory projection neuron, PIB, projects from the pleural ganglia to the buccal ganglia, via the pedal and cerebral ganglion. It is tonically active and when stimulated it releases FMRFamide which strongly inhibits all types of feeding neuron, including the CGC (Alania & Sakharov, 2000; Alania *et al.*, 2004). CV1a is the only feeding cell that shows 1:1 IPSPs from PIB, demonstrating its importance in feeding modulation.

Despite a detailed understanding of the output of these three modulatory projection neurons, very little is known about presynaptic neurons that control their activity. Only recently it was discovered that PIB receives monosynaptic excitation during aversive touch, from a withdrawal neuron known as PeD12 (Pirger *et al.*, 2014).

This provides the neural pathway for the behavioural precedence of withdrawal over feeding.

The aim of this work, summarised in **Figure 5.1** was to search for and identify another neuron which could control modulatory projection neurons. This neuron will be termed parietal dorsal 4 (PD4) and will be characterised in terms of its morphology and connections. Then its effect on different behavioural networks will be studied. Lastly, its response to sensory stimulation and extracellular nerve stimulation will be tested.

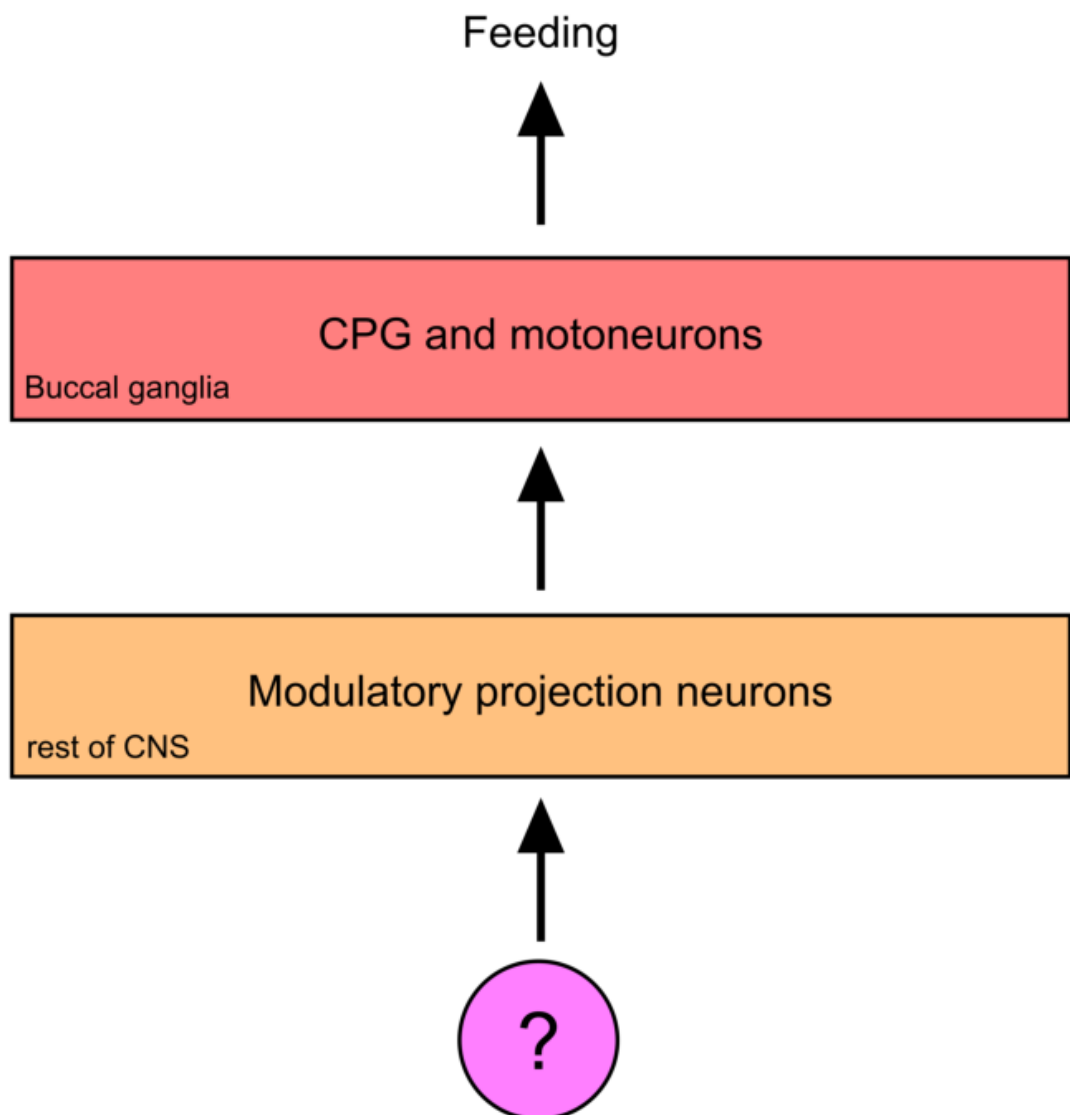


Figure 5.1. The aim of this chapter was to identify a neuron presynaptic to the modulatory projection neurons of the feeding system.

5.2. Methods

5.2.1. Preparations

The most commonly used isolated CNS preparation consisted of the entire brain with the dorsal surface facing upwards and the cerebral commissure severed. In some cases both the cerebral and pedal commissures were kept intact and the cerebral ganglia were turned over to access the CGC. When the connections between left PD4 and the buccal ganglia were tested, the left CGC was hyperpolarised and the right CBC was severed. This helped to reduce polysynaptic effects.

In order to test the response of PD4 to sensory stimuli it was necessary to use semi-intact preparations. As described in the previous chapter the lip was kept attached to the brain via the lip and tentacle nerves. To test chemosensory responses the preparation was continuously perfused with NS and then sucrose was applied for 2 minutes. To test tactile responses in the same preparation a glass capillary was touched against the lip using a manipulator. CGC was always recorded to confirm known chemosensory and tactile responses (Kemenes *et al.*, 1986).

5.2.2. Cell identification

All the known neurons in the *Lymnaea* CNS were identified by a combination of their position, their characteristic firing activity and their connections with other cells. For example, PD4 was always identified by co-recording a CGC with it and observing an excitatory connection. Therefore, all recordings of PD4 also contained a CGC, but for simplicity this was not always shown in figures. A general summary diagram of all the neurons recorded in the chapter is shown below in **Figure 5.2**.

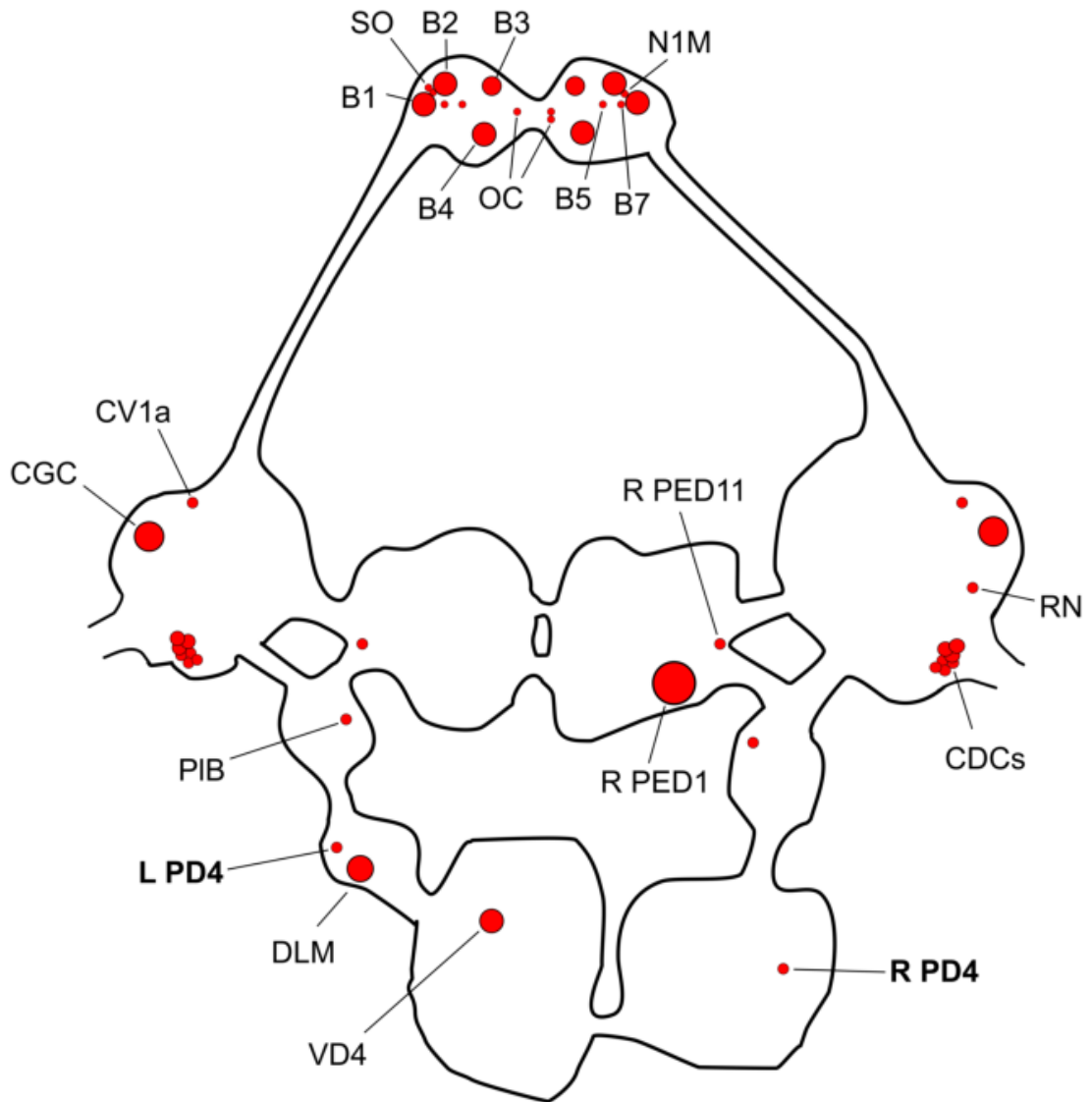


Figure 5.2. Simplified diagram of the dorsal view of the CNS in *Lymnaea* showing all of the identified cells recorded in this chapter. Note that PD4 can be found in both the left and right parietal ganglia. B1-7: buccal motoneurons, N1M: N1 medial, SO: slow oscillator, OC: octopamine cell, CGC: cerebral giant cell, CV1a: cerebral ventral 1a, CDCs: caudodorsal cells, RN: ring neuron, R PeD1: right pedal dorsal 1, R PeD11: right pedal dorsal 11, PIB: pleural-buccal interneuron, PD4: parietal dorsal 4, DLM: dorsal longitudinal muscle motoneuron, VD4: visceral dorsal 4. For simplicity all nerves have been omitted.

5.2.3. Intracellular dye filling

To examine cellular morphology, the AlexaFluor 568 dye (Thermo Fisher Scientific, Molecular Probes) was dissolved to a final concentration of 10 mM, in 200 mM potassium chloride (Sigma-Aldrich) electrolyte solution. A glass electrode was then backfilled with the dye solution and placed into the bath. During impalement continuous positive current was passed through the electrode, to reduce dye leakage into not-target cells. Once a stable impalement of the desired cell had been achieved a neurolog NL301 pulse generator was activated which injected negative current pulses of >1 nA lasting for 0.5 s and occurring at a rate of 1 Hz (0.5 s on, 0.5 s off). This pulsing was carried out for at least 20 minutes and for up to an hour. Once the recording was completed the preparation was stored at 4 °C overnight in a solution containing NS and 10 mM probenecid (Sigma-Aldrich). Probenecid is thought to reduce anion dye leakage from the cell (Steinberg *et al.*, 1987; Perry *et al.*, 1998).

The next day the preparation was returned to a Sylgard dish containing NS. The cerebral commissure was severed, allowing the brain to be laid flat. The brain was then transferred to a glass cavity slide, placed under a cover slip and viewed using a Leica SP8 laser scanning confocal microscope in Leica application Suite X software. In order to obtain an image of the dye filled neuron the preparation was excited using a 15% intensity Argon 561nm laser and emission was collected in the 575-660nm range using a 2 AU pinhole and HCX PL APO CS 10x/0.40 dry objective. Due to the large size of the cell it was necessary to collect Z stacks of overlapping tile regions (x: 2048 pixels, 1550 μ m, Y: 2048 pixels 1550 μ m, Z: 66 pixels 282.27 μ m). In ImageJ each z stack was converted to a single image using maximum projection. All the regions were then combined using the MosaicJ and TurboReg plugins (Thevenaz & Unser, 2007).

5.2.4. Modified saline

In a small number of experiments a high divalent (HiDi) saline was used throughout to assess the nature of synaptic connections between PD4 and other cells. This HiDi saline consisted of 35 mM NaCl, 2 mM KCl, 8.0 mM MgCl₂.6H₂O, 14 mM CaCl₂.2H₂O and 10 mM HEPES in reverse osmosis water adjusted to a PH of 7.9 using NaOH (Sigma-Aldrich). The effect of HiDi saline is to raise the spike threshold of neurons, reducing

the likelihood of polysynaptic connections (Berry & Pentreath, 1976; Winlow *et al.*, 1981).

5.2.5. Nerve stimulation

Nerves were identified as according to Kyriakides *et al.* (1989). Once found the nerve was sucked into a glass electrode of suitable size, along with normal saline. The glass electrode was contained in a custom holder with one silver wire within the electrode saline and the other in the bath. Once PD4 had been successfully impaled, stimulation was triggered by a TTL pulse from the ADC to a Grass SD9 stimulator. The standard stimulation was of 5 V lasting for a total of 0.5 s (biphasic, <2 ms delay, 5 ms duration, 10 Hz).

5.3. Results

5.3.1. PD4 has a widespread morphology

The initial search for a cell with connections to modulatory projection neurons involved searching with a sharp electrode within the cerebral ganglia. Repeated short-term recordings by chance from a location in the cerebral ganglia indicated the existence of a modulatory input to the CGCs. Simultaneous dye filling during these recordings revealed that the site of the recording was the axon of a cell, with the soma located in the distant parietal ganglion ($n = 2$). The soma was subsequently impaled with an electrode on the dorsal surface of the parietal ganglion, making it possible to make long-term recordings and to optimally dye fill the cell. Based on the cell's anatomical location it was termed parietal dorsal 4 (PD4).

Dye filling using the PD4 soma reveals an extensive cellular morphology that passes through many different ganglia, as can be seen in **Figure 5.3/4** ($n = 7$). The soma is located within the parietal ganglion and is approximately 40 μm in diameter. It gives rise to a large axon that projects through the pleural ganglion into the cerebral ganglion. Within the cerebral ganglion the axon branches extensively. One major axonal branch continues straight up the CBC, into the ipsilateral buccal ganglion and then crosses the midline via the buccal commissure. Another branch crosses the midline via the cerebral commissure and then passes up the contralateral CBC, again

entering the buccal ganglion. The end result is that PD4 enters the buccal ganglia via both CBCs. Interestingly within both the ipsilateral and cerebral ganglion additional branches travel to the anterior lobe where they form looped barrel structures. Given the strong synaptic connection between PD4 and CGC it seems plausible that this is the location of the CGC soma being wrapped by the axon of the PD4.

Another projection is also observed within the visceral ganglion but no direct connection can be seen to the parietal soma. This projection can be seen passing into a visceral nerve which is either the anal or intestinal nerve, which lie on top of one another. Additionally, there is an unknown soma within the pedal ganglion, of similar diameter to the primary soma (40 μm). This soma remained unidentified.

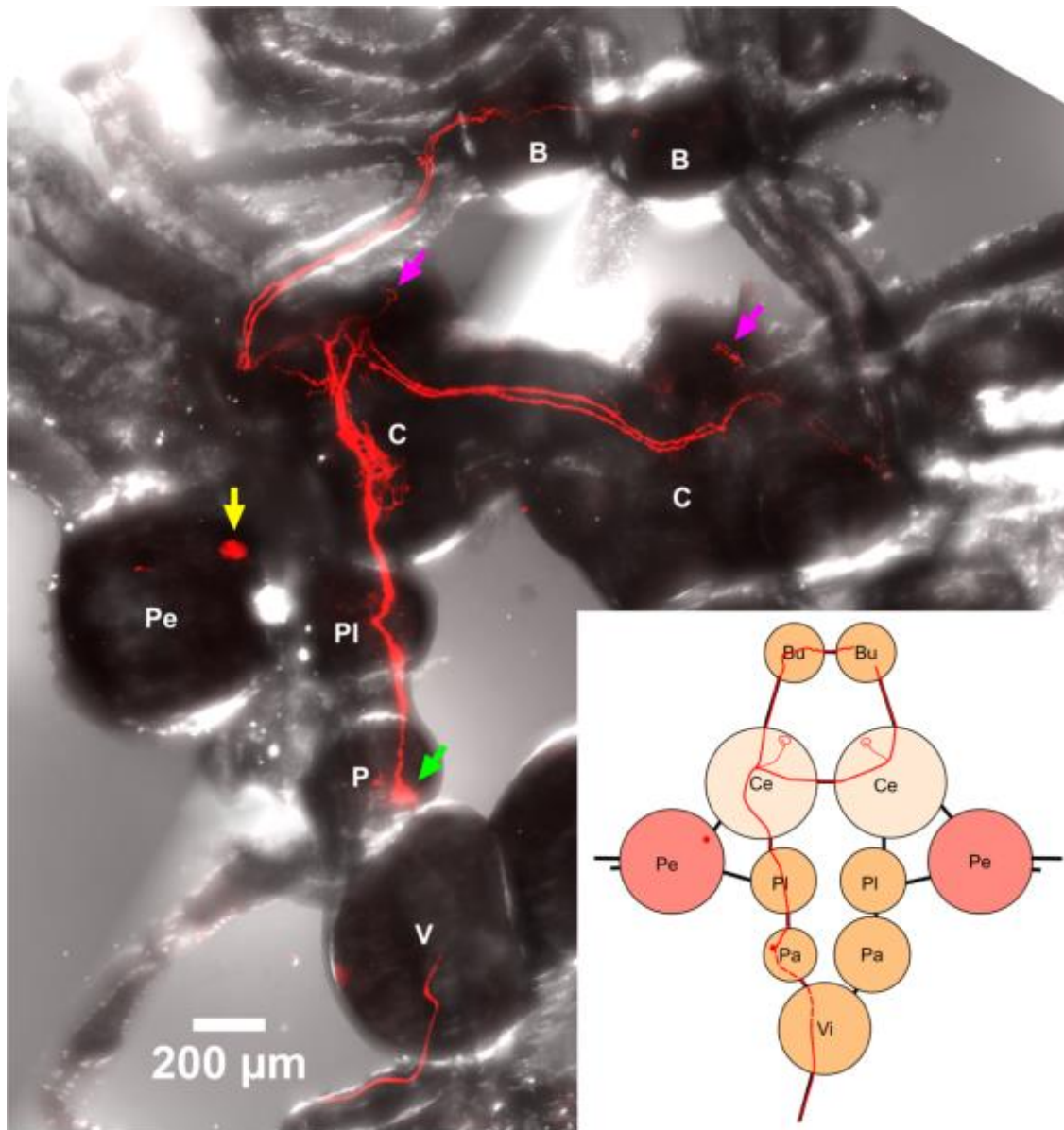


Figure 5.3. PD4 has an extensive morphology on both sides of the brain. Dorsal view of the brain after intracellular dye filling of PD4 with Alexa Fluor 568. The light green arrow indicates the PD4 soma, the light pink arrows indicate barrel-like structures formed by PD4 axon, the yellow arrow indicates an unknown soma within the pedal ganglion. Inset is a cartoon image summarising the morphology of the cell. The dashed line is inferred to be axon unobserved below the surface. B – buccal ganglion, C – cerebral ganglion, Pe – pedal ganglion, Pl – pleural ganglion, P – parietal ganglion, V – visceral ganglion.

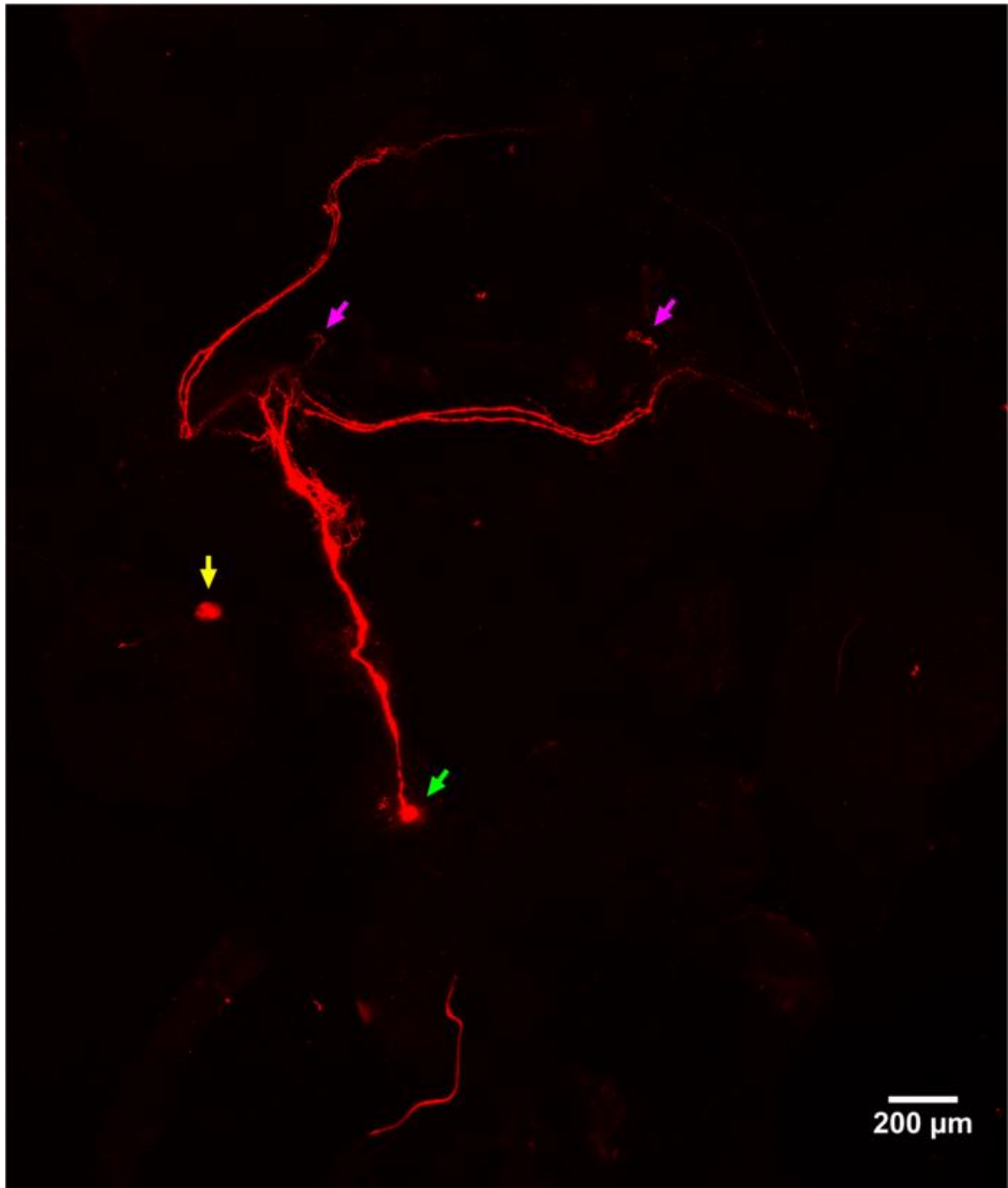


Figure 5.4. PD4 morphology following intracellular dye filling. The same preparation as the previous figure, but showing only the fluorescence. The light green arrow indicates the PD4 soma, the light pink arrows indicate barrel-like structures formed by PD4 axon and the yellow arrow indicates an unknown soma within the pedal ganglion.

5.3.2. Each PD4 directly excites both the ipsilateral and contralateral CGC

Once the PD4 morphology was known its connections with the modulatory projection neurons of the feeding system were more closely studied. The cell was usually quiescent, so it was necessary to depolarise the cell using intracellular current. When this was done, strong excitation of both the ipsilateral and contralateral CGC could be observed, as in **Figure 5.5A**. Surprisingly stimulation of PD4 had no effect on its contralateral partner ($n = 2$), unlike CGC and PIB, which synapse in the buccal ganglia (**Figure 5.5A**).

Figure 5.5B shows a recording from a reduced preparation, where the buccal ganglia were removed, so that the CGCs were no longer connected to each other. This abolishes synchronous action potentials between the two CGCs, showing that PD4 both strongly excites the ipsilateral CGC and weakly excites the contralateral CGC ($n = 12$). Furthermore, this connection persists in HiDi saline, and 1:1 EPSPs that follow PD4 action potentials are reliably observed (**Figure 5.5C**, $n = 6$). Furthermore, the EPSP from PD4 to the ipsilateral CGC appears to be both of greater amplitude and duration than that in the contralateral CGC (but note that each CGC was hyperpolarised).

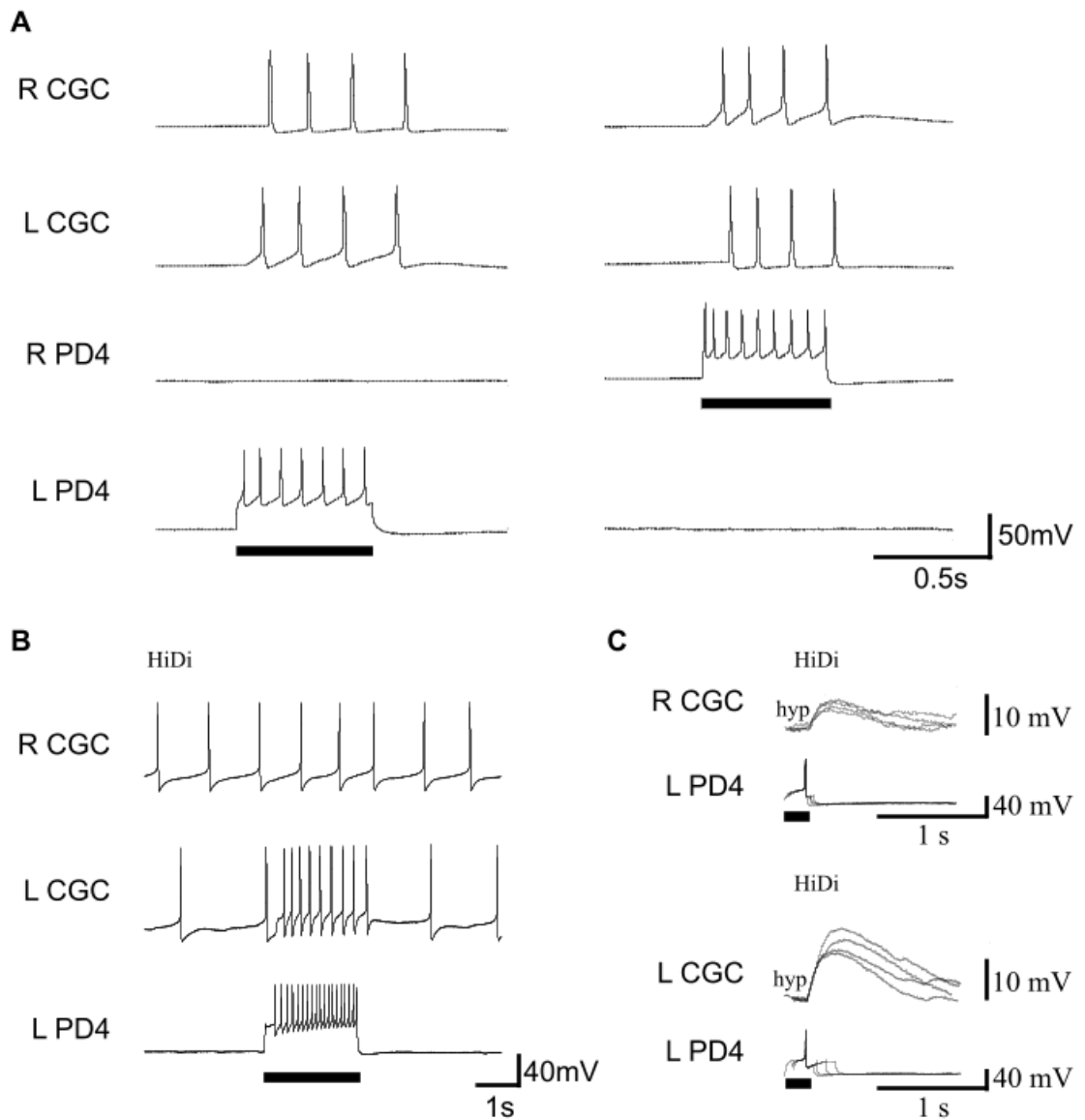


Figure 5.5. PD4 directly excites both the ipsilateral and contralateral CGC. **A.** PD4 exists on both sides of the nervous system and can excite CGC. Each PD4 does not excite its contralateral partner ($n = 2$). **B.** In a reduced preparation bathed in HiDi saline, PD4 activation causes an increase in firing of both the ipsilateral and the contralateral CGC ($n = 6$). Note that the effect is stronger in the ipsilateral CGC. **C.** Closer inspection reveals 1:1 EPSPs from PD4 onto both the contralateral and ipsilateral CGC. Black bars under a trace indicate depolarising current to the cell.

5.3.3. PD4 also synapses with other modulatory projection neurons of the feeding system

Given that PD4 synapses with CGC it seemed likely that it also had connections with other modulatory projection neurons. For example, it was possible that it had an effect on the tonic inhibitory neuron PIB and the rhythmic excitatory neuron CV1a. Indeed, stimulation of PD4 resulted in a slow inhibition of PIB which caused the cell to stop firing, as can be seen in **Figure 5.6A** (n = 1). This inhibition remained in HiDi saline and is shown in **Figure 5.6B** (n = 2). No 1:1 IPSPs could be observed on PIB. The effect of PD4 on PIB outlasted the stimulation time.

Stimulation of PD4 was also found to cause a slight depolarisation of CV1a that was not strong enough to cause the cell to fire (**Figure 5.6C**, n = 5). This connection persisted in HiDi saline, but again no 1:1 PSPs could be seen (**Figure 5.6D**, n = 3). It is possible that it is the cessation of firing in PIB that causes the CV1a depolarisation, through a drop in inhibition. This cannot be ruled out because HiDi saline did not prevent PIB from firing spontaneously, as can be seen in **Figure 5.6B**. In support of this possibility the effects of PD4 stimulation also outlasted activity in the cell again.

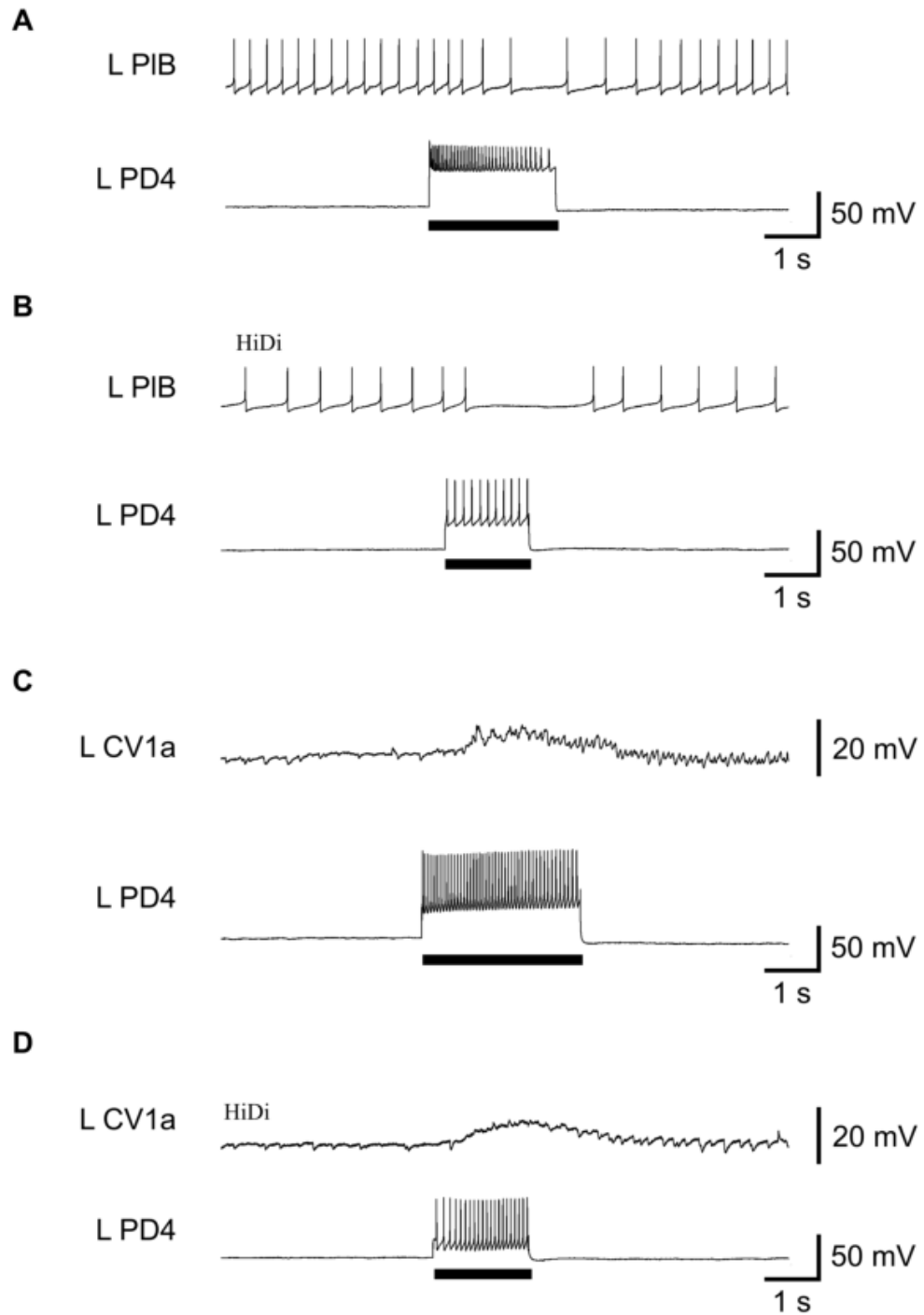


Figure 5.6. PD4 stimulation causes slow inhibition of PIB and slow excitation of CV1a. A. When PD4 is artificially stimulated this causes a reduction in the firing activity of PIB ($n = 1$). **B.** Inhibition from PD4 to PIB persists in HiDi saline ($n = 2$). **C.** Artificial stimulation of PD4 also causes a depolarisation in CV1a ($n = 5$). **D.** In the presence of HiDi saline PD4 still causes a depolarisation of CV1a ($n = 3$). Black bars under a trace indicate depolarising current to the cell.

5.3.4. PD4 does not synapse with identified dorsal buccal feeding neurons

PD4 was also tested for possible effects on dorsal buccal feeding neurons as dye filling had revealed that the cell projects to this ganglion. In order to reduce polysynaptic effects CGC was hyperpolarised during this experiment and the contralateral CBC was cut.

Given that PD4 had already been found to synapse with modulatory projection neurons, it seemed plausible that it also had control over buccal modulatory neurons. Two well characterised buccal modulatory neurons are the octopamine cell, which promotes feeding via polycyclic effects (Elliott & Vehovszky, 2000), and the slow oscillator which can initiate feeding (Rose & Benjamin, 1981). However, when PD4 was activated it had no effect on either the octopamine cell ($n = 2$) or the slow oscillator ($n = 1$) (**Figure 5.7A, B**).

It was also possible that PD4 had a direct connection with the key CPG neuron N1M. This would allow PD4 to directly initiate feeding. However artificial activation of PD4 did not cause any change in the N1M membrane potential ($n=3$), as can be seen in **Figure 5.7C**. In addition, most of the major motor neurons were also recorded whilst stimulating PD4. As can be seen in **Figure 5.7D-I** this had no effect on any of the motor neurons (B1 $n = 2$, B2 $n = 1$, B3 $n = 5$, B4 $n = 10$, B5 $n = 1$, B7 $n = 1$). In summary no connection was found from PD4 to any identified dorsal buccal feeding neurons.

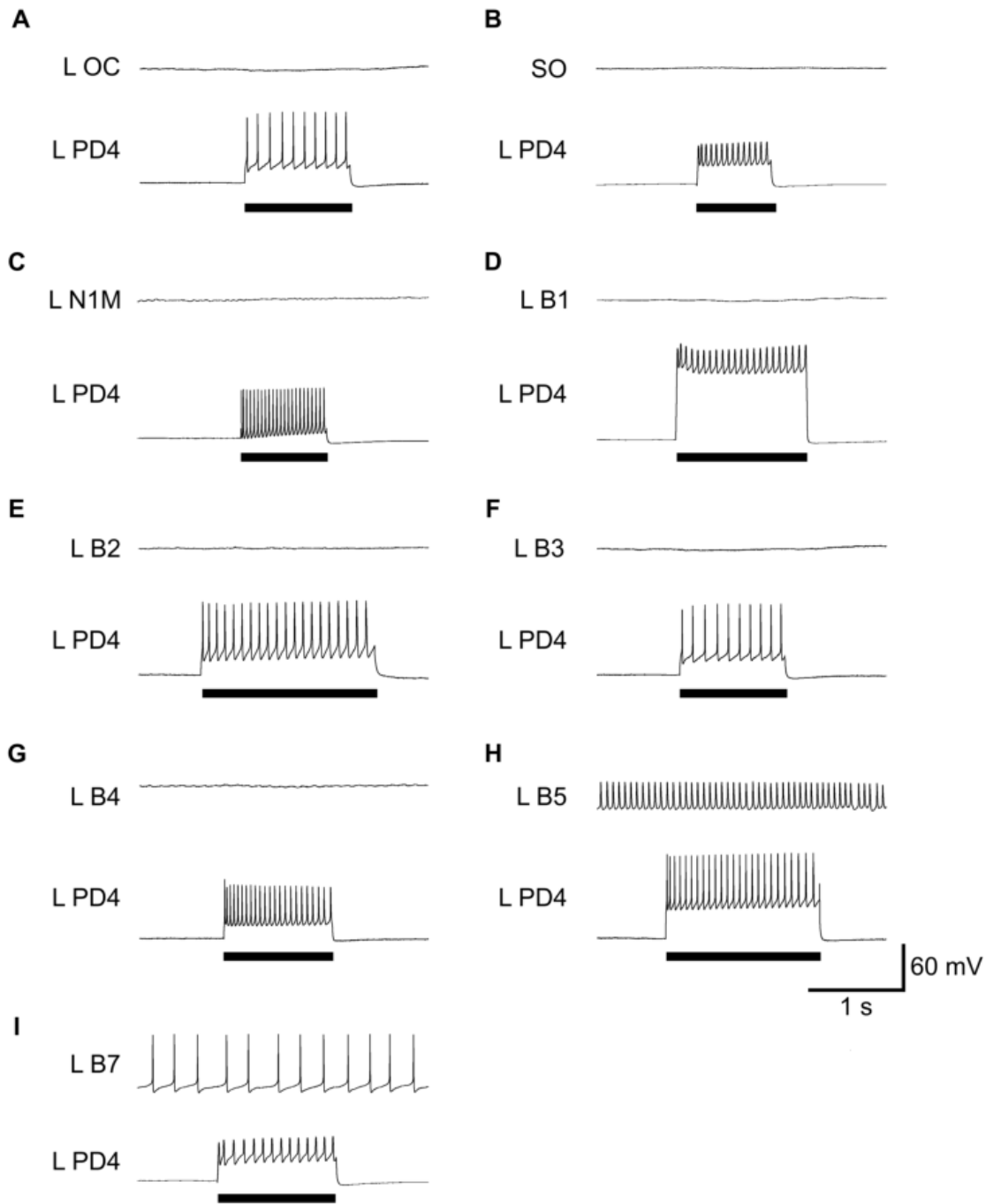


Figure 5.7. PD4 stimulation does not affect identified dorsal buccal feeding neurons.

Recordings were made in preparations with a hyperpolarised left CGC (not shown) and a cut right CBC. Firing of the left PD4 did not cause an effect on the buccal feeding neurons OC (**A**, $n = 2$), SO (**B** $n = 1$), N1M (**C** $n = 3$), B1 (**D**, $n = 2$), B2 (**E**, $n = 1$), B3 (**F**, $n = 5$), B4 (**G**, $n = 10$), B5 (**H**, $n = 1$), or B7 (**I**, $n = 1$). Note that SO and OC are modulatory, N1M is a CPG neuron and B1-7 cells are motor neurons. Black bars under a trace indicate depolarising current to the cell.

5.3.5. PD4 influences feeding but is not a command neuron

The finding that PD4 depolarised higher order neurons that promote feeding (CGC, CV1a) and hyperpolarised a higher order neuron that inhibits feeding (PIB), suggested that this cell could be a feeding command neuron, as defined by Kupfermann and Weiss (1978). To test this hypothesis PD4 was stimulated in the isolated brain whilst rhythmic feeding neurons were recorded. Weak stimulation of PD4 was capable of causing fictive feeding, as shown in **Figure 5.8A**. However, this effect was not reliable and a stronger stimulation of PD4 did not guarantee fictive feeding, as shown in **Figure 5.8B** (n = 9). Interestingly long-lasting depolarisation of PD4 in a preparation already showing feeding rhythms actually prevented their occurrence. An example of this can be seen in **Figure 5.8C**. This inhibitory effect may be due to PD4 causing polysynaptic excitation of the inhibitory neuron N3t via CGC (Yeoman *et al.*, 1996).

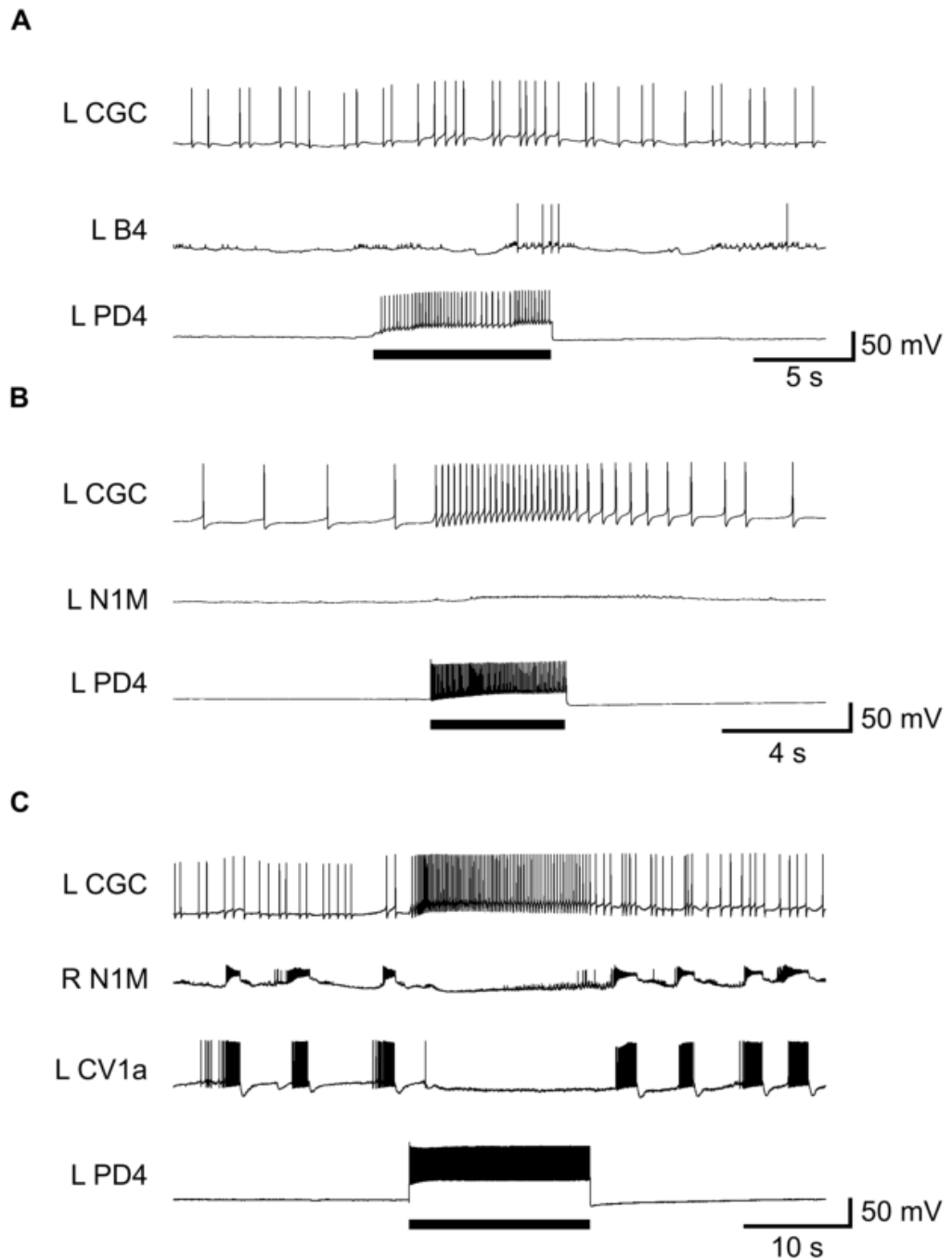


Figure 5.8. PD4 can initiate or end fictive feeding depending on its activation. A. A relatively light depolarisation of PD4 causes two fictive feeding cycles observed using the swallow motor neuron B4. **B.** In a different preparation strong stimulation of PD4 does not cause fictive feeding i.e. N1M does not become active. **C.** In a preparation showing spontaneous fictive feeding prolonged strong stimulation of PD4 inhibits rhythmic activity. Once activity in PD4 ceases fictive feeding begins again. Black bars under a trace indicate depolarising current to the cell.

5.3.6. PD4 responds to touch but not sucrose to the lips

As well as examining the output effects of PD4 within the brain it was also important to identify inputs to the cell. One possibility was that PD4 played a role in known lip sensory pathways. It had already been found that CGC was excited by both touch and sucrose applied to the lips (Kemenes *et al.*, 1986) and it was possible that PD4 was upstream and necessary for this response. To test this hypothesis semi-intact lip-brain preparations were created (description in methods) and simultaneous recordings of CGC and PD4 were made (n=7). Both cells showed a touch response but they were opposite, with a depolarisation in the CGC and a hyperpolarisation in PD4. This can be seen in **Figure 5.9A**. When sucrose was applied to the lips, CGC responded with an increase in firing rate as expected. PD4 meanwhile remained completely quiescent, as shown in **Figure 5.9B**. Therefore, PD4 does not play an upstream role in the depolarisation of CGC, during tactile or chemosensory stimuli applied to the lips.

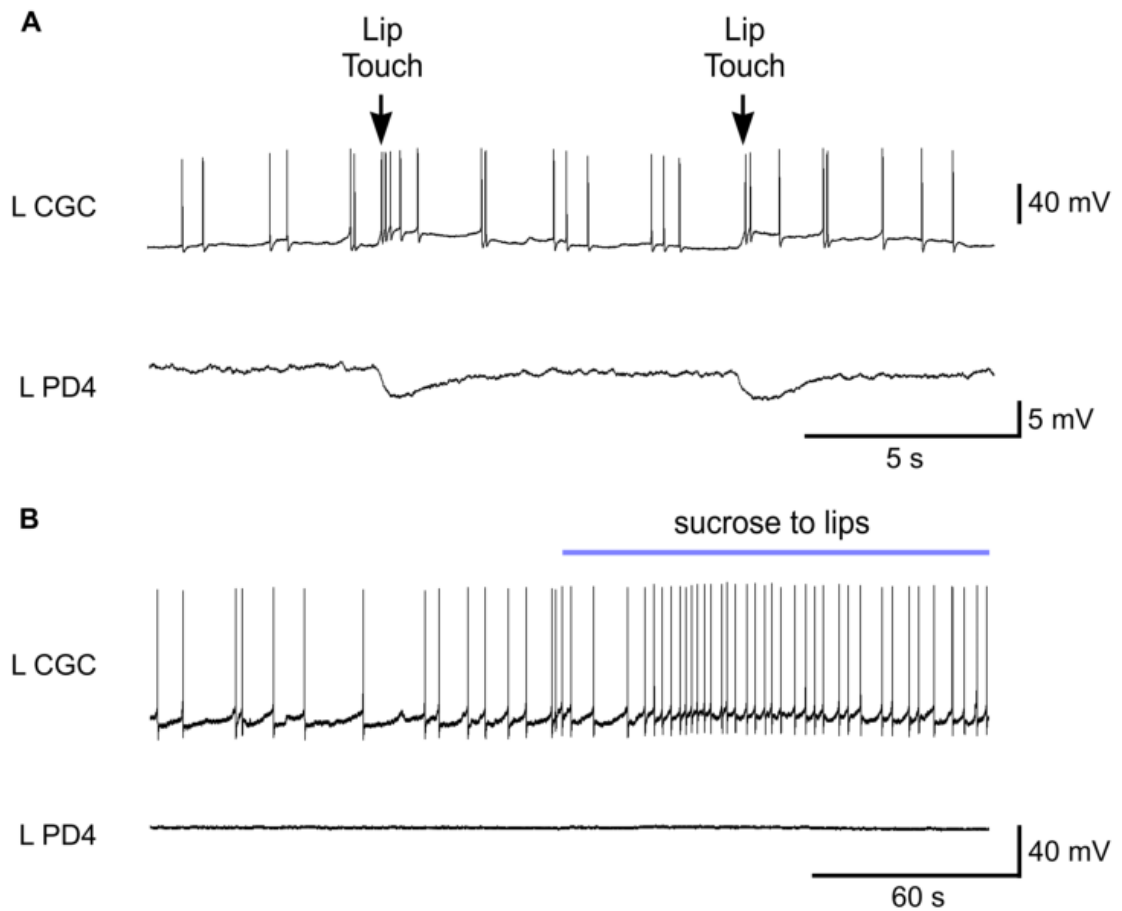


Figure 5.9. PD4 is not active during tactile and chemosensory responses. Recordings were made from lip-brain semi-intact preparations ($n = 7$). **A.** Tactile stimulation of the lip reliably causes a depolarisation of CGC and a hyperpolarisation of PD4. **B.** Applying sucrose to the lips increases the firing rate of CGC but has no effect on PD4 which remains quiescent.

5.3.7. PD4 inhibits the egg laying neurons

Given PD4's distant location from the buccal ganglia and connection with higher order neurons it seemed probable that the cell may interact with behavioural networks other than feeding. An obvious candidate was egg laying, which also utilises the buccal CPG and is known to cause an increase in the firing frequency of CGC (Jansen *et al.*, 1997; Jansen *et al.*, 1999). Egg laying is initiated by the neurohormonal caudodorsal (CDC) cells of the cerebral ganglia (Geraerts & Bohlken, 1976; Ter Maat *et al.*, 1989). Stimulation of either the left or right PD4 resulted in a long-lasting inhibition of ipsilateral CDC cells ($n=4$). No spontaneous afterdischarge in the CDCs was observed,

likely due to the severing of the cerebral commissure in these recordings. It was possible that inhibition of CDCs was via the ring neuron (RN) which is located in the right cerebral ganglia (Jansen & ter Maat, 1985) but although PD4 did excite this cell it remained below the threshold for firing ($n=2$). These findings are summarised in **Figure 5.10**.

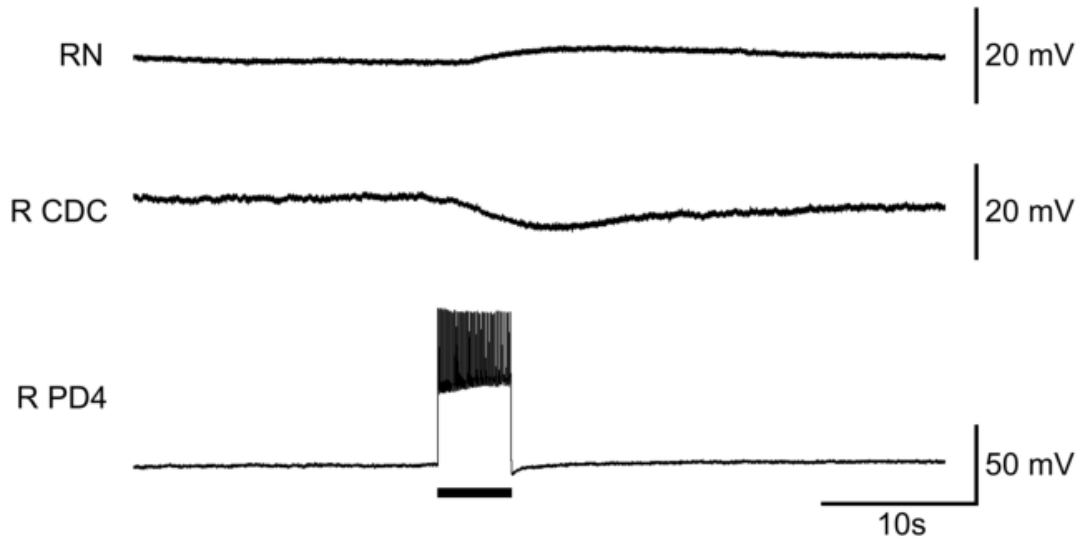


Figure 5.10. Stimulation of PD4 causes prolonged excitation of the ring neuron and inhibition of the CDCs. Black bars under a trace indicate depolarising current to the cell.

5.3.8. PD4 does not synapse with key cells of the cardiorespiratory and withdrawal networks

As PD4 had been found to synapse with more than one behavioural network it was also recorded alongside the withdrawal and cardiorespiratory networks. Specifically, stimulation of PD4 did not cause any change in the membrane potential of two cardiorespiratory CPG neurons, right pedal dorsal 1 (R PeD1, $n = 12$) and visceral dorsal 4 (VD4, $n = 1$), which remained inactive (Buckett *et al.*, 1990; Syed & Winlow, 1991b). PD4 stimulation also had no effect on the multifunctional neuron R PeD11 ($n = 1$) and the withdrawal neuron left parietal dorsal longitudinal muscle (DLM) motoneuron ($n = 1$) (Ferguson & Benjamin, 1991a; Syed & Winlow, 1991a). These results are shown in **Figure 5.11**.

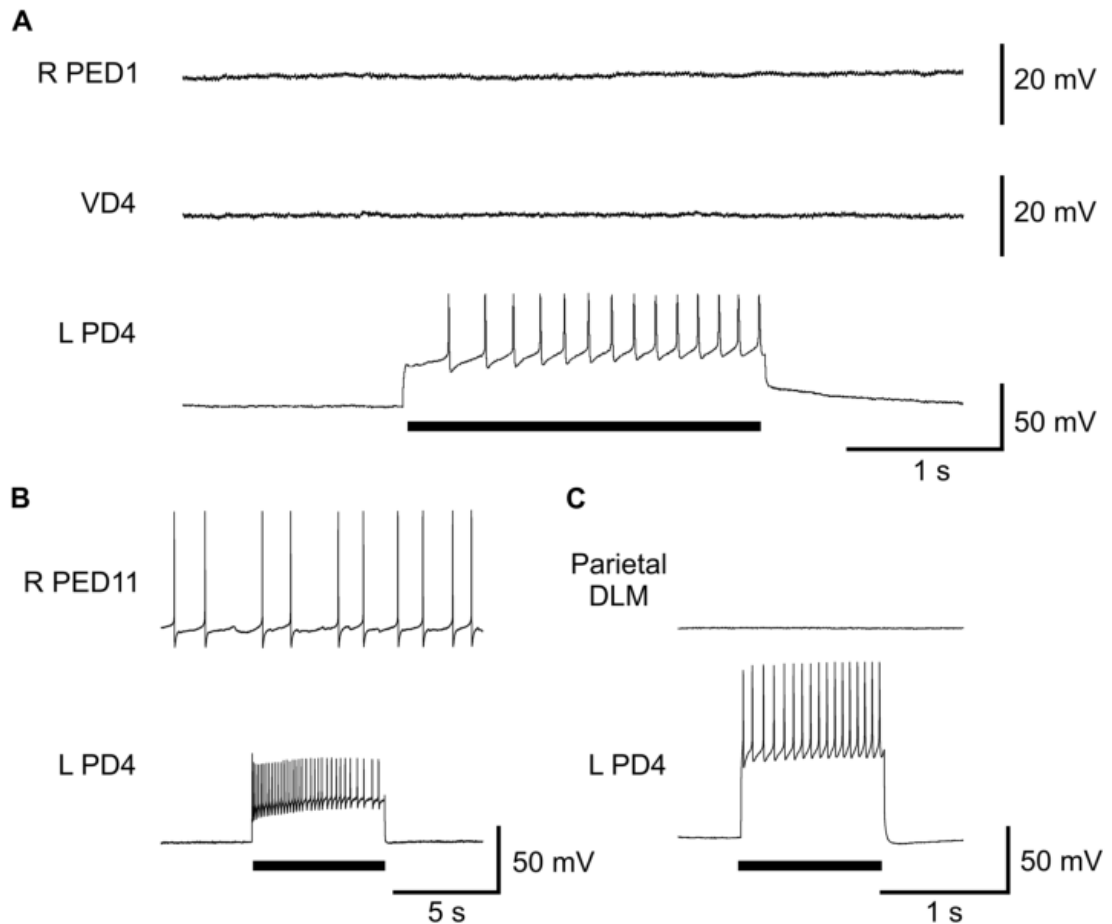


Figure 5.11. Stimulation of PD4 does not affect neurons of the cardiorespiratory and withdrawal networks. **A.** Depolarisation of PD4 does not cause an effect on R PeD1 or VD4 which are part of the respiratory CPG. **B.C.** Activity in PD4 does not affect neurons of the withdrawal system R PeD11 and parietal DLM motoneuron respectively. Note that R PED11 also influences cardiac neurons. Black bars under a trace indicate depolarising current to the cell.

5.3.9. PD4 can be activated by nerve stimulation

As relatively natural sensory stimuli had failed to activate PD4, extracellular stimulation of different nerves was tested in the isolated brain. PD4 was found to be activated by the stimulation of numerous different nerves including the superior lip nerve ($n = 5$), median lip nerve ($n = 5$), left parietal nerve ($n = 4$), right internal parietal nerve ($n = 6$) and anal/intestinal nerve ($n = 3$). Stimulation of the anal and intestinal nerves was carried out in the same preparations, as they both project from the same

ganglion and are of similar size. The two nerves were difficult to distinguish anatomically from one another, but stimulation of either in the same preparation could activate PD4. **Figure 5.12** which summarises the nerve stimulation data is shown below. Note that this shows data from a single visceral nerve which may have been either the anal or intestinal nerve, the two could not be distinguished.

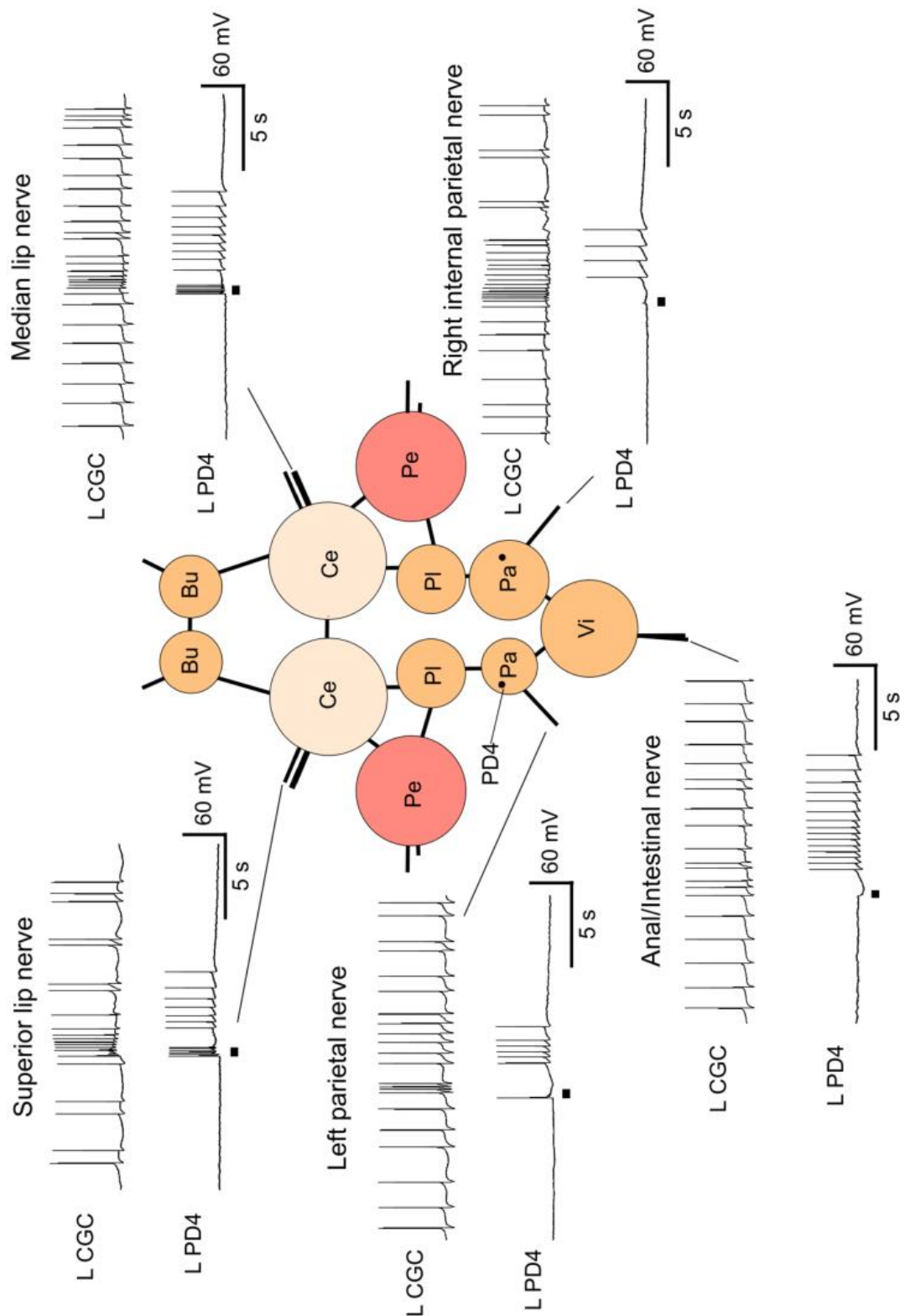


Figure 5.12. PD4 is activated by nerve stimulation. Note that PD4 was active during stimulation of the lip nerves and left parietal nerve but not the anal/intestinal or right internal parietal nerve. Black bars indicate extracellular nerve stimulation. For clarity many additional nerves are not shown.

5.4. Discussion

As shown in **Figure 5.13**, PD4 has a broad range of output effects in the brain but does not appear to receive any return inputs. In other words, all synapses that have been found are asymmetric, such that PD4 has control over feeding and egg laying cells. PD4 is also normally quiescent in isolated brains and semi-intact preparations, so it was necessary to artificially depolarise PD4 to study its output effects.

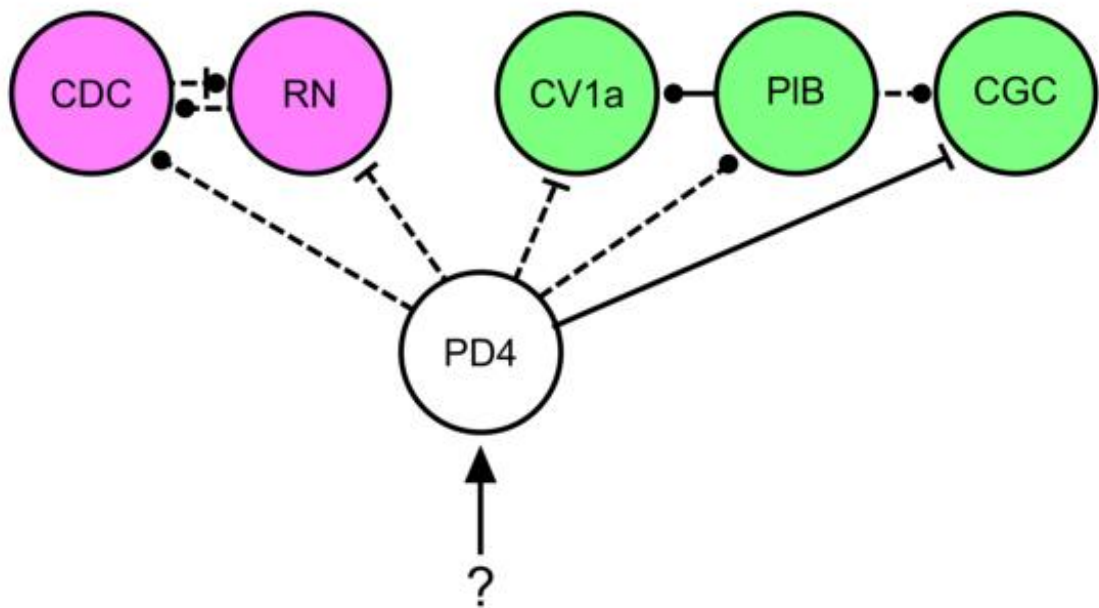


Figure 5.13. Summary circuit of the connections between PD4 and the rest of the brain.

Green cells represent feeding cells whilst purple cells represent reproductive cells. Solid lines represent monosynaptic connections whilst dashed lines represent polysynaptic/hormonal connections. Excitatory synapses are shown by bars and inhibitory synapses by dots. Note that the connection drawn between PD4 and CV1a may not exist, as inhibition of PIB could be sufficient to cause a depolarisation in CV1a.

5.4.1. PD4 influences feeding through modulatory projection neurons

Interestingly it appears that PD4 does not influence feeding directly through the CPG but instead acts on modulatory projection neurons. Based simply on the known effects

of these modulatory projection neurons, and the polarity of the synaptic connections, one would assume that PD4 would act to promote feeding. This would be supported by the strong, presumably monosynaptic activation of PD4 during stimulation of the superior and median lip nerves. However, it is important to note that the strongest connection is excitatory to the CGC, with large long lasting monosynaptic EPSPs. This gives a complicated effect on the feeding system because strong activation of PD4 can drive firing in CGC well in excess of 1 Hz. At these frequencies it appears that a polysynaptic pathway between PD4, CGC and N3t dominates, and causes strong inhibition of the feeding CPG (N1M). This effect on feeding through N3t has previously been reported for very strong stimulation of CGC (see Figure 6A, in Yeoman *et al.*, 1996). It demonstrates the importance of knowing the natural (physiological) *in vivo* firing rates of a cell in order to understand its effects on a network. Based on the current data it seems likely that long-term low frequency activity in PD4 will promote feeding, whereas short-term higher frequency activity is likely to inhibit feeding. This raises the problem that modulation of feeding often occurs over long time scales, making the output effects of the cell more difficult to study. For example, slow modulatory effects on the buccal feeding CPG have been reported from the OC and CGC lasting for several minutes (Yeoman *et al.*, 1996; Vehovszky *et al.*, 2004). It is certain that PD4 is not a feeding command neuron as activity in this cell did not reliably initiate fictive feeding.

5.4.2. PD4 may play a role in the later stages of egg laying

In addition to its effects on feeding it was also discovered that PD4 had important connections with reproductive cells. Reproduction is very complex in *Lymanaea* as each individual is hermaphroditic and can reproduce both sexually and asexually (Koene, 2010). The best characterised part of the reproductive network is female and consists of the CDCs, a large group of electrically coupled neuropeptide cells, found close to the cerebral commissure (de Vlieger *et al.*, 1980). Through both their electrical connections and autoexcitatory transmitters the CDCs can carry out an all or nothing afterdischarge, consisting of high frequency synchronous firing that lasts for several minutes (Ter Maat *et al.*, 1986). This afterdischarge is responsible for the initiation of egg laying behaviour.

Once initiated, egg laying consists of four distinct sequential behaviours; resting, turning, oviposition and inspection (Ter Maat *et al.*, 1989). Resting lasts for around 40 minutes, and is followed by a turning phase, where the animal begins to locomote within a small area, and the shell is repeatedly rotated in respect to the foot, for approximately an hour. This is followed by the oviposition phase, lasting for 10 minutes, when the animal lays the egg sac on to the substrate. Finally, the animal inspects the egg sac by passing along it and making contact with the lips and tentacles. Throughout both the turning and oviposition phase the buccal CPG is active, with the radula used to clean the surface on which the egg sac will be stuck (Jansen *et al.*, 1997; Jansen *et al.*, 1999). CGC firing frequency is also elevated during these two phases (Jansen *et al.*, 1999).

Given the data above, it is plausible that PD4 plays a role in the egg laying process. Specifically, PD4 could become active in the turning and oviposition phases, that occur after the CDC afterdischarge, and could drive CGC activity and rasping. In support of this idea, severing of the intestinal nerve has been reported to be necessary for the turning behaviour, suggesting a signal from peripheral reproductive organs is necessary (Ferguson *et al.*, 1993). Through its peripheral projection PD4 may be a component in a unidirectional pathway from the reproductive organs to the feeding system. This would also make sense as PD4 activity during the turning phase would suppress the CDC afterdischarge. Tactile feedback when the lips touch the egg sac during the inspection phase could also act to inhibit PD4.

Despite PD4's peripheral projection it only showed a delayed excitation during anal/intestinal nerve stimulation, probably via a polysynaptic pathway. During the extracellular stimulus PD4 showed an inhibition, seemingly counterintuitive when stimulating the nerve. One possible explanation is that there was a monosynaptic connection from an inhibitory cell on to PD4 which overrides excitation during the extracellular stimulation. In some cases, neuronal somata have been found within nerves and would likely be more strongly activated by the extracellular stimulation (Elekes *et al.*, 1991).

In addition to connections to the CDCs, PD4 was also found to excite the RN. The function of the RN is less well understood, but it is known to inhibit the CDCs

(Jansen & Bos, 1984; Jansen *et al.*, 1985). In turn the CDCs appear to indirectly both excite and inhibit the RN by delayed actions (Jansen & Bos, 1984). Some have hypothesised that the ring neuron is male as it only exists on the right side, and receives EPSPs when the penis nerve is stimulated (Jansen *et al.*, 1985). Alternatively, the RN could be female and simply involved in a later phase of egg laying following the afterdischarge. In support of this, stimulation of RN affects motor neurons of the columellar muscle, which could be involved in the turning phase (Jansen & ter Maat, 1985).

5.4.3. PD4 was not found to have connections with the withdrawal or cardiorespiratory networks

The connections of PD4 with behavioural networks other than feeding and reproduction were also tested. The withdrawal network is a well characterised group of electrically coupled cells, which become active together, following sufficiently aversive stimuli (Ferguson & Benjamin, 1991b; Syed & Winlow, 1991a; Pirger *et al.*, 2014). Despite this, artificial PD4 stimulation did not induce activity in R PED11 or the parietal DLM, ruling out activation of the entire withdrawal network.

If PD4 activity represented a general arousal state in the snail, connections would be expected with the cardiorespiratory network. To examine this PD4 was artificially stimulated whilst recording key neurons of this network. It was shown that activation of PD4 does not cause any activation or rhythm in two respiratory CPG neurons, R PED1 and VD4 (Syed & Winlow, 1991b). This also suggests little effect on the cardiac network as VD4, R PED1 and R PED11 have previously been found to synapse with cardiac motor neurons (Buckett *et al.*, 1990; Syed & Winlow, 1991a). However, this does not rule out possible connections between PD4 and other downstream cell types within this network, such as cardiac motoneurons.

5.4.4. Similar higher order neurons exist in other molluscs

Similar examples of higher order neurons which act on multiple behavioural networks exist in other molluscs, except the somata are located in the cerebral ganglia. In *Aplysia* the cerebral-pedal regulator (CPR) excites the metacerebral cell (MCC) and cerebral-buccal interneuron 2 (CBI-2), which are homologous to CGC and CV1a in

Lymnaea, respectively (Teyke *et al.*, 1990; Teyke *et al.*, 1997). However, unlike PD4, CPR is activated by food and/or touch in semi-intact preparations. CPR also acts to increase cardiac activity and inhibits withdrawal neurons, effects that were not found for PD4. CPR activity also effects neck motoneuron activity which is thought to alter the animal's posture to favour feeding. In *Aplysia* two electrically coupled cerebral neurons CC9/10 that initiate locomotion also excite the MCCs monosynaptically below firing threshold (Jing *et al.*, 2008). In *Pleurobranchia* similar modulatory neurons involved in locomotion, As1-4 of the cerebral ganglia, also monosynaptically excite the metacerebral giant cell (MCG), equivalent to CGC in *Lymnaea* (Jing & Gillette, 2000). This raises the possibility that PD4 similarly modulates locomotion in *Lymnaea*. It is known that movement of *Lymnaea in vivo* increases the firing rate of CGC prior to encountering food (Yeoman *et al.*, 1994). A connection with the locomotion network could explain the unidentified pedal soma observed during the dye fill, if PD4 was electrically coupled to the cell. Such dye coupling through electrical junctions has previously been reported in *Lymnaea* in some cases using biocytin and lucifer yellow (Audesirk *et al.*, 1982; Ewadinger *et al.*, 1994).

Chapter 6: General discussion

The feeding behaviour of *Lymnaea stagnalis* is very well characterised at the behavioural, cellular and molecular levels. This has allowed for extensive study of the alteration of feeding behaviour following classical conditioning and in nearly all cases modulatory neurons have been found to be the cell type responsible (Jones *et al.*, 2003; Kemenes *et al.*, 2006; Marra *et al.*, 2010). Therefore, the aim of this thesis was to further characterise modulation of the feeding system and its role in appetitive memory formation.

In the first results chapter a key modulatory neuron, the CGC, was manipulated by inserting artificial voltage-gated ion channels into the membrane. This allowed a previously described mathematical model of the cell to be tested, to see if it could account for nonsynaptic plasticity that is known to occur >24 hours after conditioning. It was found that the artificial conductances could not depolarise the cell significantly and also caused significant changes in spike characteristics. This suggests that the voltage gated conductances that control the CGCs cellular activity are more complex than described by the model.

In the next chapter the same cell, CGC, and an inhibitory neuron, PIB, were recorded during STM, ITM and LTM following sub-optimal conditioning. This weak conditioning paradigm causes memory lapses. However, no change could be identified in the electrical activity of these two modulatory neurons, when compared to untrained individuals. This suggests that neither modulatory cell shows plasticity at these particular time points after appetitive conditioning.

In the final section a novel quiescent neuron was identified with control over all major modulatory projection neurons (CCG, CV1a, PIB). This neuron could not reliably initiate feeding, and did not respond to sucrose applied to the lips, proving it does not play a command role. The cell also had an inhibitory effect on egg laying initiation neurons (CDCs), suggesting it may coordinate feeding and egg laying, two behaviours that have previously been associated (Jansen *et al.*, 1997; Jansen *et al.*, 1999).

6.1. Using dynamic clamp to simulate nonsynaptic plasticity in a modulatory neuron

The development of dynamic clamp as technique has shown great potential in the ability to directly test mathematical models on living cells (Prinz *et al.*, 2004). In an early example Ma and Koester (1996) used dynamic clamp of the *Aplysia* R20 neuron, to examine the ionic basis of action potential broadening that occurs during spike trains. By addition and subtraction of different artificial voltage-gated potassium channels, they showed that a relative change in the maximum conductance of these channels over time determines action potential width.

6.1.1. Testing learning-induced changes predicted by a mathematical model revealed that further physiological parameters need to be taken in to consideration

In this work dynamic clamp was utilised to directly test electrophysiological parameters of a modulatory interneuron of the feeding system (CGC), that is also part of the engram coding for LTM. By using the already existing model by Vavoulis *et al.* (2010), it was tested whether a persistent depolarisation could be induced in untrained preparations. This Hodgkin-Huxley type model was created by using voltage-clamp and current clamp data from earlier studies of CGC (Staras *et al.*, 2002; Nikitin *et al.*, 2006). It was then validated by removing certain conductances, in order to replicate the effects of pharmacological blocking and ion substitution (Staras *et al.*, 2002). Once completed this model was used to predict that addition of three model conductances I_{NaP} , I_K and I_{HVA} would be sufficient to depolarise the RMP of CGC, without significant change in spike characteristics, thus emulating what is seen following appetitive conditioning (Kemenes *et al.*, 2006).

This work revealed that when applying the dynamic clamp to test nonsynaptic plasticity it was important to accurately estimate the total cell surface of CGC. This was necessary as the biophysical model gives the maximum conductance per unit area, of each channel. Initially it was thought that an approximation of a sphere, based on the visible diameter of the cell soma, would be a sufficiently good measure. However,

injection of conductances, based on this approximation, revealed little effect on cellular activity. Therefore, a more accurate method of determining the cell surface area was used prior to application of the artificial conductances. This method relies on measuring the response of the cell to subthreshold sinusoid current injection.

Calculations based on this sine wave revealed that the true surface area of CGC is approximately 9 times greater than a perfect sphere. Similar surface area disparities have previously been reported for giant molluscan neurons in *Anisodoris* (Mirolli & Talbott, 1972), *Aplysia* (Coggeshall, 1967; Graubard, 1975; Pinsker *et al.*, 1976; Fejtl *et al.*, 1995) and *Tritonia* (Longley, 1984). Therefore, to account for this, the surface area of each CGC was calculated at the beginning of each recording and the maximum conductance of each artificial channel was scaled up accordingly.

Once corrections had been made to the maximum conductance of each channel the dynamic clamp experiments were repeated. Surprisingly simultaneous injection of I_{NaP} , I_K and I_{HVA} still did not significantly alter the CGC RMP, but did cause unpredicted changes in halfwidth and spike frequency. These results suggest that the biophysical parameters underlying learning induced changes are more complex than predicted by the existing model.

6.1.2. Ectopic spikes prevent artificial CGC depolarisation

As model conductances had failed to depolarise the CGC a simpler approach was taken. At the beginning of each recording a voltage vector was extracted and 5 mV was added to each element, simulating the electrophysiological effect of classical conditioning (Kemenes *et al.*, 2006). This depolarised voltage vector was then applied back on to the same CGC using a pattern clamp configuration. When the CGC was forced into this depolarised state, this caused insuppressable ectopic spikelets to be observed, often prior to the intended action potential. By recording the contralateral CCG, it was found that the ectopic spikelets observed in the leader soma, triggered full size action potentials in the follower soma. This suggests that action potentials were being initiated in the leader CGC, outside of the soma, and passing to the follower CGC, via the buccal ganglia. Given the voltage-clamp results of Staras *et al.* (2002), it seemed reasonable to assume that axotomisation of CGC would be sufficient to prevent these space-clamp issues. However, the ectopic spikelets remained even when the CBC was

severed. This is consistent with previous reports that the spike initiation zone of CGC lies in the proximal axon, within the cerebral ganglion, and therefore escapes axotomisation (McCrohan & Benjamin, 1980a; Goldschmeding *et al.*, 1981). The disparity in space clamp issues between the voltage clamp study (Staras *et al.*, 2002), and this one, are likely explained by the difference in the pattern of activity the clamp was attempting to force on to the cell. In voltage clamp the cell is being forced immediately to a fixed value, whilst here the voltage was ramping up, within the natural spike initiation range, alongside a significant background depolarisation. This highlights a major limitation in dynamic clamp; that the microelectrode is limited to one point of current injection within the cell, normally the soma (Prinz *et al.*, 2004). This means that it is not possible to perfectly replicate the true distribution of ion channels in the cellular membrane. In relatively small neurons with simple morphologies this may not be an issue, but in larger cells such as CGC it can result in a loss of control as observed here.

6.2. Searching for the neural basis of the Kamin effect

Following weak conditioning it has been shown in numerous vertebrate and invertebrate species that memory expression can disappear and reappear during the consolidation process (Gerber & Menzel, 2000; Hosono *et al.*, 2016). This has come to be known as the Kamin effect, based on the author's early description of the phenomenon in rats (Kamin, 1957).

6.2.1. Training with different conditioning stimuli results in identical temporal occurrence of the Kamin effect

As with all other reported cases, the Kamin effect is observed in *Lymnaea* when animals show weak learning. This is achieved by the use of *in vitro* conditioning of a semi-intact preparation or *in vivo* conditioning of intact snails with a weakened US (Marra *et al.*, 2013). In both conditioning paradigms, memory expression fails at 30 minutes and 2 hours following conditioning, but at all other time points is present. As is demonstrated in this thesis, the effect is independent of the CS used, as it is present

when either amyl acetate or gamma-nonolactone are given. This supports the theory that the Kamin effect is a widespread phenomenon caused by underlying weaknesses in the molecular cascades that form memory (Marra *et al.*, 2013).

6.2.2. A functional role for two key modulatory feeding neurons, CGC and PIB, in the Kamin effect, could not be found

In addition to *Lymnaea* being an excellent model of appetitive memory consolidation, the feeding network is also very well characterised (Benjamin, 2012). This presents the ideal opportunity to observe plasticity in the nervous system before, during and after memory lapses. In this thesis two key identified modulatory neurons, the CGC and PIB, were recorded both during and outside of a 2 hour lapse point. They were chosen as targets because they have widespread connections with neurons of the feeding system, including CPG neurons, motor neurons and other modulatory neurons (McCrohan & Benjamin, 1980b; Yeoman *et al.*, 1996; Alania *et al.*, 2004). This could allow them to initiate or suppress a conditioned feeding response at different time points.

Despite examining both spontaneous firing frequency and CS response firing frequency, during lapse and non-lapse points, we did not observe significant effects in either PIB nor CGC caused by appetitive conditioning. A more detailed analysis of spike characteristics also showed no significant difference between trained and untrained preparations. This suggests that these cells may not play a role in memory consolidation at 1, 2 and 4 hours after sub-optimal conditioning. This would be consistent with previous results of Kemenes *et al.* (2006) on CGC that showed no change in firing frequency at 2 and 4 hours following optimal chemical appetitive conditioning. However due to low sample sizes the statistical power during analysis was insufficient during these experiments, meaning that a possible effect has not been conclusively excluded. Therefore, future experiments with improved sample sizes will be needed.

6.3. A newly identified neuron, PD4, has a strong influence over the feeding and egg laying networks

To better understand the control of feeding system, a search was made for neurons presynaptic to known modulatory cells. This identified a novel parietal neuron, termed parietal dorsal 4 (PD4), which is capable of strong monosynaptic excitation of CGC both ipsilaterally and contralaterally. Stimulation of this cell also caused slower acting depolarisation of CV1a and similarly delayed inhibition of PIB. In all three cases synaptic effects were asymmetric, meaning the modulatory neurons had no effect back on to PD4. Such a unidirectional network layout and the polarity of the synapses suggested that this cell could be a feeding command neuron, as defined by Kupfermann and Weiss (1978). However, excitation of PD4 did not reliably initiate feeding, and could even inhibit spontaneous buccal rhythms. This was likely due to a previously described excitatory synapse from CGC to N3t which dominates at higher PD4 firing frequencies (Yeoman *et al.*, 1996). Application of sucrose to the lips, which is known to initiate feeding activity, also had no effect on PD4. Therefore, it appears that the cell does not participate in chemosensory pathways that initiate feeding (Kemenes *et al.*, 1986; Kemenes *et al.*, 2001).

6.3.1. PD4 may coordinate feeding as part of the egg laying behaviour

Given the distant anatomical location of PD4 from the majority of feeding neurons and lack of involvement in appetitive chemosensory pathways it was probable that the cell would interact with other identified behavioural networks. Therefore, the cell was stimulated whilst recording neurons from the cardiorespiratory, withdrawal and egg laying networks. We did not observe an effect of PD4 on the former two networks, but PD4 activation did cause an inhibition of the egg laying network. More specifically, PD4 inhibited the caudodorsal cells (CDCs), which are necessary for the initiation of egg laying (Geraerts & Bohlken, 1976; Ter Maat *et al.*, 1989). PD4 also caused sub-threshold excitation of the ring neuron, which has previously been shown to inhibit the

CDCs (Jansen & ter Maat, 1985; Jansen *et al.*, 1985). Overall this suggested that PD4 acts to inhibit CDC activity.

The fact that PD4 synapses with both the feeding system and the egg laying system is very interesting, as the two behaviours have previously been associated. Specifically, during the turning and oviposition phases of egg laying, it has been shown that the buccal feeding CPG is activated, and the firing frequency of CGC is elevated (Jansen *et al.*, 1997; Jansen *et al.*, 1999). Through CPG control of the motoneurons, this causes the radula to scrape against the surface, improving the likelihood of egg sac adhesion (Ter Maat *et al.*, 1989). Coordination of these two behaviours could be carried out by the PD4 cell, which may become active during the turning and oviposition phases (**Figure 6.1.**). In support of this idea, PD4 was found to have a projection down a visceral ganglion nerve, possibly the intestinal nerve. By surgical ablation, the intestinal nerve has previously been shown to be necessary for rasping behaviour to occur during the turning phase of egg laying (Ferguson *et al.*, 1993).

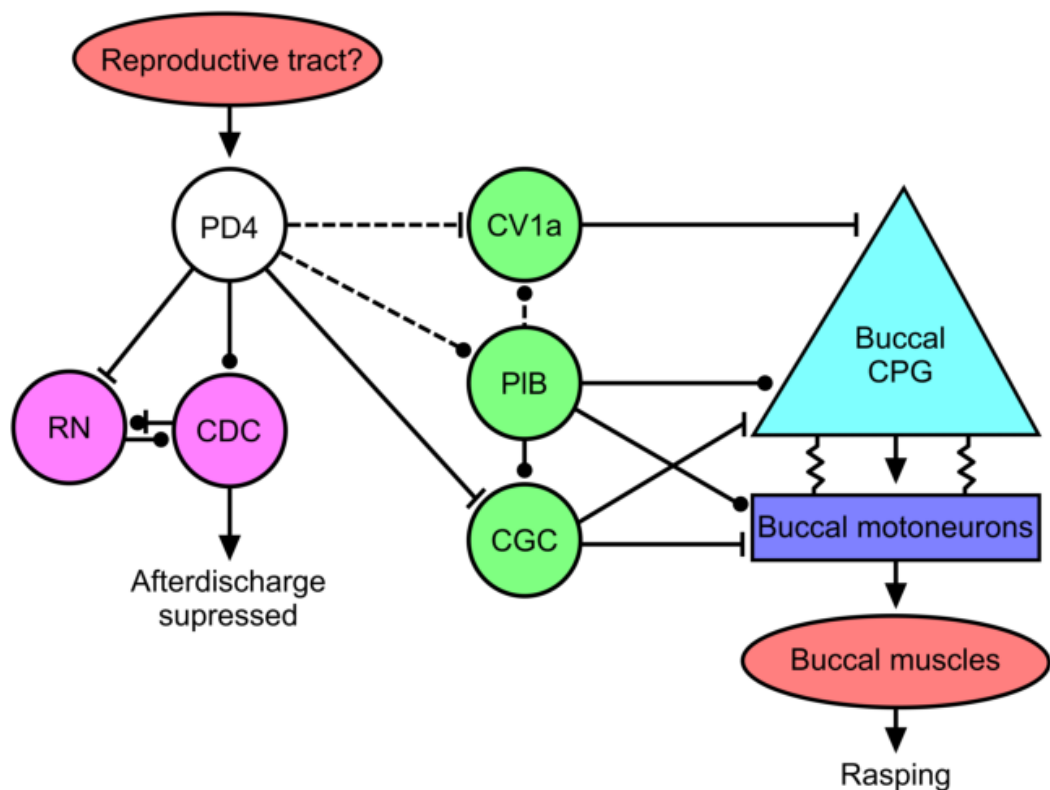


Figure 6.1. A network diagram showing a possible role for PD4 in coordination of feeding and egg laying. PD4 may become active during the turning phase due to a signal from the reproductive tract, that passes up through the visceral nerve. Through asymmetrical synapses this would act to suppress the preceding afterdischarge in the CDCs, and would promote feeding via modulatory neurons. Peripheral tissues are shown in pink, reproductive cells in purple, modulatory neurons in green, CPG neurons in light blue and motoneurons in dark blue. Excitatory synapses are shown by bars, inhibitory synapses by dots and electrical synapses by resistor symbols.

Other neurons which coordinate behaviours have been identified in *Lymnaea*, but control precedence of one behaviour over another. In both cases the neurons are part of the electrically coupled withdrawal circuit and cause inhibition of a less important behaviour. The first neuron is PeD12, which is activated by aversive touch and has been shown to monosynaptically excite the PIB, thus inhibiting feeding (Pirger *et al.*, 2014). The second neuron is the closely located right pedal dorsal 11 (R PeD11), which has been shown to inhibit respiration, through synapses with both CPG neurons and motoneurons (Inoue *et al.*, 1996a).

6.4. Future research

The findings of this thesis have raised several possibilities for future experiments and modelling both in terms of the feeding system and appetitive memory formation.

6.4.1. An alternative model of CGC nonsynaptic plasticity would be required based on the new experimental data

It has been shown that the current model of the CGC voltage-gated ion channels, developed by Vavoulis *et al.* (2010), is not sufficient to explain the nonsynaptic plasticity that underlies the conditioned feeding response. Therefore, a new CGC model will need to be developed, which could include more recent experimental data. For example, in addition to I_{HVA} and I_{LVA} , a further subtype of voltage-gated calcium channel has been characterised, that is sensitive to nifedipine application (Scutt, 2012). There was also a suggestion by Staras *et al.* (2002) that a calcium-sensitive potassium conductance may exist in the CGCs, but this has not been fully characterised.

A newer model could also utilise a different technique to estimate the parameters of the various voltage-gated conductances. In the current model the parameters were fitted to experimental data using linear and non-linear least-square fitting techniques that resulted in a very tightly tuned system. Alternative techniques using different mathematical frameworks could be used, such as that recently developed by Vavoulis *et al.* (2012).

6.4.2. Other identified neurons could play a role in the Kamin effect

The failure to find nonsynaptic or synaptic changes in PIB and CGC that could explain memory lapses means other cellular targets need to be considered. The modulatory CPG neuron N3t has been shown to reduce its spontaneous activity at the 2 hour lapse point, but also at the 1/3/4 hr non-lapse points, demonstrating that it is not responsible for the Kamin effect (Marra *et al.*, 2010). In terms of other identified neurons that could influence the whole system the most probable target is CV1a. This cell is well situated to pass a CS response signal from the lips to the buccal ganglia, and is capable of initiating feeding cycles (McCrohan & Kyriakides, 1989). CBI2 in *Aplysia*, which is homologous to CV1a in *Lymnaea*, has been shown to have enhanced CS-evoked EPSPs at 1 hour following *in vitro* classical appetitive conditioning (Mozzachiodi *et al.*, 2003). Therefore, along with the >24hr post conditioning findings of Kemenes *et al.* (2002), it is plausible that CV1a could be involved in the earlier stages of appetitive memory consolidation as well.

6.4.3. The neurotransmitter of PD4 is currently unknown

Often neurons of the feeding system of *Lymnaea* have been discovered initially via transmitter stains. In this case PD4 was identified by its effects on identified modulatory projection neurons, and therefore its transmitter is unknown. The effects of different transmitters on CGC is well characterised and this could provide clues for the nature of the PD4-CGC synapse. It is known that serotonin, dopamine and acetylcholine applied to the isolated brain will depolarise CGC (Kyriakides & McCrohan, 1989; Yeoman *et al.*, 1994). For serotonin and acetylcholine this has been replicated in isolated CGC cell culture, and it has been shown that glutamate is inhibitory (Straub,

1998). Serotonin application has also been shown to inhibit the afterdischarge in the bag cells of *Aplysia*, which are homologous to the CDCs in *Lymnaea* (Jennings *et al.*, 1981). Therefore, pharmacological blockers of serotonergic, dopaminergic and cholinergic transmission will need to be tested on PD4 output synapses.

6.4.4. PD4 projects to an unknown cell type in the buccal ganglia

Dye fills of PD4 clearly showed that the axon projects bilaterally up both CBCs and in to the buccal ganglia. However, it was not possible to identify a connection with any of the major CPG neurons and motoneurons on the dorsal surface of the buccal ganglia. This may be because PD4 synapses with neurons on the ventral surface of the buccal ganglia, such as those that have recently been implicated in egestion (Crossley *et al.*, 2018). Alternatively, PD4 could synapse with as yet unidentified non-rhythmic neurons that play a role in another behaviour, such as reproduction.

6.4.5. A stimulus that activates PD4 will need to be identified

It was initially hypothesised that PD4 became active during a known chemosensory response of the feeding system to sucrose, first described by Kemenes *et al.* (1986). However, sucrose application to the lips did not depolarise PD4, which remained quiescent, whilst CGC increased its firing frequency. This suggests that PD4 is not part of the feeding system. Instead it seems that PD4 coordinates more than one behaviour by synapsing with both modulatory feeding neurons and egg laying initiation neurons. The cell also has a peripheral projection from the visceral ganglion. Taken together, this suggests that the cell may be active during egg laying. To test this would require triggering an afterdischarge in the CDCs *in vitro* and corecording the PD4 until the turning/oviposition stages, when CGC firing should be elevated (Jansen *et al.*, 1997). The CDC afterdischarge was not triggerable by intracellular current injection during the current experiments, an effect which has previously been reported by Benjamin and Rose (1984). This was probably due to severing of the cerebral commissure, which contains the axons of the CDCs, and connects the two populations electrotonically (de Vlieger *et al.*, 1980). *In vitro* egg laying would also likely require the intestinal nerve to remain intact (Ferguson *et al.*, 1993).

6.5. Conclusion

The work of this thesis has important themes relevant for the wider neuroscientific field. This includes the importance of using techniques, such as dynamic clamp, that allow the direct testing of theoretical models on living organisms (Prinz *et al.*, 2004). A mathematical model can give the observed output, but the underlying parameters may not accurately represent the biological reality (Golowasch *et al.*, 2002). By using dynamic clamp, a causative link can be established between nonsynaptic/synaptic alterations and the change in the behavioural output of an entire neural network (Sakurai & Katz, 2017). Another important and related implication of this work, is that it can be very difficult to artificially control the activity of living cells in a precise manner. For electrophysiology, space clamp issues are particularly evident in large neurons with multiple compartments, which cannot be easily influenced by an electrode located solely in the soma (Williams & Mitchell, 2008).

This thesis also raises interesting questions about the functional role of nonsynaptic plasticity in associative memories. In many cases a correlation can be found between associative memory expression and nonsynaptic changes, but it is unknown how these changes result in stimulus specificity (Mozzachiodi & Byrne, 2010). In non-associative memories, such as sensitisation, a simple increase in the excitability of a sensory neuron for example, can result in a straightforward increase in the motor output, through a simple neural pathway (Burrell *et al.*, 2001). In *Lymnaea* the CGC can become persistently depolarised by different chemical species of CS, following classical conditioning (Crossley *et al.*, 2019). So, stimulus specificity must be achieved somewhere else in the circuit, putatively at the synapse between chemosensory CS fibres and CV1a (Kemenes *et al.*, 2006). An interestingly speculation by Mozzachiodi and Byrne (2010) is that nonsynaptic plasticity may not always be a core necessary part of the engram, but may act in initiating/priming synaptic plasticity and increasing the rate of future relearning after extinction (memory savings).

To understand the neural basis of memory it is also crucial to understand that expression is rarely continuous and that there are crucial temporal considerations. In other words, the engram is highly labile until it enters LTM and may still be subject to

reconsolidation. An interesting example of the importance of timing in learning-induced neural plasticity, is sensitisation in *Aplysia*. It was originally found that during short-term sensitisation there was spike broadening in presynaptic sensory neurons, which was thought to be responsible for observed facilitation of the EPSP (Klein & Kandel, 1978). This enhanced EPSP persists into LTM and is partially responsible for expression of the memory (Frost *et al.*, 1985). However, spike broadening was later disproven as the physiological mechanism responsible for the presynaptic facilitation during STM (Klein, 1994). Furthermore, it has now been shown that in LTM the spike broadening reverses and becomes narrower than the untrained state (Antzoulatos & Byrne, 2007). Therefore, it is clear that different temporal phases of a memory can have different underlying plasticity in the nervous system, even for one endogenous property in a single neuron.

Overall, given that the engram has been found to be highly spatially distributed and temporally-dependent during consolidation, our future understanding of associative memory will rely on techniques that can monitor and manipulate numerous different sites with high chronological accuracy.

References

- Alania, M. & Sakharov, D.A. (2000) Morphology and physiology of pleural-to-buccal neurons coordinating defensive retraction with feeding arrest in the pond snail *Lymnaea stagnalis*. *Acta Biol Hung*, **51**, 197-203.
- Alania, M., Sakharov, D.A. & Elliott, C.J. (2004) Multilevel inhibition of feeding by a peptidergic pleural interneuron in the mollusc *Lymnaea stagnalis*. *J Comp Physiol A - Neuroethol Sens Neural Behav Physiol*, **190**, 379-390.
- Alexander, J., Jr., Audesirk, T.E. & Audesirk, G.J. (1984) One-trial reward learning in the snail *Lymnaea stagnalis*. *J Neurobiol*, **15**, 67-72.
- Alkon, D.L., Sakakibara, M., Forman, R., Harrigan, J., Lederhendler, I. & Farley, J. (1985) Reduction of two voltage-dependent K⁺ currents mediates retention of a learned association. *Behav Neural Biol*, **44**, 278-300.
- Andrew, R.J. & Savage, H. (2000) Appetitive learning using visual conditioned stimuli in the pond snail, *Lymnaea*. *Neurobiol Learn Mem*, **73**, 258-273.
- Antonov, I., Antonova, I., Kandel, E.R. & Hawkins, R.D. (2003) Activity-dependent presynaptic facilitation and hebbian LTP are both required and interact during classical conditioning in *Aplysia*. *Neuron*, **37**, 135-147.
- Antzoulatos, E.G. & Byrne, J.H. (2007) Long-term sensitization training produces spike narrowing in *Aplysia* sensory neurons. *J Neurosci*, **27**, 676-683.
- Audesirk, G., Audesirk, T. & Bowsher, P. (1982) Variability and frequent failure of lucifer yellow to pass between two electrically coupled neurons in *Lymnaea stagnalis*. *J Neurobiol*, **13**, 369-375.
- Awatramani, G.B., Price, G.D. & Trussell, L.O. (2005) Modulation of transmitter release by presynaptic resting potential and background calcium levels. *Neuron*, **48**, 109-121.
- Bell, H.J., Inoue, T., Shum, K., Luk, C. & Syed, N.I. (2007) Peripheral oxygen-sensing cells directly modulate the output of an identified respiratory central pattern generating neuron. *Eur J Neurosci*, **25**, 3537-3550.
- Benjamin, P.R. (2012) Distributed network organization underlying feeding behavior in the mollusk *Lymnaea*. *Neural Syst Circ*, **2**, 4.

- Benjamin, P.R. & Rose, R.M. (1984) Electrotonic coupling and afterdischarges in the Light Green Cells: a comparison with two other cerebral ganglia neurosecretory cell types in the pond snail *Lymnaea stagnalis*. *Comp Biochem Physiol A Comp Physiol*, **77**, 67-74.
- Benjamin, P.R., Rose, R.M., Slade, C.T. & Lacy, M.G. (1979) Morphology of identified neurones in the buccal ganglia of *Lymnaea stagnalis*. *J Exp Biol*, **80**, 119.
- Benjamin, P.R., Staras, K. & Kemenes, G. (2000) A systems approach to the cellular analysis of associative learning in the pond snail *Lymnaea*. *Learn Memory*, **7**, 124-131.
- Berry, M.S. & Pentreath, V.W. (1976) Criteria for distinguishing between monosynaptic and polysynaptic transmission. *Brain Res*, **105**, 1-20.
- Brierley, M.J., Yeoman, M.S. & Benjamin, P.R. (1997) Glutamatergic N2v cells are central pattern generator interneurons of the *Lymnaea* feeding system: new model for rhythm generation. *J Neurophysiol*, **78**, 3396-3407.
- Buckett, K.J., Peters, M. & Benjamin, P.R. (1990) Excitation and inhibition of the heart of the snail, *Lymnaea*, by non-FMRFamideergic motoneurons. *J Neurophysiol*, **63**, 1436-1447.
- Burrell, B.D., Sahley, C.L. & Muller, K.J. (2001) Non-associative learning and serotonin induce similar bi-directional changes in excitability of a neuron critical for learning in the medicinal leech. *J Neurosci*, **21**, 1401-1412.
- Castellucci, V., Pinsker, H., Kupfermann, I. & Kandel, E.R. (1970) Neuronal mechanisms of habituation and dishabituation of the gill-withdrawal reflex in *Aplysia*. *Science*, **167**, 1745-1748.
- Castellucci, V.F. & Kandel, E.R. (1974) A quantal analysis of the synaptic depression underlying habituation of the gill-withdrawal reflex in *Aplysia*. *Proc Natl Acad Sci U S A*, **71**, 5004-5008.
- Coggeshall, R.E. (1967) A light and electron microscope study of the abdominal ganglion of *Aplysia californica*. *J Neurophysiol*, **30**, 1263-1287.
- Crossley, M. (2014) Neural Mechanisms of Decision Making In The Pond Snail *Lymnaea stagnalis*., DPhil, University of Sussex.

- Crossley, M., Lorenzetti, F.D., Naskar, S., O'Shea, M., Kemenes, G., Benjamin, P.R. & Kemenes, I. (2019) Proactive and retroactive interference with associative memory consolidation in the snail *Lymnaea* is time and circuit dependent. *Commun Biol*, **2**, 242.
- Crossley, M., Staras, K. & Kemenes, G. (2016) A two-neuron system for adaptive goal-directed decision-making in *Lymnaea*. *Nat Commun*, 11793.
- Crossley, M., Staras, K. & Kemenes, G. (2018) A central control circuit for encoding perceived food value. *Science Advances*, **4**, eaau9180.
- Crow, T. & Alkon, D.L. (1978) Retention of an associative behavioral change in *Hermissenda*. *Science*, **201**, 1239-1241.
- Crow, T. & Alkon, D.L. (1980) Associative behavioral modification in *Hermissenda*: cellular correlates. *Science*, **209**, 412-414.
- Crow, T. & Tian, L.M. (2002) Facilitation of monosynaptic and complex PSPs in type I interneurons of conditioned *Hermissenda*. *J Neurosci*, **22**, 7818-7824.
- Crow, T. & Tian, L.M. (2003) Neural correlates of Pavlovian conditioning in components of the neural network supporting ciliary locomotion in *Hermissenda*. *Learn Mem*, **10**, 209-216.
- Dai, J., Sheetz, M.P., Wan, X. & Morris, C.E. (1998) Membrane tension in swelling and shrinking molluscan neurons. *J Neurosci*, **18**, 6681-6692.
- de Vlieger, T.A., Kits, K.S., ter Maat, A. & Lodder, J.C. (1980) Morphology and electrophysiology of the ovulation hormone producing neuro-endocrine cells of the freshwater snail *Lymnaea stagnalis* (L.). *J Exp Biol*, **84**, 259-271.
- Elekes, K., Kemenes, G., Hiripi, L., Geffard, M. & Benjamin, P.R. (1991) Dopamine-immunoreactive neurones in the central nervous system of the pond snail *Lymnaea stagnalis*. *J Comp Neurol*, **307**, 214-224.
- Elliott, C.J. & Benjamin, P.R. (1985a) Interactions of pattern-generating interneurons controlling feeding in *Lymnaea stagnalis*. *J Neurophysiol*, **54**, 1396-1411.

- Elliott, C.J. & Benjamin, P.R. (1985b) Interactions of the slow oscillator interneuron with feeding pattern-generating interneurons in *Lymnaea stagnalis*. *J Neurophysiol*, **54**, 1412-1421.
- Elliott, C.J. & Vehovszky, A. (2000) Polycyclic neuromodulation of the feeding rhythm of the pond snail *Lymnaea stagnalis* by the intrinsic octopaminergic interneuron, OC. *Brain Res*, **887**, 63-69.
- Ewadinger, N., Syed, N., Lukowiak, K. & Bulloch, A. (1994) Differential tracer coupling between pairs of identified neurones of the mollusc *Lymnaea stagnalis*. *J Exp Biol*, **192**, 291-297.
- Farley, J. & Han, Y. (1997) Ionic basis of learning-correlated excitability changes in *Hermissenda* type A photoreceptors. *J Neurophysiol*, **77**, 1861-1888.
- Faul, F., Erdfelder, E., Lang, A.G. & Buchner, A. (2007) G*Power 3: a flexible statistical power analysis program for the social, behavioral, and biomedical sciences. *Behav Res Methods*, **39**, 175-191.
- Fejtl, M., Szarowski, D.H., Decker, D., Buttle, K., Carpenter, D.O. & Turner, J.N. (1995) Three-dimensional imaging and electrophysiology of live *Aplysia* neurons during volume perturbation: confocal light and high-voltage electron microscopy. *Microscopy and Microanalysis*, **1**, 75-85.
- Ferguson, G.P. & Benjamin, P.R. (1991a) The whole-body withdrawal response of *Lymnaea stagnalis*. I. Identification of central motoneurons and muscles. *J Exp Biol*, **158**, 63-95.
- Ferguson, G.P. & Benjamin, P.R. (1991b) The whole-body withdrawal response of *Lymnaea stagnalis*. II. Activation of central motoneurons and muscles by sensory input. *J Exp Biol*, **158**, 97-116.
- Ferguson, G.P., Pieneman, A.W., Jansen, R.F. & Ter Maat, A. (1993) Neuronal feedback in egg-laying behaviour of the pond snail *Lymnaea stagnalis*. *J Exp Biol*, **178**, 251.
- Ford, L., Crossley, M., Vadukul, D.M., Kemenes, G. & Serpell, L.C. (2017) Structure-dependent effects of amyloid-beta on long-term memory in *Lymnaea stagnalis*. *FEBS Lett*, **591**, 1236-1246.

- Ford, L., Crossley, M., Williams, T., Thorpe, J.R., Serpell, L.C. & Kemenes, G. (2015) Effects of Abeta exposure on long-term associative memory and its neuronal mechanisms in a defined neuronal network. *Sci Rep*, **5**, 10614.
- Frost, W.N., Castellucci, V.F., Hawkins, R.D. & Kandel, E.R. (1985) Monosynaptic connections made by the sensory neurons of the gill- and siphon-withdrawal reflex in *Aplysia* participate in the storage of long-term memory for sensitization. *Proc Natl Acad Sci U S A*, **82**, 8266-8269.
- Fryszak, R.J. & Crow, T. (1993) Differential expression of correlates of classical conditioning in identified medial and lateral type A photoreceptors of *Hermisenda*. *J Neurosci*, **13**, 2889-2897.
- Fryszak, R.J. & Crow, T. (1994) Enhancement of type B and A photoreceptor inhibitory synaptic connections in conditioned *Hermisenda*. *J Neurosci*, **14**, 1245-1250.
- Fryszak, R.J. & Crow, T. (1997) Synaptic enhancement and enhanced excitability in presynaptic and postsynaptic neurons in the conditioned stimulus pathway of *Hermisenda*. *J Neurosci*, **17**, 4426-4433.
- Fulton, D., Kemenes, I., Andrew, R.J. & Benjamin, P.R. (2005) A single time-window for protein synthesis-dependent long-term memory formation after one-trial appetitive conditioning. *Eur J Neurosci*, **21**, 1347-1358.
- Gandhi, C.C. & Matzel, L.D. (2000) Modulation of presynaptic action potential kinetics underlies synaptic facilitation of type B photoreceptors after associative conditioning in *Hermisenda*. *J Neurosci*, **20**, 2022-2035.
- Geraerts, W.P. & Bohlken, S. (1976) The control of ovulation in the hermaphroditic freshwater snail *Lymnaea stagnalis* by the neurohormone of the caudodorsal cells. *Gen Comp Endocrinol*, **28**, 350-357.
- Gerber, B. & Menzel, R. (2000) Contextual modulation of memory consolidation. *Learn Memory*, **7**, 151-158.
- Gerhardt, C.C., Leysen, J.E., Planta, R.J., Vreugdenhil, E. & VanHeerikhuizen, H. (1996) Functional characterisation of a 5-HT₂ receptor cDNA cloned from *Lymnaea stagnalis*. *Eur J Pharmacol*, **311**, 249-258.
- Goldschmeding, J.T., Van Duivenboden, Y.A. & Lodder, J.C. (1981) Axonal branching pattern and coupling mechanisms of the cerebral giant neurones in the snail, *Lymnaea stagnalis*. *J Neurobiol*, **12**, 405-424.

- Golowasch, J., Goldman, M.S., Abbott, L.F. & Marder, E. (2002) Failure of averaging in the construction of a conductance-based neuron model. *J Neurophysiol*, **87**, 1129-1131.
- Graubard, K. (1975) Voltage attenuation within *Aplysia* neurons: the effect of branching pattern. *Brain Res*, **88**, 325-332.
- Haque, Z., Lee, T.K., Inoue, T., Luk, C., Hasan, S.U., Lukowiak, K. & Syed, N.I. (2006) An identified central pattern-generating neuron co-ordinates sensory-motor components of respiratory behavior in *Lymnaea*. *Eur J Neurosci*, **23**, 94-104.
- Hebb, D.O. (1949) *The Organization of Behavior: A Neuropsychological Theory*. Wiley and Sons, New York.
- Hille, B. (2001) *Ion channels of excitable membranes*. Sunderland, Mass. : Sinauer.
- Hodgkin, A.L. & Huxley, A.F. (1952) A quantitative description of membrane current and its application to conduction and excitation in nerve. *J Physiol*, **117**, 500-544.
- Hosono, S., Matsumoto, Y. & Mizunami, M. (2016) Interaction of inhibitory and facilitatory effects of conditioning trials on long-term memory formation. *Learn Memory*, **23**, 669-678.
- Inoue, T., Takasaki, M., Lukowiak, K. & Syed, N. (1996a) Inhibition of the respiratory pattern-generating neurons by an identified whole-body withdrawal interneuron of *Lymnaea stagnalis*. *J Exp Biol*, **199**, 1887-1898.
- Inoue, T., Takasaki, M., Lukowiak, K. & Syed, N.I. (1996b) Identification of a putative mechanosensory neuron in *Lymnaea*: characterization of its synaptic and functional connections with the whole-body withdrawal interneuron. *J Neurophysiol*, **76**, 3230-3238.
- Jansen, R.F. & Bos, N.P. (1984) An identified neuron modulating the activity of the ovulation hormone producing caudo-dorsal cells of the pond snail *Lymnaea stagnalis*. *J Neurobiol*, **15**, 161-167.
- Jansen, R.F., Pieneman, A.W. & Maat, A.T. (1999) Pattern generation in the buccal system of freely behaving *Lymnaea stagnalis*. *J Neurophysiol*, **82**, 3378-3391.

- Jansen, R.F., Pieneman, A.W. & ter Maat, A. (1997) Behavior-dependent activities of a central pattern generator in freely behaving *Lymnaea stagnalis*. *J Neurophysiol*, **78**, 3415-3427.
- Jansen, R.F. & ter Maat, A. (1985) Ring neuron control of columellar motor neurons during egg-laying behavior in the pond snail. *J Neurobiol*, **16**, 1-14.
- Jansen, R.F., ter Maat, A. & Bos, N.P. (1985) Membrane mechanism of neuroendocrine caudo-dorsal cell inhibition by the ring neuron in the pond snail *Lymnaea stagnalis*. *J Neurobiol*, **16**, 15-26.
- Jennings, K.R., Host, J.J., Kaczmarek, L.K. & Strumwasser, F. (1981) Serotonergic inhibition of afterdischarge in peptidergic bag cells. *J Neurobiol*, **12**, 579-590.
- Jing, J. & Gillette, R. (2000) Escape swim network interneurons have diverse roles in behavioral switching and putative arousal in *Pleurobranchaea*. *J Neurophysiol*, **83**, 1346-1355.
- Jing, J., Vilim, F.S., Cropper, E.C. & Weiss, K.R. (2008) Neural analog of arousal: persistent conditional activation of a feeding modulator by serotonergic initiators of locomotion. *J Neurosci*, **28**, 12349-12361.
- Jones, N., Kemenes, G. & Benjamin, P.R. (2001) Selective expression of electrical correlates of differential appetitive classical conditioning in a feeding network. *J Neurophysiol*, **85**, 89-97.
- Jones, N.G., Kemenes, I., Kemenes, G. & Benjamin, P.R. (2003) A persistent cellular change in a single modulatory neuron contributes to associative long-term memory. *Curr Biol*, **13**, 1064-1069.
- Kamin, L.J. (1957) The retention of an incompletely learned avoidance response. *J Comp Physiol Psychol*, **50**, 457-460.
- Kamin, L.J. (1963) Retention of an incompletely learned avoidance response: some further analyses. *J Comp Physiol Psychol*, **56**, 713-718.
- Kandel, E.R., Dudai, Y. & Mayford, M.R. (2014) The molecular and systems biology of memory. *Cell*, **157**, 163-186.
- Katz, P.S. & Frost, W.N. (1996) Intrinsic neuromodulation: altering neuronal circuits from within. *Trends Neurosci*, **19**, 54-61.

- Kemenes, G. & Benjamin, P.R. (1989) Appetitive learning in snails shows characteristics of conditioning in vertebrates. *Brain Res*, **489**, 163-166.
- Kemenes, G. & Elliott, C.J. (1994) Analysis of the feeding motor pattern in the pond snail, *Lymnaea stagnalis*: photoinactivation of axonally stained pattern-generating interneurons. *J Neurosci*, **14**, 153-166.
- Kemenes, G., Elliott, C.J.H. & Benjamin, P.R. (1986) Chemical and tactile inputs to the *Lymnaea* feeding system - effects on behavior and neural circuitry. *J Exp Biol*, **122**, 113-137.
- Kemenes, G., Staras, K. & Benjamin, P.R. (2001) Multiple types of control by identified interneurons in a sensory-activated rhythmic motor pattern. *J Neurosci*, **21**, 2903-2911.
- Kemenes, I., Kemenes, G., Andrew, R.J., Benjamin, P.R. & O'Shea, M. (2002) Critical time-window for NO-cGMP-dependent long-term memory formation after one-trial appetitive conditioning. *J Neurosci*, **22**, 1414-1425.
- Kemenes, I., Marra, V., Crossley, M., Samu, D., Staras, K., Kemenes, G. & Nowotny, T. (2011) Dynamic clamp with StdpC software. *Nat Protoc*, **6**, 405-417.
- Kemenes, I., Straub, V.A., Nikitin, E.S., Staras, K., O'Shea, M., Kemenes, G. & Benjamin, P.R. (2006) Role of delayed nonsynaptic neuronal plasticity in long-term associative memory. *Curr Biol*, **16**, 1269-1279.
- Klein, M. (1994) Synaptic augmentation by 5-HT at rested *Aplysia* sensorimotor synapses: independence of action potential prolongation. *Neuron*, **13**, 159-166.
- Klein, M. & Kandel, E.R. (1978) Presynaptic modulation of voltage-dependent Ca²⁺ current: mechanism for behavioral sensitization in *Aplysia californica*. *Proc Natl Acad Sci U S A*, **75**, 3512-3516.
- Koene, J.M. (2010) Neuro-endocrine control of reproduction in hermaphroditic freshwater snails: mechanisms and evolution. *Front Behav Neurosci*, **4**, 167.
- Konorski, J. (1948) *Conditioned Reflexes and Neuron Organization*. Cambridge University Press, Cambridge.

- Koya, E., Golden, S.A., Harvey, B.K., Guez-Barber, D.H., Berkow, A., Simmons, D.E., Bossert, J.M., Nair, S.G., Uejima, J.L., Marin, M.T., Mitchell, T.B., Farquhar, D., Ghosh, S.C., Mattson, B.J. & Hope, B.T. (2009) Targeted disruption of cocaine-activated nucleus accumbens neurons prevents context-specific sensitization. *Nat Neurosci*, **12**, 1069-1073.
- Kupfermann, I. & Weiss, K.R. (1978) The command neuron concept. *Behavioral and Brain Sciences*, **1**, 3-10.
- Kyriakides, M., McCrohan, C.R., Slade, C.T., Syed, N.I. & Winlow, W. (1989) The morphology and electrophysiology of the neurones of the paired pedal ganglia of *Lymnaea stagnalis* (L.). *Comp Biochem Physiol A Comp Physiol*, **93**, 861-876.
- Kyriakides, M.A. & McCrohan, C.R. (1989) Effect of putative neuromodulators on rhythmic buccal motor output in *Lymnaea stagnalis*. *J Neurobiol*, **20**, 635-650.
- Lindau, M. & Neher, E. (1988) Patch-clamp techniques for time-resolved capacitance measurements in single cells. *Pflugers Arch*, **411**, 137-146.
- Liu, X., Ramirez, S., Pang, P.T., Puryear, C.B., Govindarajan, A., Deisseroth, K. & Tonegawa, S. (2012) Optogenetic stimulation of a hippocampal engram activates fear memory recall. *Nature*, **484**, 381-385.
- Longley, R.D. (1984) Axon surface infolding and axon size can be quantitatively related in gastropod molluscs. *J Exp Biol*, **108**, 163.
- Lowe, M.R. & Spencer, G.E. (2006) Perturbation of the activity of a single identified neuron affects long-term memory formation in a molluscan semi-intact preparation. *J Exp Biol*, **209**, 711-721.
- Lukowiak, K., Adatia, N., Krygier, D. & Syed, N. (2000) Operant conditioning in *Lymnaea*: evidence for intermediate- and long-term memory. *Learn Mem*, **7**, 140-150.
- Lukowiak, K., Cotter, R., Westly, J., Ringseis, E. & Spencer, G. (1998) Long-term memory of an operantly conditioned respiratory behaviour pattern in *Lymnaea stagnalis*. *J Exp Biol*, **201**, 877-882.
- Lukowiak, K., Ringseis, E., Spencer, G., Wildering, W. & Syed, N. (1996) Operant conditioning of aerial respiratory behaviour in *Lymnaea stagnalis*. *J Exp Biol*, **199**, 683-691.

- Ma, M. & Koester, J. (1996) The role of K⁺ currents in frequency-dependent spike broadening in *Aplysia* R20 neurons: a dynamic-clamp analysis. *J Neurosci*, **16**, 4089-4101.
- Marra, V. (2009) Cellular and Molecular Mechanisms of Different Memory Phases After Single-Trial Classical Conditioning in *Lymnaea*., DPhil, University of Sussex.
- Marra, V., Kemenes, I., Vavoulis, D., Feng, J., O'Shea, M. & Benjamin, P.R. (2010) Role of tonic inhibition in associative reward conditioning in *Lymnaea*. *Front Behav Neurosci*, **4**.
- Marra, V., O'Shea, M., Benjamin, P.R. & Kemenes, I. (2013) Susceptibility of memory consolidation during lapses in recall. *Nat Commun*, **4**, 1578.
- Mayer, M.L., Westbrook, G.L. & Guthrie, P.B. (1984) Voltage-dependent block by Mg²⁺ of NMDA responses in spinal cord neurones. *Nature*, **309**, 261-263.
- McCrohan, C.R. (1984a) Initiation of feeding motor output by an identified interneurone in the snail *Lymnaea stagnalis*. *J Exp Biol*, **113**, 351-366.
- McCrohan, C.R. (1984b) Properties of ventral cerebral neurons involved in the feeding system of the snail, *Lymnaea stagnalis*. *J Exp Biol*, **108**, 257.
- McCrohan, C.R. & Benjamin, P.R. (1980a) Patterns of activity and axonal projections of the cerebral giant cells of the snail, *Lymnaea stagnalis*. *J Exp Biol*, **85**, 149-168.
- McCrohan, C.R. & Benjamin, P.R. (1980b) Synaptic relationships of the cerebral giant cells with motoneurons in the feeding system of *Lymnaea stagnalis*. *J Exp Biol*, **85**, 169-186.
- McCrohan, C.R. & Croll, R.P. (1997) Characterization of an identified cerebrobuccal neuron containing the neuropeptide APGWamide (Ala-Pro-Gly-Trp-NH₂) in the snail *Lymnaea stagnalis*. *Invertebr Neurosci*, **2**, 273-282.
- McCrohan, C.R. & Kyriakides, M.A. (1989) Cerebral interneurons controlling feeding motor output in the snail *Lymnaea stagnalis*. *J Exp Biol*, **147**, 361-374.
- Mirolli, M. & Talbott, S.R. (1972) The geometrical factors determining the electrotonic properties of a molluscan neurone. *J Physiol*, **227**, 19-34.

- Mozzachiodi, R. & Byrne, J.H. (2010) More than synaptic plasticity: role of nonsynaptic plasticity in learning and memory. *Trends Neurosci*, **33**, 17-26.
- Mozzachiodi, R., Lechner, H.A., Baxter, D.A. & Byrne, J.H. (2003) In vitro analog of classical conditioning of feeding behavior in *Aplysia*. *Learn Mem*, **10**, 478-494.
- Nikitin, E.S., Balaban, P.M. & Kemenes, G. (2013) Nonsynaptic plasticity underlies a compartmentalized increase in synaptic efficacy after classical conditioning. *Curr Biol*, **23**, 614-619.
- Nikitin, E.S., Kiss, T., Staras, K., O'Shea, M., Benjamin, P.R. & Kemenes, G. (2006) Persistent sodium current is a target for cAMP-induced neuronal plasticity in a state-setting modulatory interneuron. *J Neurophysiol*, **95**, 453-463.
- Nikitin, E.S., Vavoulis, D.V., Kemenes, I., Marra, V., Pirger, Z., Michel, M., Feng, J., O'Shea, M., Benjamin, P.R. & Kemenes, G. (2008) Persistent sodium current is a nonsynaptic substrate for long-term associative memory. *Curr Biol*, **18**, 1221-1226.
- Nowotny, T., Szucs, A., Pinto, R.D. & Selverston, A.I. (2006) StpC: A modern dynamic clamp. *J Neurosci Methods*, **158**, 287-299.
- Pavlov, I.P. (1928) *Lectures on conditioned reflexes : twenty-five years of objective study of the higher nervous activity (behaviour) of animals*. International Publishers.
- Perry, S.J., Straub, V.A., Kemenes, G., Santama, N., Worster, B.M., Burke, J.F. & Benjamin, P.R. (1998) Neural modulation of gut motility by myomodulin peptides and acetylcholine in the snail *Lymnaea*. *J Neurophysiol*, **79**, 2460-2474.
- Pinsker, H., Feinstein, R., Sawada, M. & Coggeshall, R. (1976) Anatomical basis for an apparent paradox concerning conduction velocities of two identified axons in *Aplysia*. *J Neurobiol*, **7**, 241-253.
- Pirger, Z., Crossley, M., Laszlo, Z., Naskar, S., Kemenes, G., O'Shea, M., Benjamin, P.R. & Kemenes, I. (2014) Interneuronal mechanism for Tinbergen's hierarchical model of behavioral choice. *Curr Biol*, **24**, 2018-2024.
- Prinz, A.A., Abbott, L.F. & Marder, E. (2004) The dynamic clamp comes of age. *Trends Neurosci*, **27**, 218-224.

- Robinson, H.P. & Kawai, N. (1993) Injection of digitally synthesized synaptic conductance transients to measure the integrative properties of neurons. *J Neurosci Methods*, **49**, 157-165.
- Rose, R.M. & Benjamin, P.R. (1979) The relationship of the central motor pattern to the feeding cycle of *Lymnaea stagnalis*. *J Exp Biol*, **80**, 137-163.
- Rose, R.M. & Benjamin, P.R. (1981) Interneuronal control of feeding in the pond snail *Lymnaea stagnalis*: I. Initiation of feeding cycles by a single buccal interneurone. *J Exp Biol*, **92**, 187.
- Sakurai, A. & Katz, P.S. (2017) Artificial synaptic rewiring demonstrates that distinct neural circuit configurations underlie homologous behaviors. *Curr Biol*, **27**, 1721-1734 e1723.
- Santama, N., Brierley, M., Burke, J.F. & Benjamin, P.R. (1994) Neural network controlling feeding in *Lymnaea stagnalis*: immunocytochemical localization of myomodulin, small cardioactive peptide, buccalin, and FMRFamide-related peptides. *J Comp Neurol*, **342**, 352-365.
- Schacter, D.L. & Wagner, A.D. (2013) Learning and Memory. In Kandel, E.R. (ed) *Principles of Neural Science*. New York : McGraw-Hill.
- Scheibenstock, A., Krygier, D., Haque, Z., Syed, N. & Lukowiak, K. (2002) The soma of RPeD1 must be present for long-term memory formation of associative learning in *Lymnaea*. *J Neurophysiol*, **88**, 1584-1591.
- Schulz, D.J., Goillard, J.M. & Marder, E. (2006) Variable channel expression in identified single and electrically coupled neurons in different animals. *Nat Neurosci*, **9**, 356-362.
- Scutt, G. (2012) Age-related changes to ionic currents and excitability in the Cerebral Giant Cells of the pond snail, *Lymnaea stagnalis*., DPhil, University of Brighton.
- Semon, R. (1921) *The mneme*. George Allen & Unwin, London.
- Sharp, A.A., O'Neil, M.B., Abbott, L.F. & Marder, E. (1993) Dynamic clamp: computer-generated conductances in real neurons. *J Neurophysiol*, **69**, 992-995.
- Skinner, B.F. (1969) *Contingencies of Reinforcement: A theoretical analysis* Meredith, New York.

- Spencer, G.E., Syed, N.I. & Lukowiak, K. (1999) Neural changes after operant conditioning of the aerial respiratory behavior in *Lymnaea stagnalis*. *J Neurosci*, **19**, 1836-1843.
- Squire, L.R. & Zola-Morgan, S. (1988) Memory: brain systems and behavior. *Trends Neurosci*, **11**, 170-175.
- Staras, K., Gyori, J. & Kemenes, G. (2002) Voltage-gated ionic currents in an identified modulatory cell type controlling molluscan feeding. *Eur J Neurosci*, **15**, 109-119.
- Staras, K., Kemenes, G. & Benjamin, P.R. (1998) Pattern-generating role for motoneurons in a rhythmically active neuronal network. *J Neurosci*, **18**, 3669-3688.
- Staras, K., Kemenes, G. & Benjamin, P.R. (1999a) Cellular traces of behavioral classical conditioning can be recorded at several specific sites in a simple nervous system. *J Neurosci*, **19**, 347-357.
- Staras, K., Kemenes, G. & Benjamin, P.R. (1999b) Electrophysiological and behavioral analysis of lip touch as a component of the food stimulus in the snail *Lymnaea*. *J Neurophysiol*, **81**, 1261-1273.
- Staras, K., Kemenes, I., Benjamin, P.R. & Kemenes, G. (2003) Loss of self-inhibition is a cellular mechanism for episodic rhythmic behavior. *Curr Biol*, **13**, 116-124.
- Steinberg, T.H., Newman, A.S., Swanson, J.A. & Silverstein, S.C. (1987) Macrophages possess probenecid-inhibitable organic anion transporters that remove fluorescent dyes from the cytoplasmic matrix. *J Cell Biol*, **105**, 2695-2702.
- Straub, V.A. (1998) In Vitro Study of a Central Pattern Generator., DPhil, University of Sussex.
- Straub, V.A. & Benjamin, P.R. (2001) Extrinsic modulation and motor pattern generation in a feeding network: a cellular study. *J Neurosci*, **21**, 1767-1778.
- Straub, V.A., Grant, J., O'Shea, M. & Benjamin, P.R. (2007) Modulation of serotonergic neurotransmission by nitric oxide. *J Neurophysiol*, **97**, 1088-1099.

- Straub, V.A., Kemenes, I., O'Shea, M. & Benjamin, P.R. (2006) Associative memory stored by functional novel pathway rather than modifications of preexisting neuronal pathways. *J Neurosci*, **26**, 4139-4146.
- Straub, V.A., Staras, K., Kemenes, G. & Benjamin, P.R. (2002) Endogenous and network properties of *Lymnaea* feeding central pattern generator interneurons. *J Neurophysiol*, **88**, 1569-1583.
- Straub, V.A., Styles, B.J., Ireland, J.S., O'Shea, M. & Benjamin, P.R. (2004) Central localization of plasticity involved in appetitive conditioning in *Lymnaea*. *Learn Mem*, **11**, 787-793.
- Sugamori, K.S., Sunahara, R.K., Guan, H.C., Bulloch, A.G., Tensen, C.P., Seeman, P., Niznik, H.B. & Van Tol, H.H. (1993) Serotonin receptor cDNA cloned from *Lymnaea stagnalis*. *Proc Natl Acad Sci U S A*, **90**, 11-15.
- Syed, N.I., Bulloch, A.G. & Lukowiak, K. (1990) In vitro reconstruction of the respiratory central pattern generator of the mollusk *Lymnaea*. *Science*, **250**, 282-285.
- Syed, N.I. & Winlow, W. (1991a) Coordination of locomotor and cardiorespiratory networks of *Lymnaea stagnalis* by a pair of identified interneurons. *J Exp Biol*, **158**, 37-62.
- Syed, N.I. & Winlow, W. (1991b) Respiratory behavior in the pond snail *Lymnaea stagnalis*. 2. Neural elements of the central pattern generator (CPG). *J Comp Physiol A - Sens Neural Behav Physiol*, **169**, 557-568.
- Ter Maat, A., Dijcks, F.A. & Bos, N.P.A. (1986) In vivo recordings of neuroendocrine cells (caudo-dorsal cells) in the pond snail. *J Comp Physiol A - Sens Neural Behav Physiol*, **158**, 853-859.
- Ter Maat, A., Pieneman, A.W., Goldschmeding, J.T., Smelik, W.F.E. & Ferguson, G.P. (1989) Spontaneous and induced egg laying behavior of the pond snail, *Lymnaea stagnalis*. *J Comp Physiol A - Sens Neural Behav Physiol*, **184**, 673-683.
- Teyke, T., Weiss, K.R. & Kupfermann, I. (1990) An identified neuron (CPR) evokes neuronal responses reflecting food arousal in *Aplysia*. *Science*, **247**, 85-87.
- Teyke, T., Xin, Y., Weiss, K.R. & Kupfermann, I. (1997) Ganglionic distribution of inputs and outputs of C-PR, a neuron involved in the generation of a food-induced arousal state in *Aplysia*. *Invertebr Neurosci*, **2**, 235-244.

- Thevenaz, P. & Unser, M. (2007) User-friendly semiautomated assembly of accurate image mosaics in microscopy. *Microsc Res Tech*, **70**, 135-146.
- Thorndike, E.L. (1911) *Animal Intelligence*. Macmillan, New York.
- Tonegawa, S., Liu, X., Ramirez, S. & Redondo, R. (2015) Memory engram cells have come of age. *Neuron*, **87**, 918-931.
- Vavoulis, D.V., Nikitin, E.S., Kemenes, I., Marra, V., Feng, J., Benjamin, P.R. & Kemenes, G. (2010) Balanced plasticity and stability of the electrical properties of a molluscan modulatory interneuron after classical conditioning: a computational study. *Front Behav Neurosci*, **4**, 19.
- Vavoulis, D.V., Straub, V.A., Aston, J.A.D. & Feng, J.F. (2012) A self-organizing state-space-model approach for parameter estimation in hodgkin-huxley-type models of single neurons. *PLoS Comp Biol*, **8**, 31.
- Vavoulis, D.V., Straub, V.A., Kemenes, I., Kemenes, G., Feng, J. & Benjamin, P.R. (2007) Dynamic control of a central pattern generator circuit: a computational model of the snail feeding network. *Eur J Neurosci*, **25**, 2805-2818.
- Vehovszky, A. & Elliott, C.J. (2001) Activation and reconfiguration of fictive feeding by the octopamine-containing modulatory OC interneurons in the snail *Lymnaea*. *J Neurophysiol*, **86**, 792-808.
- Vehovszky, A. & Elliott, C.J. (2002) Heterosynaptic modulation by the octopaminergic OC interneurons increases the synaptic outputs of protraction phase interneurons (SO, N1L) in the feeding system of *Lymnaea stagnalis*. *Neuroscience*, **115**, 483-494.
- Vehovszky, A., Elliott, C.J.H., Voronezhskaya, E.E., Hiripi, L. & Elekes, K. (1998) Octopamine: a new feeding modulator in *Lymnaea*. *Philos Trans R Soc Lond, Ser B: Biol Sci*, **353**, 1631-1643.
- Vehovszky, A., Hiripi, L. & Elliott, C.J. (2000) Octopamine is the synaptic transmitter between identified neurons in the buccal feeding network of the pond snail *Lymnaea stagnalis*. *Brain Res*, **867**, 188-199.
- Vehovszky, A., Szabo, H. & Elliott, C.J. (2004) Octopamine-containing (OC) interneurons enhance central pattern generator activity in sucrose-induced feeding in the

snail *Lymnaea stagnalis*. *J Comp Physiol A Neuroethol Sens Neural Behav Physiol*, **190**, 837-846.

- Vehovszky, A., Szabo, H. & Elliott, C.J. (2005) Octopamine increases the excitability of neurons in the snail feeding system by modulation of inward sodium current but not outward potassium currents. *BMC Neurosci*, **6**, 70.
- Weiss, K.R., Cohen, J.L. & Kupfermann, I. (1978) Modulatory control of buccal musculature by a serotonergic neuron (metacerebral cell) in *Aplysia*. *J Neurophysiol*, **41**, 181-203.
- Whelan, H.A. & McCrohan, C.R. (1996) Food-related conditioning and neuronal correlates in the freshwater snail *Lymnaea stagnalis*. *J Molluscan Stud*, **62**, 483-494.
- Williams, S.R. & Mitchell, S.J. (2008) Direct measurement of somatic voltage clamp errors in central neurons. *Nat Neurosci*, **11**, 790.
- Winlow, W., Haydon, P.G. & Benjamin, P.R. (1981) Multiple postsynaptic actions of the giant dopamine-containing neurone RPeD1 of *Lymnaea stagnalis*. *J Exp Biol*, **94**, 137.
- Woody, C.D. & Black-Cleworth, P. (1973) Differences in excitability of cortical neurons as a function of motor projection in conditioned cats. *J Neurophysiol*, **36**, 1104-1116.
- Yeoman, M.S., Brierley, M.J. & Benjamin, P.R. (1996) Central pattern generator interneurons are targets for the modulatory serotonergic cerebral giant cells in the feeding system of *Lymnaea*. *J Neurophysiol*, **75**, 11-25.
- Yeoman, M.S., Pieneman, A.W., Ferguson, G.P., Ter Maat, A. & Benjamin, P.R. (1994) Modulatory role for the serotonergic cerebral giant cells in the feeding system of the snail, *Lymnaea*. I. Fine wire recording in the intact animal and pharmacology. *J Neurophysiol*, **72**, 1357-1371.
- Yeoman, M.S., Vehovszky, A., Kemenes, G., Elliott, C.J. & Benjamin, P.R. (1995) Novel interneuron having hybrid modulatory-central pattern generator properties in the feeding system of the snail, *Lymnaea stagnalis*. *J Neurophysiol*, **73**, 112-124.